Proton-Proton Colliding-Beam Storage Rings for the National Accelerator Laboratory

Design Study 1968

Proton-Proton Colliding-Beam Storage Rings for the National Accelerator Laboratory

Design Study 1968

national accelerator laboratory

Batavia Illinois

Universities Research Association
for the United States Atomic Energy Commission

INTRODUCTION

This report describes the design studies on colliding-beam storage rings carried out at the National Accelerator Laboratory in the summer and fall of 1968. These studies were under the direction of Lee C. Teng. M. Stanley Livingston also played an important part in catalyzing the studies. Dr. Teng's preface, immediately following, gives a chronology of the study and lists the participants in various aspects.

The purpose of the study has been to develop realistic cost estimates upon which future plans can be based. It is to be emphasized that this is not a proposal for construction.

The major results of the study are that 100-100 BeV colliding-beam rings can be built for approximately 75 million dollars (in 1968 dollars), utilizing conventional steel and copper magnets. This estimate includes no equipment for physics experiments.

A system utilizing steel magnets that are excited by superconducting coils is estimated to cost somewhat less. A similar system using cryogenic aluminum coils appears to be slightly more costly at this time than the conventional magnet.

A number of storage rings built of superconducting magnets have also been analyzed on the premise (undemonstrated as yet) that they would in fact operate satisfactorily. Such magnets designed using present technology for relatively low fields, about 40 kG, appear to be competitive with conventional magnets.

Evidently a total colliding-beam facility, including experimental equipment, could be built at NAL for a sum of the order of 100 million 1968 dollars. It should be added that the terms of reference of these design studies gave emphasis to a straightforward, conservative design. Further design work and advances in technology might very well result in a significant reduction in cost or, at the same cost, provide for a greater scope.

Robert Rathbun Wilson

PREFACE

The present effort on the study of storage rings for the NAL accelerator was begun in July 1968 in response to a recommendation from Sub-panel A of the High Energy Physics Advisory Panel of the Atomic Energy Commission. The immediate goal of the study is to produce one or a few desirable designs based on the present and extrapolated status of high energy physics and accelerator technology. As a working hypothesis it was assumed that actual construction would start in about three years. Adequate design details are worked out to allow making reasonably reliable cost estimates.

Because of the necessary close collaboration with a large spectrum of experimental physicists and because of the heavy involvement of the NAL staff in the design and construction of the 200 BeV accelerator, we have relied heavily on manpower from outside the Laboratory. During the last two weeks of the NAL Summer Study at Aspen, Colorado, which ended on August 16, 1968, intensive discussions on the design criteria for the beam collision region were carried out with several of the participating physicists. The non-NAL physicists actively involved were

Giuseppe Cocconi (CERN
Hans Frauenfelder (U. of Ill.)
David Frisch (MIT)
Clemens Heusch (CIT)
Lawrence Jones (U. of Mich.)
Alan Krisch (U. of Mich.)
Donald Meyer (U. of Mich.)
Lynn Stevenson (LRL)
Karl Strauch (CEA).

A work session was then held during the following two weeks from August 19 through August 30. More than a dozen people, most of whom were accelerator physicists and engineers from various laboratories in the U. S. and from CERN, participated for various lengths of time. Intensive design efforts were spent based on the result of discussion with experimentalists at Aspen. The first approximations of several designs were generated during this session. Non-NAL participants were

Richard Britton (BNL)	Frederick Mills (PSL)
Ernest Courant (BNL)	Brian Montague (CERN)
Gordon Danby (BNL)	James Patterson (CEA)
Michael Green (LRL)	John Purcell (ANL)
Lawrence Jones (U. of Mich.)	Ednor Rowe (PSL)
Eberhard Keil (CERN)	Andrew Sessler (LRL)
Donald Meyer (U. of Mich.)	Wolfgang Schnell (CERN).

During the week of September 30 through October 4 a one-week session was held to study the experimental utilization of the storage rings as designed. As a result of this study further modifications of the design of the intersecting region were made. The following physicists from outside of NAL participated for various lengths of time during this period:

Clemens Heusch (CIT)	Kent Terwilliger (U. of Mich.)
Lynn Stevenson (LRL)	Alan Krisch (U. of Mich.)
John Rees (AEC)	Donald Meyer (U. of Mich.)
Robert Little (CEA)	Gerald O'Neill (Princeton)
Lawrence Jones (U. of Mich.)	W. H. K. Panofsky (SLAC)
Andrew Buffington (LRL)	Richard Wilson (Harvard).

Throughout the study the continuity and detailed design efforts were provided by NAL staff members. Those who participated most actively were

Miguel Awschalom	James MacLachlan
Roy Billinge	Lincoln Read
Thomas Collins	Lloyd Smith
Alper Garren	Stanley Snowdon
Edward Hubbard	John Stekly
Quentin Kerns	Lee Teng
Stanley Livingston	Arie van Steenbergen
Ernest Malamud	Robert Wilson.

In addition S. M. Marcowitz and R. J. Lari of ANL assisted in performing computer calculations. For engineering and cost estimating we engaged the service of W. M. Brobeck & Associates.

Section I of the Design Report on "High Energy Physics on Proton-Proton Storage Rings" was mostly written by J. J. Sakurai of the University of Chicago. Other people who assisted in the writing were

A. A. Garren (Section III)

S. C. Snowdon (Section IV)

Q. A. Kerns (Sections VI and IX)

E. D. Courant (Section VII)

L. Smith (Section VIII)

W. M. Brobeck & Associates (Sections IX, X, XI and XII).

Z. J. Stekly (Appendix A).

The design presented here, tentative and incomplete as it is, shows nevertheless that a proton-proton colliding beam storage ring as described is practical, will be a very useful facility for high energy physics experimentation, and can be built at approximately the cost estimated.

Lee C. Teng

TABLE OF CONTENTS

I. High Energy Physics on Proton-Proton Colliding Beam Storage Rings 1

II. Choice of Major Parameters 8

III. Lattice and Orbit 17

(A) Ring Lattice

(B) Aperture Requirements

(C) Space Charge Limits

(D) Luminosity

IV. Magnet System 30

(A) Conventional Magnets

(B) Iron Magnet with Superconducting Coil

(C) Iron Magnet with Cryogenically Cooled Aluminum Coil

(D) Trimming Magnets

V. Vacuum System 41

(A) Vacuum Chamber

(B) Linear Ion Pump

(C) Cryosorption Pump

(D) Sector Valves

(E) Clearing Electrodes

VI. Radiofrequency System 48

(A) RF Cavity

(B) RF Supply and Control

VII. Injection and Beam Transport 52

(A) Injection Beam Transport

(B) Injection Procedure

(C) Kicker Magnet

(D) Beam Stacking

VIII. Radiation, Shielding, and Beam Dump System 60

(A) General Shielding

(B) Beam Scrapers

(C) Beam Dump System

IX. Monitoring and Control Systems 67

(A) Beam Monitoring

(B) Control System

X. Ring Enclosures and Experimental Halls 72

(A) Injection Transport Enclosure

(B) Enclosures of Regular Lattice and Injection Areas

(C) Experimental Halls

XI. Support Buildings and Utilities 77

(A) Service Buildings

(B) Staff and Space Requirements

(C) Mechanical Utilities

(D) Electric Power Distribution

XII. Construction Cost Estimate 83

Appendix A - High Field Superconducting Magnet Storage Rings

Appendix B - List of Parameters

Appendix C - Bibliography

I. HIGH ENERGY PHYSICS ON PROTON-PROTON COLLIDING BEAM STORAGE RINGS

A high energy accelerator is one of the most complex and costly facilities for basic research in science. Bigger and bigger accelerators have been built to yield higher and higher energies at correspondingly higher costs. Although there is no technological limitation to the highest energy attainable, the high cost of accelerators will surely impose an economic limitation. A technological breakthrough which will significantly reduce the cost of accelerators is not yet in sight. The next order of magnitude increase in energy from that of the NAL accelerator is most likely attainable in practice only by the technique of colliding beams.

Several electron-electron and electron-positron storage rings have been built in the past few years. Notable among these are the 300 MeV electron-electron machine at Stanford and the 400 MeV range electron-positron machines at Novosibirsk and at Orsay. All these storage rings have proven to be highly productive in physics research. A 1.5 BeV electron-positron storage ring has recently been completed at Frascati, Italy. Several electron-positron storage rings in the range of 3 BeV are currently under design or construction at SLAC, CEA, DESY, and Novosibirsk.

No proton colliding beam storage ring has yet been operated. At CERN, Switzerland, a set of intersecting storage rings (ISR)

for proton-proton collisions at energies up to 28 BeV is under construction and is expected to be operating in 1971. This will produce center-of-mass energies equivalent to those attainable with a conventional accelerator of 1780 BeV. At Novosibirsk, USSR, design and construction are underway for a colliding beam storage ring in which protons and antiprotons will collide at 25 BeV. This is equivalent to a 1430 BeV antiproton beam on a stationary target; to produce such an antiproton beam would probably require a conventional accelerator well above 2000 BeV.

In the U. S. the construction of proton-proton storage rings was recommended by the Ramsey Panel in 1963. The most appropriate accelerator for which the storage ring should be built at that time was the 33 BeV AGS at Brookhaven. With the funding of the 200 BeV NAL accelerator, and since the CERN-ISR is expected to be operating at 28 BeV in 1971, it is clearly most reasonable now to consider storage rings for the 200 BeV accelerator.

Proton-proton colliding beam storage rings considered here provide center-of-mass energies which are too costly to be attained with a proton beam colliding with protons at rest. For example, to obtain the proposed center-of-mass energy of 200 BeV using the conventional technique we need an accelerator of 22,000 BeV which might cost many billions of dollars. The large center-of-mass energy available with the storage ring enables us to perform qualitatively different experiments as well as more conventional experiments at enormously high energies.

It is unfortunately true, however, that colliding beam experiments are difficult and are limited as to the classes of experiments which can be performed. With this limitation in mind, we may discuss various colliding beam experiments.

(A) Search for New Particles

One of the more obvious experiments to be performed at p-p colliding beam facilities is to search for new stable or metastable particles. It has been proposed by some theoreticians that all the known hadrons (strongly interacting particles) are made up of more "basic" particles belonging to a triplet representation of unitary symmetry. The conjectured basic triplets may have either integral or fractional charges ("quarks" with $\pm e/3$, $\pm 2e/3$). Such particles have been searched for at the Brookhaven AGS and the CERN CPS with negative results. It is possible that the energies of these machines are too low for the production of these particles.

Another massive particle whose existence has often been speculated theoretically is a W boson (or several kinds of W bosons) which is believed to act as the carrier of the weak interactions in much the same way as the photon is the carrier of the electromagnetic interactions. It is interesting to note that the production cross section for W bosons can be relatively large if the W-mass m_W is high; this is because the dimensionless coupling constant for the W boson varies as Gm_W^2 where G is the usual four-fermion weak coupling constant ($G \sim 10^{-5} m_p^{-2}$, m_p = proton mass).

(B) Search for New Phenomena

The present theory of weak interactions based on current-current interactions is a phenomenological theory and is expected to be valid only at low or medium energies. For this reason the possibility that the "weak" interaction becomes effectively "strong" at high energies should be seriously investigated. In particular one may look for apparent breakdown of conservation laws obeyed by the usual strong and electromagnetic interactions, e.g. violation of parity conservation and strangeness conservation with appreciable magnitude.

Recent experiments of the Utah cosmic ray group have revealed an anomalous zenith distribution of very high energy cosmic ray muons at sea level. One possible explanation for this interesting effect is that in high energy proton-proton collisions there exists a mechanism for copious production of muons which are not decay products of long-lived particles such as pions and kaons. Even though more underground and above-ground experiments are being planned along this line, it is likely that to obtain a better understanding of the Utah anomaly we must await new facilities such as proton-proton storage rings.

(C) Proton-Proton Total Cross Section

At AGS energies (laboratory momentum $p_{lab} \leq 30$ BeV/c) the proton-proton total cross section can be parametrized by the formula

$$\sigma_{tot}(pp) \approx (a + b\, p_{lab}^{-0.99}).$$

Using the proposed storage ring we will be able to find out whether this parametrization is valid up to p_{lab} = 22,000 BeV/c. Whether σ_{tot}(pp) approaches the value a = 38 mb given by the formula and the manner in which it approaches the asymptotic value are both of considerable interest. Some theoreticians even speculate that σ_{tot}(pp) in fact vanishes at infinite energy.

(D) Elastic Proton-Proton Scattering

Various theoretical models suggest that elastic proton-proton scattering becomes much "cleaner" as we go to very high energies. In the Regge pole approach, for instance, the effect of the so-called secondary (ω, P', ρ etc.) trajectories is predicted to be insignificant at the storage ring energy; we therefore have an excellent opportunity to study the nature of the Pomeranchuk trajectory (or, if it is not a trajectory at all, whatever is responsible for diffraction scattering at extremely high energies). In particular, one should study whether $d\sigma/dt$ becomes independent of s, as required by the old-fashioned diffraction model, or $d\sigma/dt$ shrinks with s, as is the case if the Pomeranchuk trajectory is normal in the sense of the Regge pole theory. It is also worth examining whether the amplitude for p-p scattering becomes purely imaginary at extremely high energies, as required by most theoretical models. (At the highest AGS energy the ratio of the real to imaginary part of the p-p scattering amplitude is about -15%.)

Recent differential cross section measurements indicate that there are definite kinks in the p-p angular distribution at $t \approx -1 (\text{BeV/c})^2$ and $\approx -3 (\text{BeV/c})^2$. It is of considerable theoretical importance to find out whether: 1) these kinks persist at the same values of t at higher energies, and 2) these breaks in $d\sigma/dt$ become more pronounced as we go to higher energies. We should not discount the possibility that these anomalies in $d\sigma/dt$ ultimately appear as genuine diffraction minima at extremely high energies.

There are theoretical proposals to relate high momentum transfer p-p scattering to the electromagnetic form factor $G_E(t)$ of the proton determined from electron-proton scattering by the relation

$$\frac{d\sigma}{dt} (pp \to pp) \propto G_E^4 (t).$$

The presently available proton energy is insufficient to provide crucial tests for these interesting speculations.

If polarized protons can be stored in the ring, we may even learn something about the spin dependence of high energy p-p scattering.

(E) Inelastic Proton-Proton Interactions

At AGS energies nucleon isobars with the same isospin (T=1/2) and natural parity (e.g. $J^P = 5/2^+$) as the nucleon are produced with sizeable cross sections (mb range) and without any appreciable energy dependence by a process known as diffraction dissociation. We may therefore speculate that these

"quasi-elastic" processes still occur when the center-of-mass energy is increased by more than an order of magnitude.

Cosmic ray physicists have been using two-center models (or two-fireball models) for proton-proton interactions up to energies of 10^{15}eV. With the proposed storage ring it should become possible to test such models in an unambiguous way for the first time. It is also of interest to examine the mean transverse momentum of secondary particles in high energy collisions to see whether it is indeed approximately independent of the incident particle energy, as indicated by cosmic ray data.

The experimental programs discussed above are indicative of the new range of physical phenomena potentially accessible through the use of colliding beams. However, the enthusiasm expressed by physicists for a storage ring facility is undoubtedly colored by the feeling that while these are visible problems whose resolution justifies the required effort, there is a high probability that entirely new phenomena will appear that would cut through our present confusion in a much more profound manner.

II. CHOICE OF MAJOR PARAMETERS

A large variety of storage ring sizes and configurations were examined during the early part of this study[1,2,3]. The primary considerations in the choice of design parameters are, of course, the utilization of the facility for performing high energy physics experiments. These are

(a) The peak energy should be sufficiently higher than that available elsewhere to make this a unique facility. In addition, the energy should be continuously variable from the peak value down to at least the highest value available at another similar facility.

(b) The design should contain provision to serve as many simultaneous experiments as considered optimal.

(c) The facility should have the capability of attaining the highest possible luminosity or interaction rate. In addition the design of the beam collision region should provide maximum flexibility for doing experiments.

(d) The design should minimize the interference of the storage ring operation with the regular 200 BeV experimental program.

To these one should add the obvious requirement that imposes moderating influences, namely:

(e) The cost of the facility should be kept reasonable and for given design capabilities the cost should be minimized.

The weighing of relative merit and cost is a lengthy and sometimes not totally rational process. It is gratifying, however, that the present choice of major parameters and the gross features

of design have withstood several re-examinations by different groups of both experimentalists and accelerator physicists.

(A) Evaluation of the Bypass-Storage Ring Scheme

The bypass-ring scheme[4,5] was conceived during the summer study of 1967 and was described in Section 18 of the NAL Design Report. In this scheme a part of the beam stacked in a single storage ring is reinjected into the main ring of the accelerator which is then operated at dc as the other storage ring. This part of the beam is made to collide with the part of the beam remaining in the single storage ring on a bypass added to the main ring. Compared to the conventional two-ring scheme where the accelerator is used only as an injector to fill the two rings, the bypass-ring scheme suffers the following drawbacks:

(1) In the bypass-ring scheme whenever colliding beam experiments are being performed, the main ring of the accelerator is tied up and not available for regular experiments in the experimental areas. Since the storage rings have to be filled only once or twice a day and the filling time is only a few minutes, tying up the main ring represents a serious operational disadvantage.

(2) Since the single beam stacked in the one ring is shared between the ring and the bypass-plus-main ring and since the circumference of the main ring is longer than that of the storage ring the luminosity and duty factor of the beam interaction region are much lower than those in the two-ring scheme.

(3) Because of the necessary improvement of the main ring vacuum system to obtain the 10^{-9} torr pressure necessary for

beam storage operation and because the length of the bypass is comparable to the circumference of a storage ring, the bypass-ring scheme may have an economic disadvantage compared to the two-ring scheme[6].

(4) The very large amount of stored energy in the stacked beam makes the operation of a storage ring hazardous at best. It is difficult to justify subjecting the main ring of the accelerator to this hazard when it can easily be avoided.

For these reasons we have adopted the two-ring scheme.

(B) Choice of Energy and Magnetic Field

In making a choice of beam energy and magnetic field, one has to consider on the one hand the 2 x 28 BeV energy of the CERN-ISR and, on the other hand, the 2 x 400 BeV energy potentially available at NAL. For this study we have chosen an energy of 2 x 100 BeV at a magnetic field of 20 kG. This field is obtainable with conventional magnets and the energy is sufficiently higher than that of the ISR to make the NAL facility uniquely interesting. For the same geometry, an energy of 2 x 400 BeV could be reached with superconducting magnets at 80 kG, a field level that is certainly in the range of future possibilities. Thus the choice of this radius conservatively provides a signficiant increase in energy from the ISR and optimistically allows for exploitation of the full potential of the accelerator. In this report, the conservative parameters are emphasized for the purpose of establishing a realistic cost estimate, but the entire concept should be constantly reviewed for the possibility of revising the energy upwards in response to advances in the technology of superconductors.

(C) Number of Experimental Areas

Discussions with high energy experimental physicists indicated the desirability of having at least the capability of eventually providing four or more beam collision points for the simultaneous installation of four or more experimental set-ups. Configurations where the rings are externally tangent to each other can provide only one, or at most two, closely adjacent beam collision points and are hence discarded. We have focused our attention on a concentric ring configuration with six symmetrically located beam collision points. Special magnet sequences are inserted into the regular magnet lattice of the rings in the neighborhood of the beam collision points to produce desired beam characteristics at these points. Two of these insertions will be used for injection of beam into the storage rings leaving four for the performance of colliding beam experiments. We have further assumed that only three of the four experimental areas will be developed initially.

(D) Choice of Radius

The choice of six long insertions and of 100 BeV at 20 kG leads naturally, if rather arbitrarily, to a ring radius of $\frac{1}{3}$ km. Although not crucial, it is simplest to have a storage ring radius which is an integral fraction of the main ring radius. The beam extracted in one turn from the main ring will then fill the storage ring exactly an integral number (in this case three) of turns.

(E) Positioning of the Storage Ring on the Laboratory Site

The positioning of the storage ring relative to the main

ring of the accelerator is based largely on economic considerations. The 100 BeV beam in the main ring will be extracted in one turn from the long straight section immediately downstream from the one for injection into the main ring and extraction to the external proton beam. This puts the storage ring in a position closest to the center of activity of the Laboratory and minimizes the lengths of roads and utility connections.

Two storage ring insertions 120° apart are used for injection. This choice minimizes the total length and bending angle of the beam transport lines from the accelerator main ring to the storage ring. The bending magnetic field for the beam transport is also taken to be 20 kG. Fig. II-1 is the master plan showing the layout of the storage ring on the NAL site in relation to the 200 BeV accelerator. Fig. II-2 is an enlarged view of the storage ring showing the injection transport lines, the storage ring enclosure, the three experimental halls, and other buildings and structures.

(F) Antiproton Storage

The capability of performing proton-antiproton colliding beam experiments would greatly enhance the usefulness of the storage ring facility. Straight-forward injection of the low phase space density antiproton beam produced from a target into a storage ring will not give a beam of useful intensity. An ingenious scheme has been proposed by G. I. Budker[7] to increase the transverse phase space density of an antiproton beam. In this scheme a high intensity electron beam having the same speed is made to coalesce and travel along with the antiproton beam.

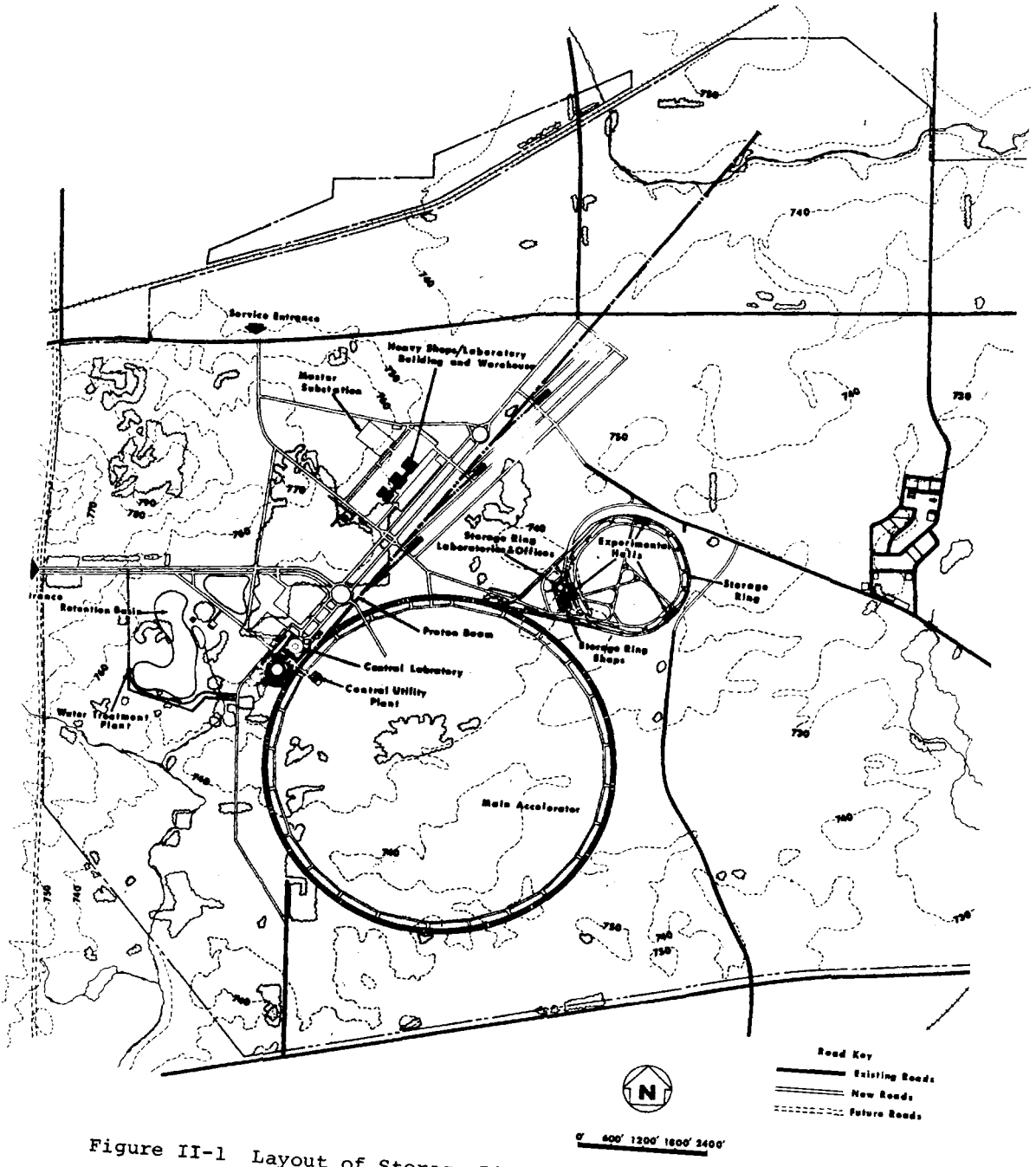

Figure II-1 Layout of Storage Ring on NAL Site

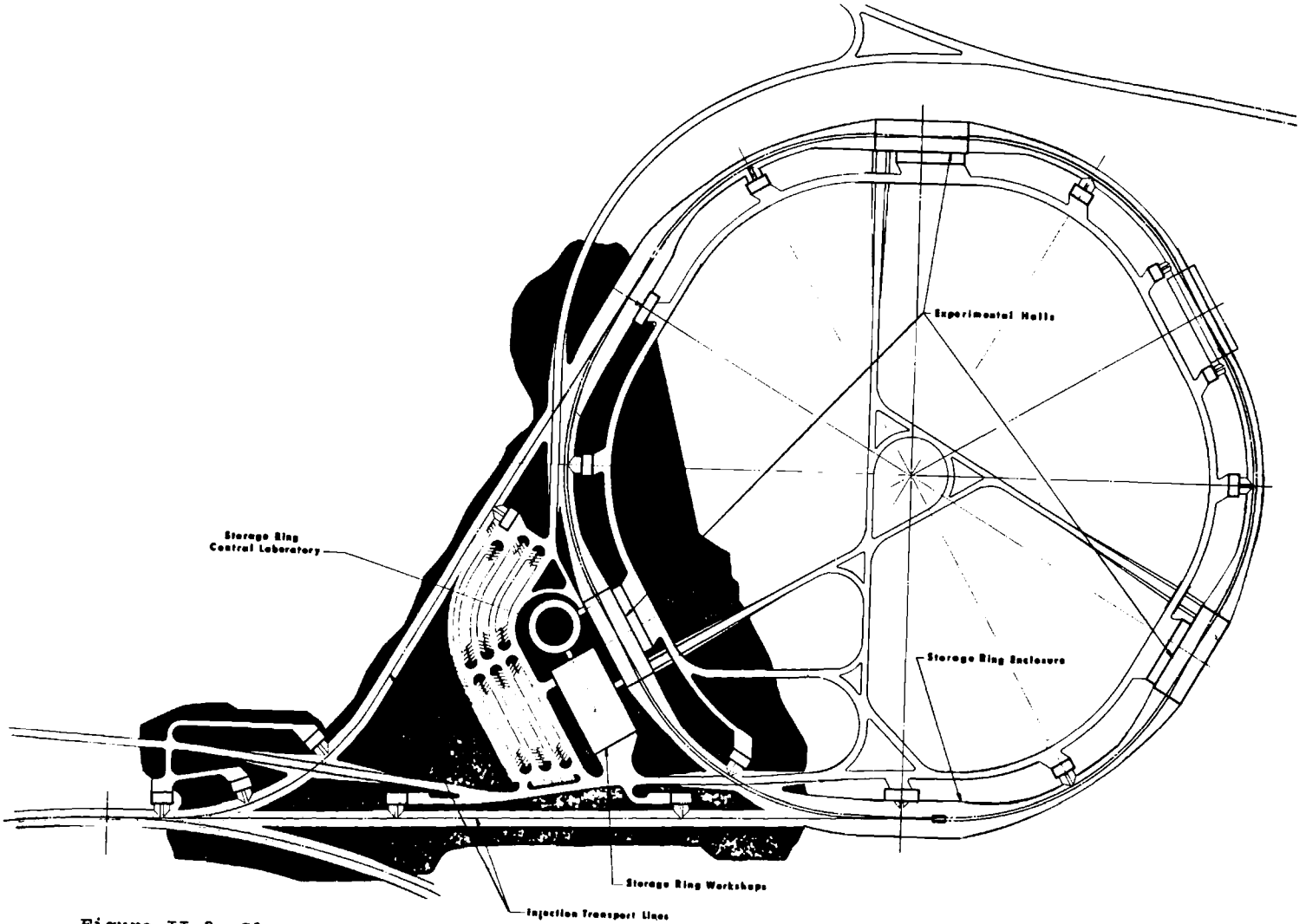

Figure II-2 Close-up of Storage Ring Layout

The energy of the transverse motion of the antiprotons is reduced through equipartition exchange with the much lower transverse energy of the electrons. The transverse phase space volume occupied by the antiproton beam is, thereby, reduced. Although on paper this scheme looks sound, its validity has not yet been demonstrated in practice. For this study we have therefore chosen not to consider the storage of an antiproton beam.

(G) Design Considerations for the Ring Lattice and Magnets

In addition to these choices of major design parameters, the following general considerations for design of more detailed features are also worth discussing.

(1) Ring Regular Lattice

The beam geometry and characteristics in an insertion are specified by the function of the insertion and are crucial to the performance and usefulness of the storage ring. In the regular magnet lattice connecting the insertions, however, there is no special demand on either beam geometry or beam characteristics except that they should be compatible with minimum cost. Recent developments[8,9,10] have made it clear that by using properly designed magnet trains it is generally possible, within broad limits, to match the beam characteristics in any chosen regular lattice to any functionally desirable characteristics in the insertion. For the regular lattice the studies made for the accelerator main ring are directly applicable and indicate that the separated function FODO lattice is most economical.

(2) Beam Geometry in Insertion

The two beams in an insertion can assume two different basic geometries, namely, either without or with a crossing. The former geometry gives better accessibility to each beam separately and is therefore more advantageous for beam injection. However, to do experiments we must use additional steering magnets to make the beams collide. The latter geometry assures a beam collision and provides more flexibility for experiments. The crossing angle, and hence, the length and luminosity of the beam interaction region can be adjusted by additional beam steering magnets. The obvious choice of four crossing and two no-crossing insertions does not lead to a configuration which is acceptable from the point of view of orbit geometry and stability. Since the advantage of no-crossing geometry for injection is only minor and since crossing geometry provides the important flexibility for experiments we have adopted the crossing geometry for all six insertions.

(3) Horizontal or Vertical Beam Crossing

In the configuration where the beams cross in a vertical plane the two rings would be placed directly one above the other. In this case the secondary particles being produced mainly in the directions of the incident beams would be going either upward or downward in the vertical plane which makes the setting up of experimental equipment awkward. For this reason we have chosen to have the storage rings and the beam crossings in a horizontal plane.

(4) Separate or Combined Ring Magnets

For concentric rings in a horizontal plane, it is possible to combine the magnets for the two rings if the separation between the beams is not made too large. A single magnet with two gaps side by side having oppositely directed fields could be used for the two beams going in opposite directions and could lead to some cost saving. However, for some experiments it is desirable to have the capability of storing beams of unequal energies in the two rings. Combining the magnets of the two rings makes it difficult to provide this capability. For this capability and for the flexibility of being able to trim the two rings separately we decided on two separate and independent rings.

(5) Ring Magnet Design

For a magnet with 20 kG field an iron yoke has definite advantages. To energize the magnet several types of coils can be employed. Conventional room temperature copper coils are simplest to design and give the greatest assurance of success. However, such magnets are large and consume large amounts of electric power. High purity aluminum, when cryogenically cooled to $16^{\circ}K$, has a resistivity about $\frac{1}{5000}$ that of aluminum at room temperature. Iron magnets with cryogenically cooled aluminum coils have been developed for some applications. High field niobium alloy superconductors are commonly used for applications in which fields higher than 40 kG are desired. Still, the use of superconducting coils in 20 kG iron-yoke magnets[11] clearly presents definite advantages. For both the superconducting Nb

alloy coil and the cryogenic Al coil, the power consumption is greatly reduced. On the other hand, cryogenic jackets and refrigeration systems are needed for these coils. Designs of iron-yoke 20 kG magnets with all three types of coils were studied.

In addition, a cursory study of 100 BeV storage rings using 40 kG and 60 kG high field superconducting magnets was also made. The results of this study are given in Appendix A and indicate that at the present time the application of these high field superconducting magnets, aside from the technical feasibility which has yet to be demonstrated, gives no economic advantage. However, the rapid advances in this field may in the near future drastically alter the picture.

References

1 M. S. Livingston, Study Paper on the NAL Storage Ring Design, NAL Report FN-162, July 2, 1968.

2 M. S. Livingston, Storage Ring Study Paper #2, NAL Report TM-3, August 14, 1968.

3 M. S. Livingston, Dimensional Study of Intersecting Storage Rings, NAL Report TM-24, August 30, 1968.

4 E. D. Courant, et al, Bypass-Storage Ring Option for NAL, NAL Report 5, August 30, 1967.

5 E. D. Courant, L. W. Jones, B. W. Montague, E. M. Rowe, and A. M. Sessler, Bypass-Storage Ring Option for NAL, Nucl. Instr. and Methods 60, 29-35, 1968.

6 P. J. Reardon, Cost Guestimate for Storage Ring, NAL Memo, July 25, 1968.

7 G. I. Budker, An Effective Method of Damping Particle Oscillations in Proton and Antiproton Storage Rings, Translation from Atomnaya Energiya, Vol. 22, no. 5, p. 346, May, 1967.

8 T. L. Collins, Long Straight Sections for AG Synchrotrons, Cambridge Accelerator Report CEA-86, July 10, 1961.

9 A. A. Garren, Design of Long Straight Sections for Synchrotrons, Proc. of the V International Conf. on High Energy Accel., CNEN Rome, p. 22, 1966.

10 P. L. Morton and J. R. Rees, The Design of Low-β Insertions for Storage Rings, IEEE Trans. on Nucl. Sci., p. 630, June, 1967.

11 R. R. Wilson, A Superferric Storage Ring, NAL Report FN-173, September 25, 1968.

III. LATTICE AND ORBITS

(A) Ring Lattice

During the early phases of the study simple storage ring lattices[1] were developed for the express purpose of providing some definite designs for cost estimating. These lattices although valid, do not contain special matching insertions to produce beam characteristics optimal for injection or for experimentation. The more ambitious program of designing special function insertions to match optimal beam characteristics in the insertion to those in a regular lattice chosen for economy was undertaken later. The design of these matching insertions although straight forward involves extensive and time-consuming computer work using computer programs, such as TRANSPORT and SYNCH. The lattice presented here is only an intermediate design. A subsequent modification[2] gives ν values more appropriate for injection and further reduces the vertical beam height at the experimental crossing point leading to a higher luminosity. Continuing work in refining the lattice will further improve the performance and utilization of the storage ring.

(1) General Description

The storage ring consists of two rings crossing each other at six symmetrically located points. Three of the crossings, where the intersecting beams are inwardly directed, are

designed to yield beam characteristics most suitable for colliding beam experiments. The beams are made narrow vertically at the crossing points to enhance the luminosity, and the beam widening due to momentum spread is made zero to localize the interaction region as closely as possible. These will be referred to as experimental (E) crossings.

Two of the other three crossings are needed for injection of beam into the rings and for extracting and dumping the beams in the rings when desired. These functions require the beams to be wide horizontally and have large momentum widening[3]. For symmetry reasons, all three crossings will have identical design and will be called Injection (I) crossings.

The E and I crossings alternate so that each ring has three superperiods. Each superperiod thus consists of the magnet lattice insertions for an E and an I crossing connected by normal separated function FODO cells[4]. The beam characteristics in the E and I insertions are matched to those in the normal cells.

(2) Geometry

The usefulness of the storage ring depends principally on the design of the experimental insertion. To provide maximum flexibility for carrying out experiments, the clear drift lengths on either side of the beam crossing point should be as long as possible. On the other hand, the beam widths will get excessively large over too long a drift space. This is especially true in the vertical plane since the height of the

beam is to be very small at the crossing point, which implies a large angular spread. For the given beam emittance, the longest practical drift length on either side of the intersection is about 40 m. At the end of this drift length the separation between the two beams should be about 2 m to provide space for particle detectors for experiments. This leads to a beam crossing angle of about 50 mrad. Thus the outer arc of the regular lattice connecting two neighboring insertions should have a bending angle 100 mrad greater than that of the inner arc. This is accomplished simply by adjusting the bending angle of a normal cell to be 100 mrad and making the outer arc contain one more normal cell than the inner arc. The exact geometrical parameters so developed are given in Table III-1.

(3) Normal Cell

The normal cell shown schematically in Fig. III-1 is a compact separated function FODO design similar to that of the main ring of the accelerator. The phase advance is chosen so as to minimize the β-function. The bending magnetic field is about 20 kG, as discussed in Section II. As will be discussed later in Section IV, the 4.2 m bending magnet is actually split into two rectangular sections with a common coil. The 1.6 m drift space will contain a trimming magnet package, a beam sensing electrode package and a pump out port. Detailed parameters are given in Table III-1.

(4) Experimental (E) Insertion

The insertion is between the mid-points of normal cell

Table III-1 Lattice Structure and Orbit Parameters
(*Numbers in parentheses are bending magnet fields and quadrupole field gradients at 100 BeV)

1.	Normal cell (C)		
	a. Length of bending magnet (B1 and B2)	4.2 m	(19.99kG)*
	b. Length of cell quadrupole magnet (QF and QD)	1.4 m	(248.5kG/m)
	c. Length of minimum separation between magnets (0)	0.3 m	
	d. Length of short straight section (00)	1.6 m	
	e. Cell structure	(QF/2)00(B1)0(B2)0-(QD)00(B2)0(B1 0(QF/2)	
	f. Total length of cell	24 m	
	g. umber of cells in each ring	48	
2.	Injection Insertion (I)		
	a. Length of end quadrupole (QDI = QD/2)	0.7 m	(248.5kG/m)
	b. Length of bending magnet (BI)	4.2 m	(19.99kG)
	c. Lengths of quadrupoles in triplets		
	QFI1	1.3 m	(237 kG/m)
	QDI2	2.14 m	(-190 kG/m)
	QFI3	0.85 m	(141 kG/m)
	d. Drift lengths between		
	QDI and BI (LI1)	3.40 m	
	BI and BI (0)	0.3 m	
	BI and QFI1 (LI2)	6.14 m	
	QFI1 and QDI2 (LI3)	4.7 m	
	QDI2 and QFI3 (LI4)	3.86 m	
	QFI3 and crossing point (inside) (LI5)	39.28 m	
	Crossing point and QFI3 (outside) (LI6)	29.49 m	
	e. Insertion point in normal cell	Midpoint of QD	
	f. Structure of insertion I (in beam direction from inside to outside)	(QDI)LI1(B2)0(B1)0(BI)0(BI)LI2(QFI1)LI3(QDI2)LI4(QFI3)LI5-LI6(QFI3)LI4(QDI2)LI3(QFI1)LI2-(BI)0(BI)0(B1)0(B2)LI1(QDI)	
	g. Total length of I-insertion	149.35 m	
	h. Number of I-insertions	3	

3. Experimental insertion (E)

a.	Length of end quadrupole (QFE) -	0.94 m	(248.5kG/m)
b.	Length of bending magnet (BE)	4.2 m	(19.99kG)
c.	Lenths of quadrupoles in outer triplet		
	QFE1	1.8 m	(214kG/m)
	QDE2	2.5 m	(-196kG/m)
	QFE3	1.4 m	(165 kG/m)
	Lengths of quadrupoles in inner triplet		
	QDE4	1.8 m	(-179kG/m)
	QFE5	2.5 m	(183kG/m)
	QDE6	1.4 m	(-120kG/m)
d.	Drift lengths between		
	QFE and B1 (LE1)	0.78 m	
	BE and BE(0)	0.3 m	
	BE and QFE1 (LE2)	1.93 m	
	QFE1 and QDE2(LE3)	4.03 m	
	QDE2 and QFE3(LE4)	3.86 m	
	QDE3 and crossing point (LE5)	32.55 m	
	Crossing point and QDE4(LE6)	39.97 m	
	QDE4 and QFE5(LE7)	3.54 m	
	QFE5 and QDE6(LE8)	4.68 m	
	QDE6 and BE(LE9)	5.29 m	
e.	Insertion point in normal cell	Midpoint of QF	
f.	Structure of insertion E (in beam direction from outside to inside)	(QFE)LE1(B1)0(B2)0(BE)0-(BE)0(BE)0(BE)LE2(QFE1)-LE3(QDE2)LE4(QFE3)LE5-LE6(QDE4)LE7(QFE5)LE8-(QDE6)LE9(BE)0(BE)0(BE)-0(BE)0(B2)0(B1)LE1(QFE)	
g.	Total length of E-insertion	164.78 m	
h.	Number of E insertions	3	

4. Superperiod

a.	Half cells		
	from mid-QF to mid-QD	$\frac{C}{2}$	
	from mid-QD to mid-QF	$\frac{C}{2}$	
b.	Structure of superperiod	ECCCCCCC$\frac{C}{2}$I$\frac{C}{2}$CCCCCCCC	
c.	Total length of superperiod	698.13 m	
d.	Number of superperiods	3	

5. Orbit properties

a.	Betatron oscillation wave-number (ν)	14.8	
	Betatron Oscillation wave-length	141.4 m	

5. Orbit functions - Continued

b. Betatron Oscillation amplitude function (β)

Normal cell	
$\beta_{x\ max} = \beta_{y\ max}$	39.5 m
$\beta_{x\ min} = \beta_{y\ min}$	10.2 m
Injection insertion	
$\beta_{x\ max}$	140 m
$\beta_{y\ max}$	102 m
Experimental insertion	
$\beta_{x\ max}$	224 m
$\beta_{y\ max}$	618 m
Experimental crossing point	
β_x	27 m
β_y	4 m

c. Momentum excursion function (x_p)

Maximum in normal cell	2.18 m
Minimum in normal cell	1.20 m
Injection insertion	3.65 m
Experimental insertion	0

quadrupoles QF. The momentum excursion functions x_p and x'_p are first brought to zero in the middle of the insertion by properly placing at each end one focusing quadrupole QFE and six bending magnets BE. The low β_y at the intersection is then obtained by six quadrupoles QFE1, QDE3, QFE3, QDE4, QFE5, and QDE6, three at each end inboard of the x_p-matching magnets. The matching magnets are so positioned that the free drift lengths on either side of the crossing point are as long as is practical. The parameters are given in Table III-1 and the insertion is shown in Fig. III-1.

When desired, the six low-β_y matching quadrupoles QFE1 to QDE6 can be adjusted to give high β_y values at the crossing point. This will result in small beam divergence at this point, which is required by certain classes of experiments.

(5) Injection (I) Insertion

The injection insertion has overall dimensions similar to those of the experimental insertion. But, in this case it is desirable to have large x_p and β_x in the middle of the insertion, as well as the longest practical free drift lengths. Also, for this insertion the beam properties at the crossing point are of no special importance. To simplify matters, we have adopted a symmetric insertion design having reflection symmetry about the midpoint. The I insertion is between mid-points of normal cell quadrupoles QD. The high-x_p matching is accomplished by one quadrupole QDI and four bending magnets

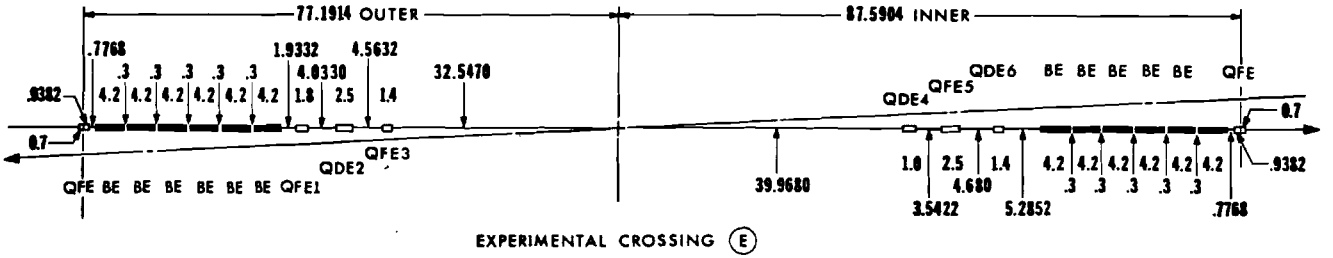

EXPERIMENTAL CROSSING (E)

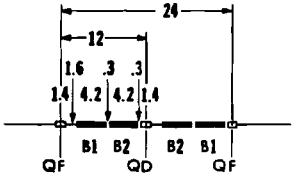

NORMAL CELL

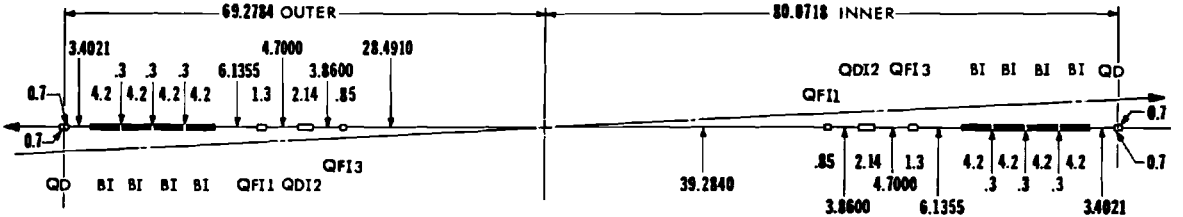

INJECTION CROSSING (I)

Figure III-1 Storage Ring Lattice Showing a Normal Cell, An Experimental Insertion and an Injection Insertion

BI at each end of the insertion. The β matching is again obtained by three quadrupoles QDI1, QFI2 and QDI3, at each end inboard of the x_p matching magnets. The insertion is shown in Fig. III-1 and the geometrical and orbit parameters are given in Table III-1.

Two of these insertions 120° apart are used for injection and beam dumping. The third one is reserved for future development into an experimental area. Because of the large values of x_p and β_x and the shorter downstream drift spaces, this crossing is thought to be less useful for doing experiments than the E insertions, but could be developed into an experimental area as occasion might demand.

Fig. III-2 shows a sextant of the storage ring with 16 normal cells and one each of E and I insertions. Fig. III-3 shows the complete storage ring together with the injection beam transport lines. Fig. III-4 are plots of the orbit functions β_x, β_y, and x_p.

(B) Aperture Requirements

The beam properties at injection into the storage ring based on the accelerator performance given in the NAL Design Report are

$$E_{xi} = 0.92\pi \text{ mm-mrad}$$

$$E_{yi} = 0.36\pi \text{ mm-mrad}$$

$$(\Delta p/p)_i = \pm 0.41 \times 10^{-4} \text{ debunched}$$

where a factor of two dilution in betatron phase space during

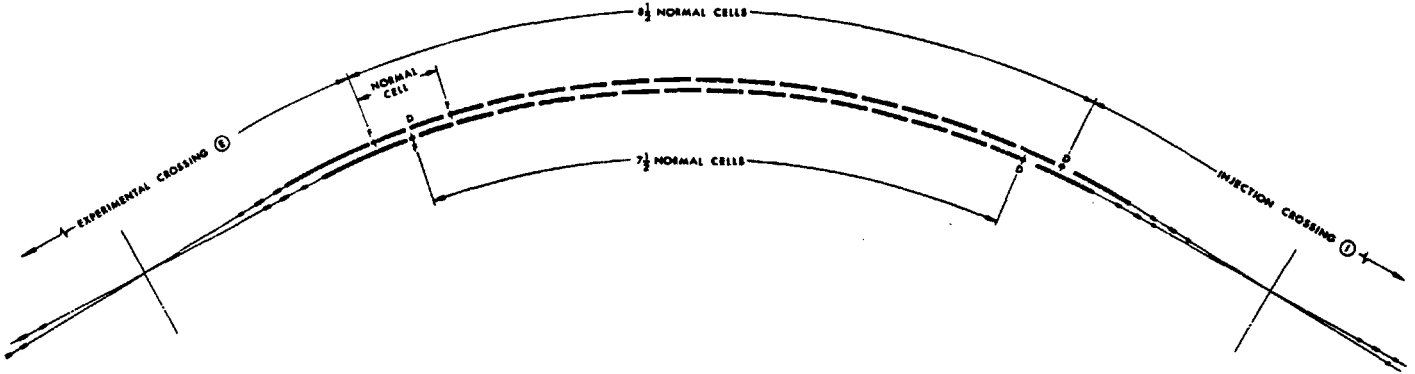

Figure III-2 A Sextant of the Storage Ring Lattice

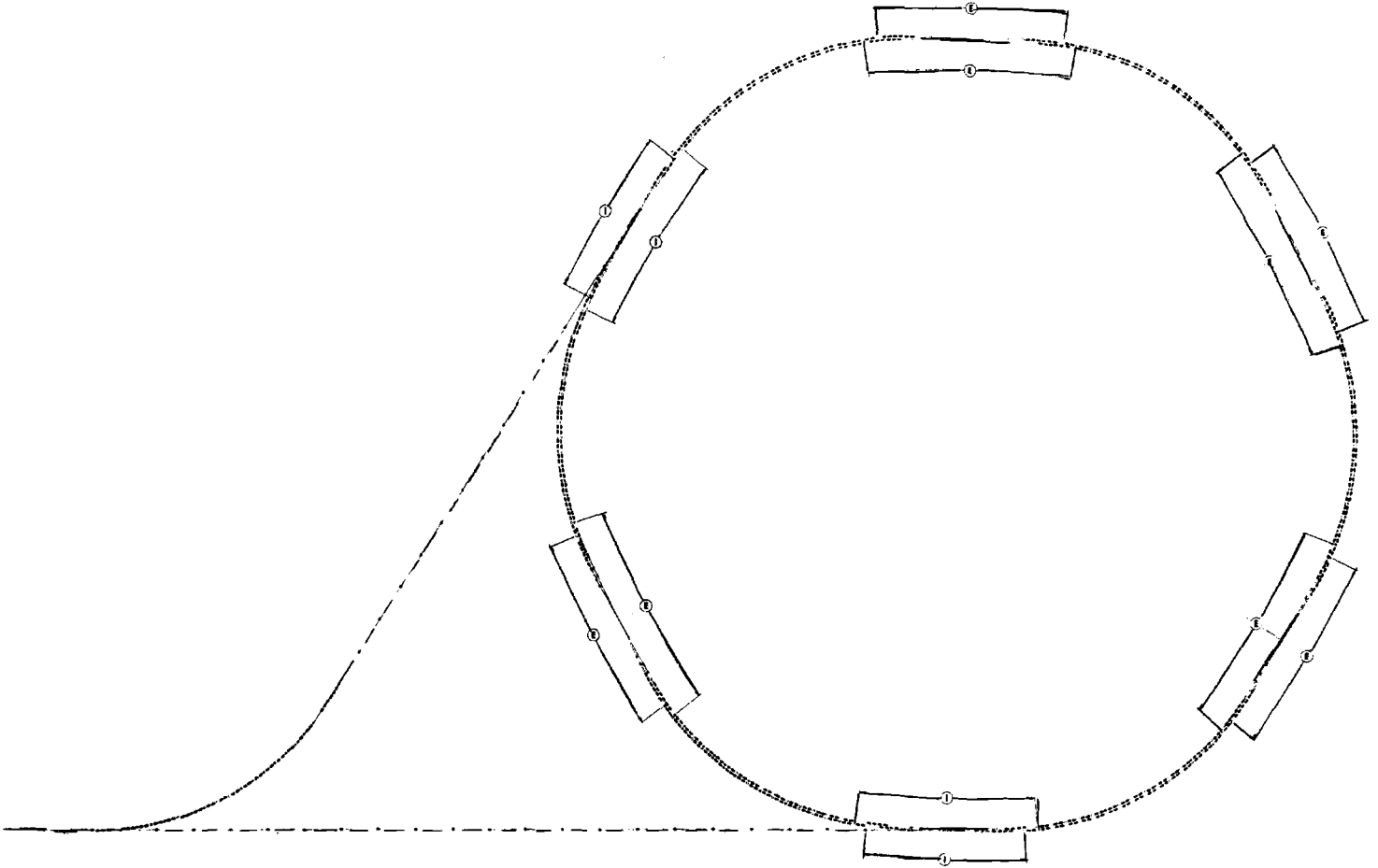

Figure III-3 Layout of Storage Ring and Injection Beam Transport Lines

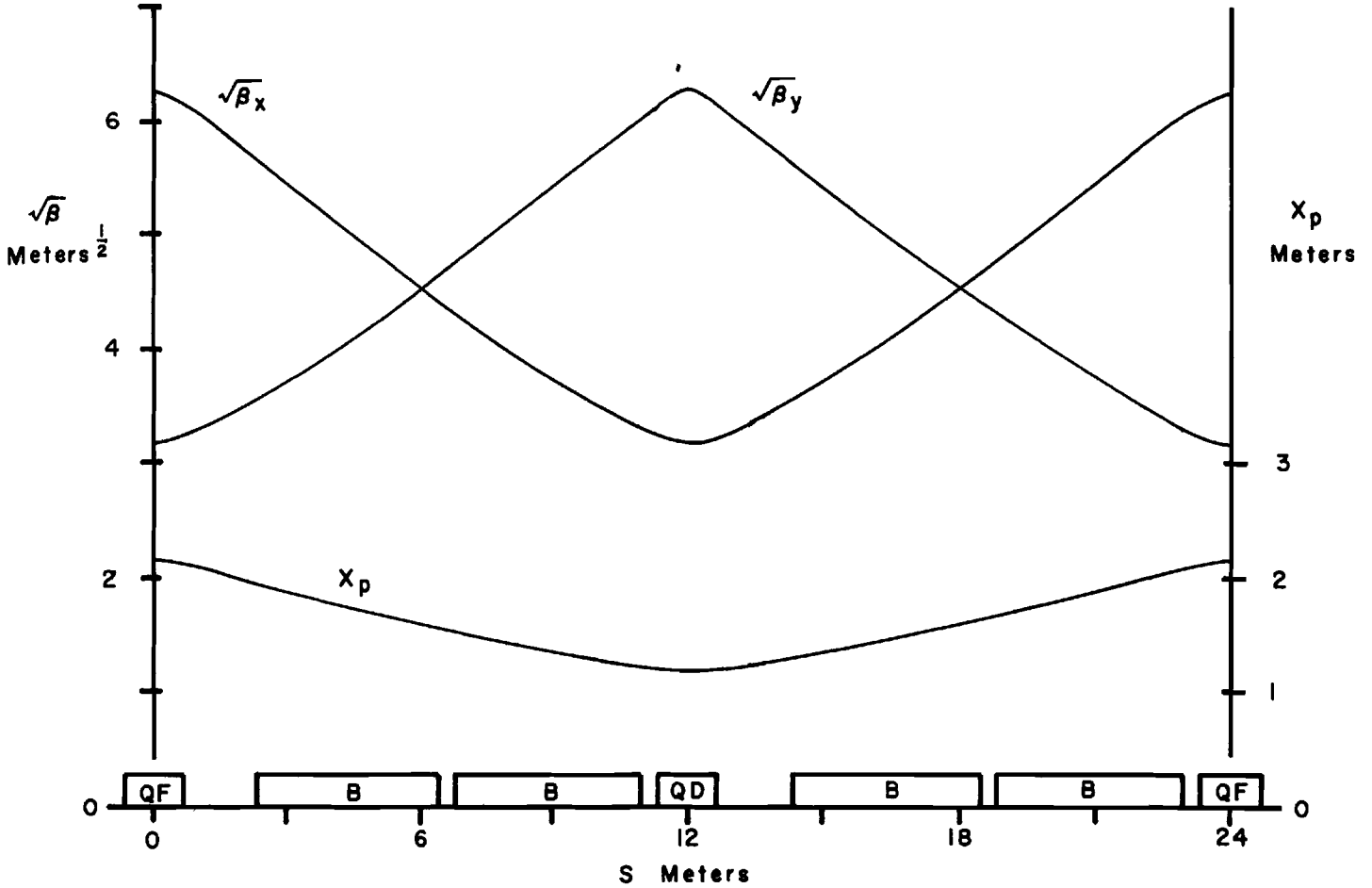

Figure III-4A Orbit Functions in Normal Cell

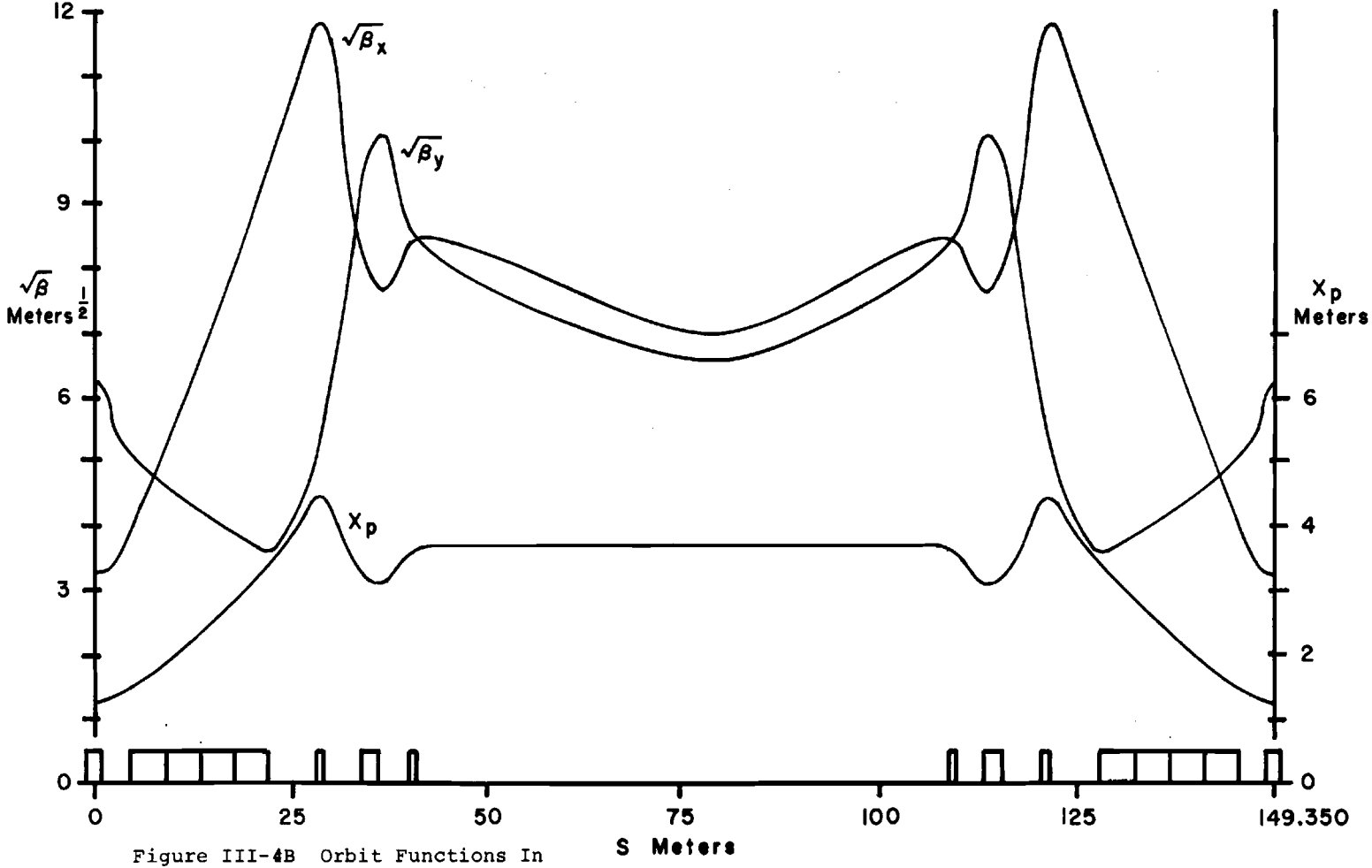

Figure III-4B Orbit Functions In Injection Insertion

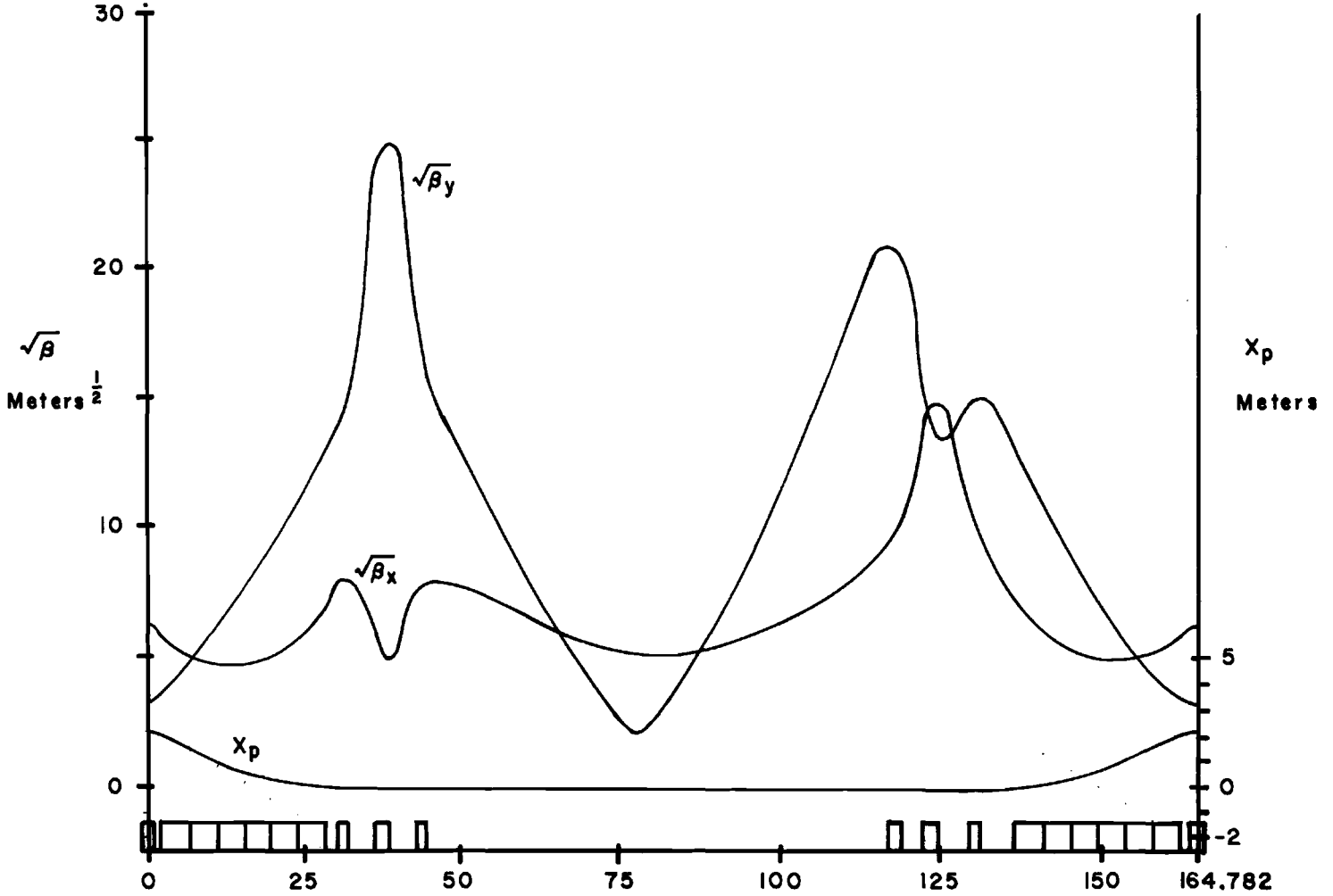

Figure III-4C Orbit Functions in Experimental Insertion

transfer from the accelerator main ring to the storage ring, and a total dilution factor of eight in synchrotron phase space during the complete accelerator cycle have been included.

Each pulse of the main ring is injected into the storage ring as three turns. These three turns are stacked in horizontal betatron phase space. With a 2 mm injection magnet septum thickness, one finds that the area of the phase ellipse enclosing all three turns is 6.25 times that of a single turn. The injected beam in the storage ring, therefore, has E_x = 5.7π mm-mrad, and $E_y = 0.36\pi$ mm-mrad.

Twenty main-ring pulses are to be injected and stacked in synchrotron phase space. Assuming reasonable stacking efficiency, the resultant momentum spread of the stacked beam will be about $\Delta p/p = \pm 10^{-3}$.

(1) Horizontal Aperture

Horizontal aperture is required for:

(a) Betatron width of stacked beam = $2\sqrt{\beta_x E_x/\pi}$

(b) Momentum width of stacked beam = $2x_p(\Delta p/p)$

(c) The stacked beam must be separated in momentum from the injected beam so that it will clear the septum when the kickers are turned on. The required spatial separation at the septum is approximately $\sqrt{\beta_{xs} E_x/\pi} \equiv A_{xs}$. At an arbitrary point in the lattice, the corresponding separation = $\dfrac{x_p/\sqrt{\beta_x}}{x_{ps}/\sqrt{\beta_{xs}}} A_{xs}$.

(d) Closed orbit deviation at 70% confidence level corresponding to assumed errors

$\left(\frac{\Delta B}{B}\right)_{rms} = \left(\frac{\Delta L}{L}\right)_{rms} = 5 \times 10^{-4}$ for bending magnets, and

$(\Delta x)_{rms} = 10^{-4}$m for quadrupoles, is $2.92\sqrt{\beta_x (\text{in m})}$ mm.

The resulting full horizontal aperture required for the normal cell magnets, the septum position S, and the experimental crossing point E are

QF	B1	B2	QD	S	E
64.3 mm	65.2 mm	54.4 mm	40.0 mm	87.1 mm	39.5 mm

(2) Vertical Aperture

Vertical aperture must provide for the following:

(a) Betatron height = $2\sqrt{\beta_y E_y/\pi}$

(b) Closed orbit deviation corresponding to: $(\Delta\theta)_{rms}$ = 5×10^{-4} rad for bending magnets, and $(\Delta y)_{rms} = 10^{-4}$m for quadrupoles, is $2.92\sqrt{\beta_y \text{ (in m)}}$ mm.

This gives the following required full vertical aperture:

QF	B1	B2	QD	S	E
13.4 mm	19.3 mm	25.0 mm	25.8 mm	32.5 mm	8.2 mm

From this consideration the good field apertures for B1 and B2 should, therefore, be 0.76 in. x 2.57 in. and 0.98 in. x 2.14 in. respectively. But as we shall see later these vertical apertures give a rather tight space charge limit for the design intensity of 10^{15} protons. To arrive at a design where the aperture is better matched to the eventual space charge limited beam after all closed orbit errors are corrected we should increase the vertical aperture and reduce the horizontal aperture as given by this calculation. We have, therefore, chosen an aperture of 1.0 in x 2.5 in. for B1 and an aperture of 1.25 in. x 2.0 in. for B2.

(3) Special Magnets

The bending magnets and quadrupoles in the E and I insertions require larger apertures than do those in the normal cells. The aperture requirements for these magnets are as follows:

	QFE	BE	QDE	QFI	BI	QDI
Full width (mm)	115.4	73.9	47.3	111.5	99.2	78.6
Full height (mm)	63.5	56.8	107.8	25.1	21.1	43.4

(C) Space Charge Limits

It is planned to inject 20 main ring pulses of 5×10^{13} protons each into each storage ring. The stacked beam in each ring will, therefore, contain 10^{15} protons. We consider, now, the various space charge effects

(1) Beam-Beam Interaction

Computations indicate that instability occurs if the change in ν of one beam due to its interaction with the other exceeds a threshold of approximately 0.05 to 0.10 per intersection region. This shift is given by[5]:

$$\Delta\nu = \frac{N\, r_p \beta_y}{2\pi R \alpha \gamma b}$$

where

N = number of protons per ring = 10^{15}

r_p = classical proton radius = 1.53×10^{-18} m

R = ring radius = 333 m

β_y = vertical β at crossing point = 4 m

α = crossing angle = 0.05 rad

γ = 107.6

b = beam half height at crossing point = 1.2 mm.

These numbers lead to $\Delta\nu = 4 \times 10^{-4}$, which is negligible.

(2) Incoherent Single Beam Limit

In this case, the image forces dominate and lead to the ν-shift[6]

$$\Delta\nu = \frac{Nr_p R}{\pi\gamma\nu h^2} \left(\varepsilon_1 + \frac{h^2}{g^2}\varepsilon_2\right)$$

With image coefficients $\varepsilon_1 = 0.16$, ε_2 = negligible and h = average half vertical aperture = 1.3 cm, we get $\Delta\nu = 0.25$ for $N = 2.5 \times 10^{15}$ which is comfortably above the design intensity of 10^{15}.

(3) Resistive wall instability

The threshold for this instability leads to a lower space-charge limited intensity. But it has been demonstrated on many accelerators that coherent oscillations of the beam can be damped out by the use of electronic feed-back circuits.

From the above three results it is reasonable to expect that at least 20 main ring pulses can be stacked stably in each storage ring to give a beam of 10^{15} protons or a current of about 23A. It is likely that after all closed-orbit errors are corrected, a factor of two increase in intensity can be realized.

(D) Luminosity

The interaction rate at each crossing point is σL $\sec^{-1}$, where σ is the interaction cross-section and L is the luminosity. The luminosity is related to the beam characteristics by[7]

$$L = \frac{c}{\alpha b}\left(\frac{N}{2\pi R}\right)^2 .$$

For the present design, we get $L = 1.14 \times 10^{32}$ cm^{-2} sec^{-1} at each of the three E-crossings.

At the I crossing reserved for experimental use, the minimum beam half height would be 0.38 cm, corresponding to a luminosity of 0.36×10^{32} cm^{-2} sec^{-1}.

References

1 A. A. Garren, Storage Ring Study, NAL Report TM-2, August 15, 1968.

2 A. A. Garren and J. L. MacLachlan, Modification of the Lattice of the Colliding Beam Storage Ring for the National Accelerator Laboratory, NAL Report TM-103, December, 1968.

3 A. van Steenbergen, Injection Criteria Storage Ring, NAL Report FN-171, August 28, 1968.

4 L. C. Teng, FODO Lattice for Storage Ring, NAL Report TM-55, September 20, 1968.

5 E. Keil and A. M. Sessler, Performance Capabilities of Proton Storage Rings, CERN Report ISR-TH/67-37, July 21, 1967.

6 L. J. Laslett, On Intensity Limitations Imposed by Transverse Space Charge Effects in Circular Particle Accelerators, Brookhaven National Laboratory Report, BNL-7534, p. 324, July 19, 1963.

7 A. Schoch, CERN Studies on Proton Storage Rings, Proceedings of the 1963 Summer Study on Storage Rings, Accelerators and Experimentation at Super-High Energies, BNL-7534, p. 128, 1963.

IV. MAGNET SYSTEM

For the magnet system, the design using conventional iron-copper magnets was worked out in the greatest detail, although the designs of iron-yoke magnets with Nb-Ti superconducting coils and cryogenically cooled Al coils were also studied. The top field for all 3 types of magnets is taken to be 20 kG. A storage ring using high field air-core magnets with superconducting coils will be discussed in Appendix A, since the consequences of higher fields give rise to larger perturbations in the system design than those due to the use of superconducting or cryogenic coils in an iron magnet.

Figure III-2 shows the disposition of bending and focusing magnets in a sextant of the twin ring separated function lattice. In each sextant, there are 84 bending magnets of two distinct types differing in aperture requirements, 42 of each type. There are also 34 regular quadrupole magnets, and 12 special matching quadrupoles.

(A) Conventional Magnets

(1) General Description

Each bending magnet block consists of a top and bottom slab 4.2 m long. The sides consist of four slabs each 2.1 m long pinned and bolted to the top and bottom slabs such that the angle

required for minimum effect from sagitta is maintained between the two 2.1 m sections of the magnet. The poles consist of forgings shaped to produce the desired field characteristics, pinned and bolted to the top and bottom slabs again with an angle between the two magnet sections to reduce the effects of sagitta on the required aperture to a minimum. Azimuthal field shaping and transition blocks are bolted to the ends of the poles such that the total length of each pole including these blocks is about 2.1 m.

Excitation of the 4.2 m long magnet block is accomplished by surrounding both poles on the top side by a single coil bent up by 25° at the ends and on the bottom side by a similar coil bent down by 25° at the ends. The coils are wound using 40 turns for the B_1 magnet and 50 turns for the B_2 magnet each of 3/4 in. square hollow copper conductor with a 3/8 in. diameter hole. The space allowed in the coil window for insulation and positioning errors is about 3/8 in. horizontally by 5/8 in. vertically.

The quadrupoles are made in four quadrants from forgings each containing a shaped pole and a coil surrounding the pole. As with the bending magnets, longitudinal field shaping at the entrance and exit of each quadrupole must be obtained by using properly shaped end plates.

One bending magnet block and one quadrupole are mounted on two channel iron supports to provide a focusing-bending unit which is to be positioned in the ring. Details of the bending magnets

and quadrupole magnet are shown in Fig. IV-1.

Power and cooling water are fed to the coils by bus bars and manifolds mounted on the top and bottom of each magnet block.

Magnet power will be distributed around the accelerator enclosure as shown schematically in Fig. IV-2. The bending magnets are supplied from two 34.5 kV transformers from the mains. Twenty-four silicon controlled rectifiers supply the current required by the bending magnets of both rings, each ring being provided with twelve symmetrically located rectifiers delivering a current of 1169 A regulated to within .01%.

The quadrupoles are supplied with power independently of the bending magnets through a single 13.8 kV transformer from the mains. Six silicon controlled rectifiers provide the 258 A required by the quadrupoles, each ring being supplied by three symmetrically located rectifiers regulated to .01%.

The special matching quadrupoles, of which there are twelve per sextant of the ring, will each be provided with silicon controlled rectifiers independently.

(2) Magnet Block Design and Fabrication

The bending and focusing magnets are made from commercial SAE-1010 steel forged to assure optimum mechanical and magnetic properties. The surfaces of the upper, lower, and side yokes are flat and lend themselves to routine production and machining. The pole pieces, on the other hand, should be shaped in such a way as to provide the maximum width of uniform field. This will be

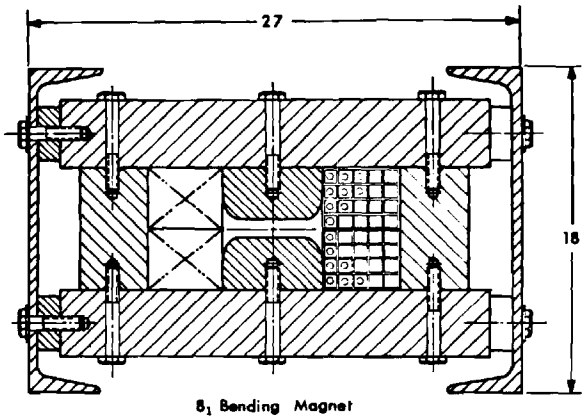

B_1 Bending Magnet

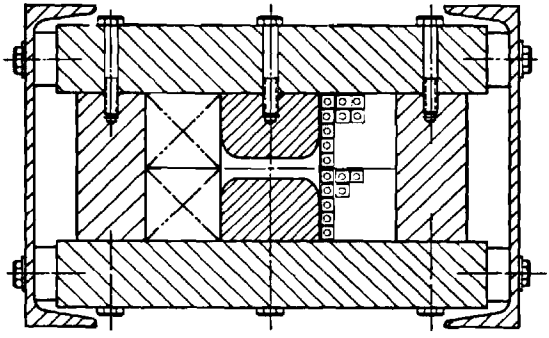

B_2 Bending Magnet

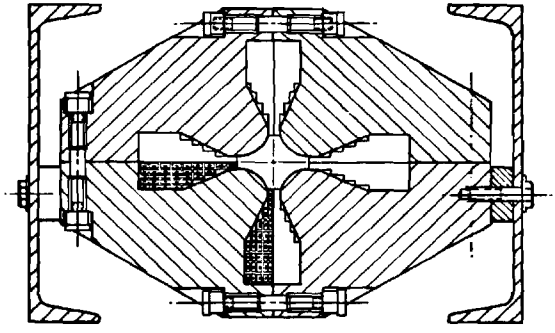

Quadrupole Magnet

Figure IV-1. Cross Sections of Bending and Quadrupole Magnets

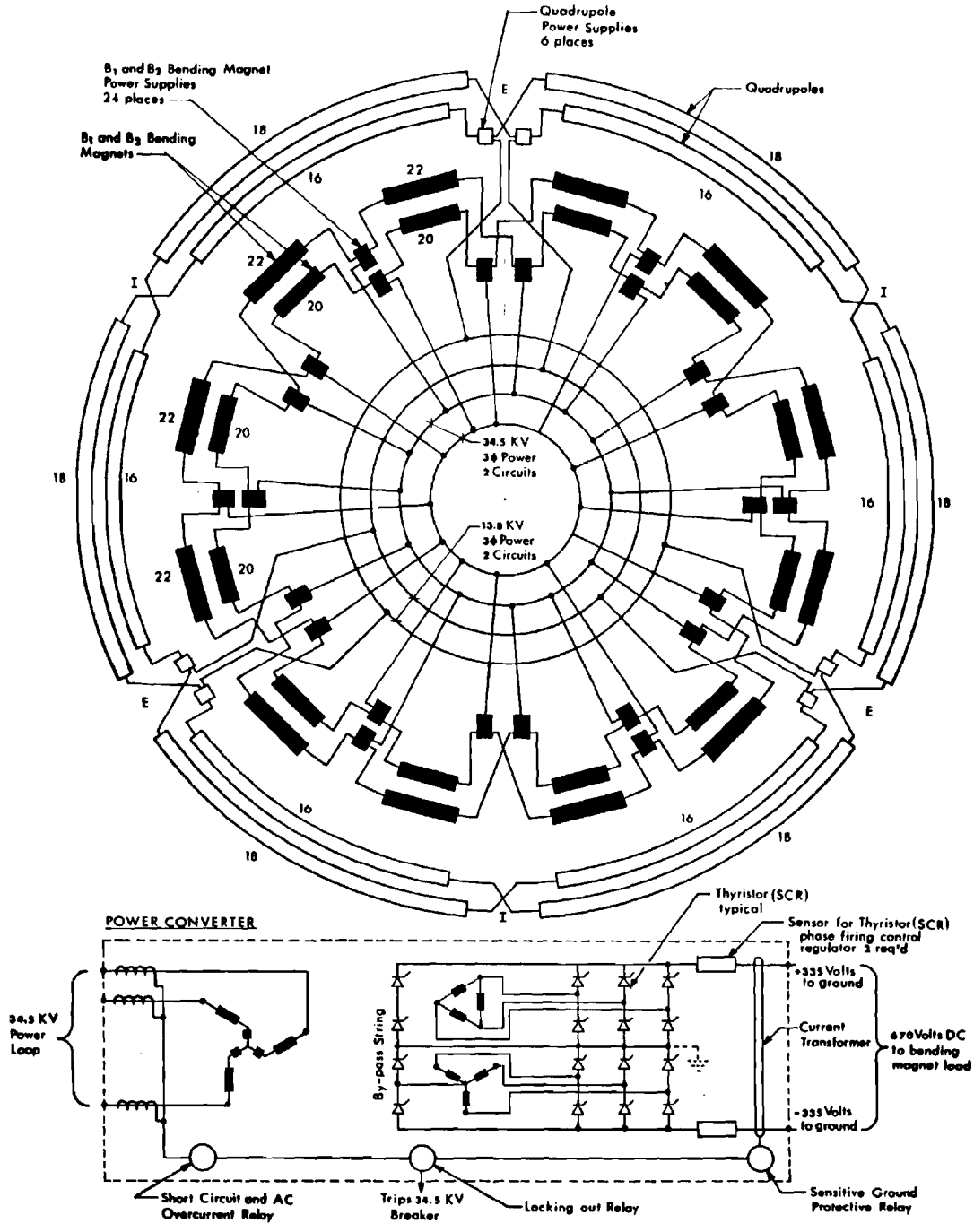

Figure VI-2. Magnet Power Distributions

accomplished either with a shaper or through the use of tape controlled milling. In addition, control of the flux distribution within the iron will be needed to permit an adjustment of the magnetic field over a range corresponding to 28 BeV to 100 BeV particle energy. This will be accomplished through the use of subsurface voids whose size and location will be determined with the aid of magnetostatic computer programs and modeling.

The quadrupole focusing magnets will be fabricated from forgings of commercial SAE-1010 steel. Pole contours will be formed using a shaper.

Table IV-1 lists the important magnet parameters.

(3) Coil Design and Fabrication

The windings on the bending magnets use water cooled, hollow, copper conductors of square cross section 3/4 in. by 3/4 in. outside dimensions with a 3/8 in. diameter hole. Turns, layers, and coils will be wrapped with glass tape and potted with a radiation resistant epoxy resin for insulation. The insulation will consist of a double wrap of .010 in. glass tape on each turn with a .010 in. spacer between turns, and a single wrap of .010 in. glass tape on each layer with a .20 in. spacer between layers. The coils will be provided with a single .010 in. wrap and potted to specified outside dimensions in radiation resistant epoxy. The coils will then be secured in place with the magnet assembly bolts after appropriate spacers are inserted.

Table IV-1. Storage Ring Magnet Parameters

	B1	B2	Q
Magnet Length (m)	2 x 2.1	2 x 2.1	1.4
B_o, magnet center, (kG)	20.0	20.0	-
B'_Q (kG/m)	±.15	±.15	248.5
Magnet Gap (in)	1.00	1.25	1.30
Good Field Width (in)	2.50	2.00	2.80
Coil Turns	40	50	31/pole
Conductor Current (A)	1169	1169	258
Power (kW)	32.2	41.6	6.04
Inductance (H)	0.042	0.053	-
Cooling Water Press. Drop (psi)	100.	100.	-
No. Water Paths/Coil	4	5	-
Water Temp. Rise (^oC)	14.	14.	15.
Magnet Iron Weight (lbs)	11200	12000	5700
Copper Coil Weight (lbs)	2200	2700	530

The windings on the quadrupoles use water cooled, hollow, copper conductors of rectangular cross section 0.560 in. by 0.280 in. outside dimensions, with a 0.200 in. diameter hole. The insulation is similar to that of the bending magnet coils in that turns, layers, and coils will be wrapped with glass tape and potted with a radiation resistant epoxy.

Table IV-2 gives the design parameters of the coils. Approximately 16% excess amp-turns over the air gap excitation is included to account for saturation in the iron. A temperature rise of about 15° C is allowed in estimating the cooling water requirements.

Table IV-2. Coil Weight, Power, and Cooling (two rings)

	Coil Weight (Ton)	Power (kW)	Cooling Water Flow (gal/min)
Bending (B1+BI)	255	7900	2000
Bending (B2+BE)	430	13300	3300
Focusing (regular)	53	1200	300
Focusing (matching)	136	3000	750
Total	874	25400	6350

(B) Iron Magnet with Superconducting Coil

In view of the reasonably long lead time for the project, we have looked into some less conventional types of magnet design that may lead to overall cost savings. One such design is to

utilize superconducting coils[1]. This will greatly reduce the cross-sectional area of the coil and hence, the cross-sectional area of the whole magnet. Fig. IV-3 shows a conceptual design of an iron core magnet for which the required field of 20 kG is obtained using a Nb - Ti superconducting coil cooled to 4.2° K by liquid helium and carrying 20000 A/cm^2. Magnetostatic computer programs such as TRIM indicate the possibility of obtaining the necessary width of good field with the overall dimensions as shown. Slight shaping of the pole face is sufficient to cancel the effects of saturation in the iron and of the absence of current between the poles above and below the coil.

The construction envisaged makes use of an inner vacuum envelope of stainless steel into which is placed the cryosorption pump elements. The liquid helium cooling channels and the superconducting coil are placed external to, but in intimate thermal contact with, the vacuum chamber. Stainless steel straps around both the superconducting coil sides, the liquid helium channels, and the vacuum chamber serve to provide an integral structural unit capable of withstanding the outward magnetic forces on the coil sides.

The coil-coolant-chamber unit maintained at 4.2° K is centered within the room temperature iron yoke window by low thermal conductivity supports leaving a 1/4 in. insulation space all around. The insulation space is filled with many layers of

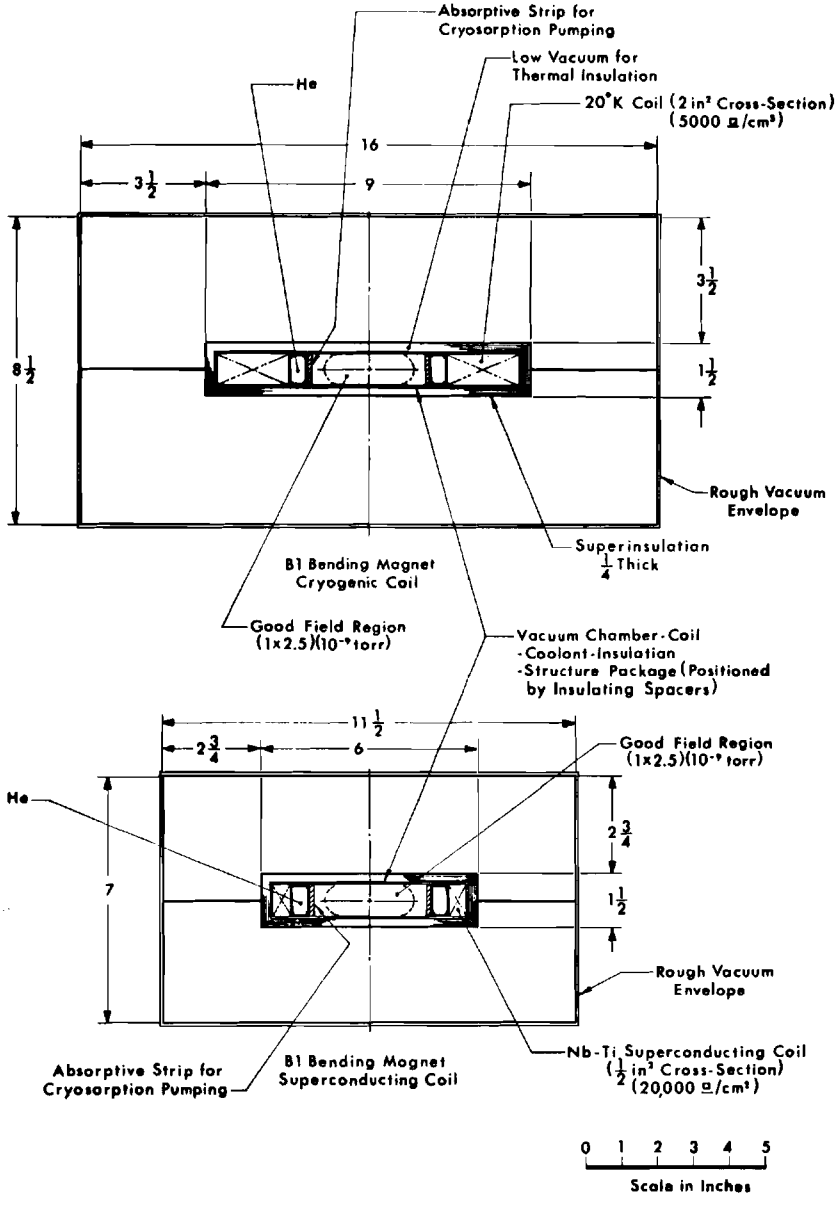

Figure IV-3. Top: Cross-Section of Bending Magnet with Iron Yoke and Cryogenically Cooled Aluminum Coils

Bottom: Cross-Section of Bending Magnet with Iron Yoke and Superconducting Niobium-Titanium Coils.

high reflectivity thin aluminized mylar sheet (superinsulation) to reduce conduction by radiation and is evacuated to about 10^{-5} torr using stainless steel sheet over the magnet yoke as an outer vacuum box.

The excitation current which may be of the order of 1000 A, depending on the number of turns, is brought in and out of the cryogenic enclosure through thermal stacks, and the connections between magnets will be superconducting joints inside an uninterrupted cryogenic enclosure leading from one magnet to the next. Table IV-3 gives the approximate refrigeration requirements for both rings.

Table IV-3. Liquid Helium Refrigeration Load at 4.2°K for Storage Ring with Superconducting Coil Iron Magnets

Radiation (magnet yoke to inner vacuum chamber including transfer lines and expansion loops)	2.20 kW
Conduction through supports	0.36
Heat loss in conductor joines	0.60
Beam power loss @ 0.1 W/m	0.42
Electrical feed throughs (thermal stack)	0.24
Circulating pump power	1.00
Cool down, standby, two transfer lines	3.00
Total Refrigerator Capacity Required	7.82 kW

The power supply is very modest. A few kilowatts of power regulated to within .01% is all that is required. A simple

silicon controlled rectifier system with transistor regulation will meet the demands adequately.

Some amount of development work is necessary to make this type of magnet practical, but there is no doubt as to its technological feasibility.

(C) Iron Magnet with Cryogenically Cooled Aluminum Coil

Another possibility that permits an increase in the conductor current density is to use cryogenically cooled high purity aluminum conductors[2]. When cooled by gaseous helium to 16^{o}K, the resistivity of aluminum is reduced by a factor of about 1/5000, and a current density of about 5000 A/cm^2 in such a conductor becomes practical.

Figure IV-3 shows a conceptual design of a cryogenically cooled aluminum coil magnet. The design is identical to that of the superconducting coil iron magnet except now the coil cross-section is larger by a factor of 4, and the coolant is gaseous instead of liquid helium. Table IV-4 gives the approximate refrigeration requirements for both rings.

Table IV-4. Refrigeration Requirements for Storage Ring with Cryogenically Cooled Aluminum Coil Magnets

Radiation (magnet yoke to inner vacuum chamber including transfer lines and expansion loops)	3.30 kW
Conduction through supports	0.36
Power loss in aluminum coil	150.00
Heat loss in conductor joints	1.50

Beam power loss @ 0.1 W/m	0.42
Electrical feed throughs (thermal stack)	0.24
Circulating pump power loss	2.00
Cool down, standby, two transfer lines	20.00
Total Refrigerator Capacity Required	177.82

The power supply must provide a current of approximately 1000 A and a power of about 150 kW. Silicon controlled rectifiers with transistor regulation will maintain the current to .01%.

Similarly here, some development work on this type of magnet is needed, but there is no doubt as to its technological feasibility.

(D) Trimming Magnets

A trimming magnet package will be inserted in every 1.6 m straight section. Its function is to provide for correction of closed orbit errors, elimination of coupling between vertical and horizontal oscillations, and adjustment of the radial dependence of oscillation tunes. Figure IV-4 shows a schematic of the trimming magnet package. Table IV-5 lists the maximum adjustments possible with the trimming magnet package.

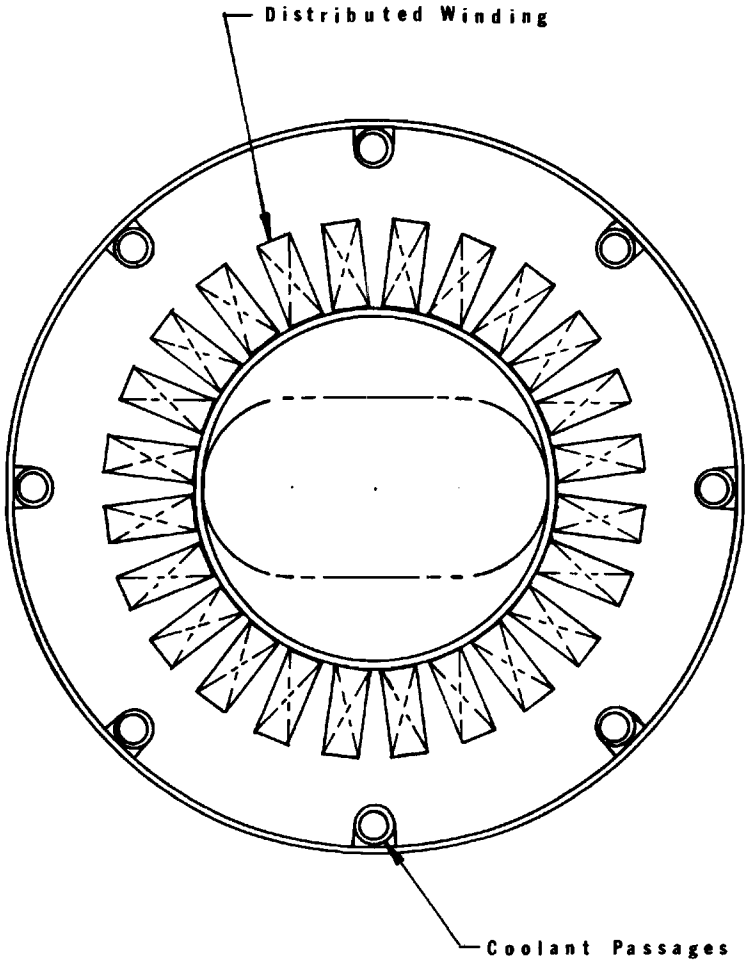

Figure IV-4. Cross-Section of Trimming Magnet Package

Table IV-5. Trimming Magnet Parameters

		Equiv. Curr. Sheet(A/in)
B	±0.6 kG	1213 Cos θ
B'	± 2.5 kG/m	253 Cos 2θ
B"	±700 kG/m^2	1769 Cos 3θ
Magnet Length	0.3 m	

The distribution of currents at an aperture diameter of 4 in. is given by the equivalent current sheet distribution and is to be approximated by currents distributed in the coil slots shown in Figure. IV-4. A construction employing stamped laminations is contemplated although no details have as yet been worked out.

References

1 R. R. Wilson, A Superferric Storage Ring, NAL Report FN-173, September 25, 1968.

2 G. T. Danby, J. E. Allinger, and J. W. Jackson, Synchrotron Magnets with Cryogenic Excitation Coils, Proceedings Summer Conference on Superconductivity, Brookhaven National Laboratory, August 6, 1968.

V. VACUUM SYSTEM

Special attention must be paid to the vacuum system to attain the very high vacuum required. High vacuum is needed to reduce scattering of the stored beams by residual gas atoms to an acceptably low level. In the first place, the radiation and radioactivity caused by particles scattered out of the beam must not be excessive. In the second place, gas scattering degrades the stored beam and limits its useful lifetime. An average pressure of 10^{-9} torr of N_2 over the entire beam is necessary to give a reasonable beam half-life. Furthermore, to keep the background radiation caused by residual gas in the experimental beam crossings down to a level acceptable for the performance of colliding beam experiments, we need a vacuum in the neighborhood of 10^{-11} torr.

(A) Vacuum Chamber

In storage rings using conventional magnets with copper coils, a separate vacuum chamber is required. During operation the vacuum chamber will be at room temperature. For designs in which cryogenic temperature coils are used, the vacuum chamber will be an integral part of the chamber-coil-coolant-insulation structure and will be at the same cryogenic temperature as the coolant and the coil. In either case, the chamber should be all metal in construction with only welded joints. The chamber material will be either stainless steel or titanium. In the separate room-temperature chamber a wall thickness of 0.05 in. is adequate to withstand atmospheric pressure.

Experience at SLAC[1] indicates that for stainless steel, when the surface has been chemically etched and prebaked at 400°C for 48 hours, an outgassing rate of $<10^{-12}$ torr liter/sec cm^2 can be obtained, and the residual gas is more than 99% hydrogen. If the surface is subsequently exposed to moist air, the same outgassing rate can be regained after about four days of pumping at room temperature. The duration of exposure to air has no significant effect on subsequent pumpdown behavior. For exposure to dry nitrogen, the pumpdown time required is reduced by about a factor of three. We have therefore assumed that the chamber will be chemically etched and vacuum baked at 400°C for more than 48 hours prior to installation. Care will be taken, thereafter, to handle the chamber only in dry nitrogen atmosphere. No bakeout in situ should be necessary after installation.

Because of the rather small aperture of the vacuum chamber the conductance along the length of the chamber is very limited. The conventional system of tying pumps onto the vacuum chamber at intervals along the length becomes extremely costly. It is therefore desirable that pump elements be installed directly inside the vacuum chamber.

(B) Linear Ion Pump

For conventional magnets with copper coils, sputter-ion pumping will be used. The pump elements will be mounted directly inside the vacuum chamber, using the field of the ring magnet for confining the discharge. This system has been tested at SLAC and used at Novosibirsk. Fig. V-1 shows a layout of the linear pump

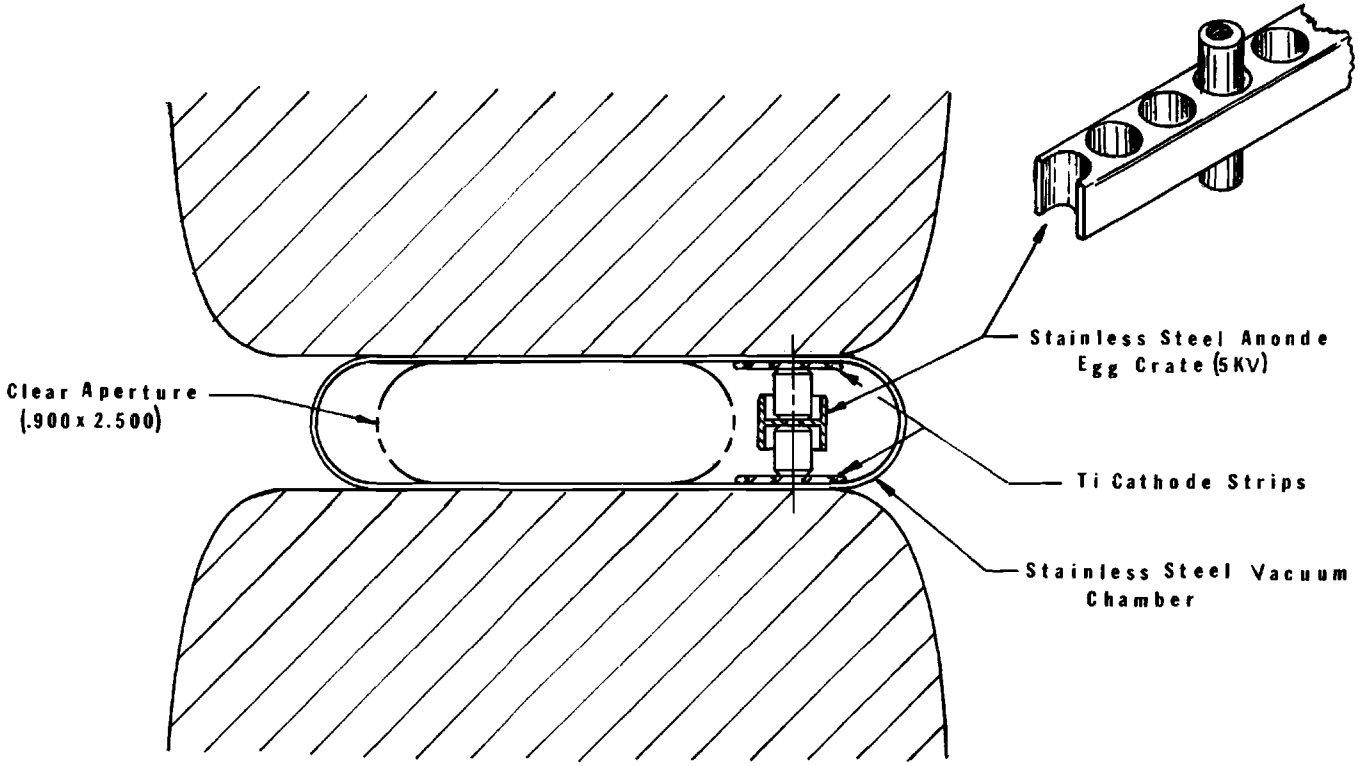

Figure V-1 Linear Ion Pump

elements inside the vacuum chamber. The pump element is mounted on either side in the chamber aperture, where a free space over 1 in. wide exists which is not useful for the beam because of excessively poor magnetic field quality. The grounded cold cathodes could be two long titanium strips attached to the top and the bottom of a stainless steel vacuum chamber or the chamber can be made of titanium, thereby providing automatically grounded titanium surfaces as cathodes. The anode, or "egg-crate", is made simply by drilling a row of $\frac{3}{8}$ in. diameter holes in a $\frac{1}{2}$ in. x $\frac{3}{8}$ in. cross-section stainless steel bar stock. The anode is supported by alumina insulators from the cathode strips and is connected to a 5 kV power supply. Since the storage ring will be operated over a range of proton energies, the magnetic field will range from perhaps 5 kG to 20 kG; the latter value is higher than that normally used for ion pumps, but should significantly improve the low pressure pumping characteristics.

Using the empirical formulas obtained by the Novosibirsk group[2] at a field of 20 kG, one gets a pumping speed for this system of about 3 ℓ/sec per cm length down to about 10^{-12} torr. This pumping speed is more than adequate to handle the approximately 0.03 ℓ/sec per cm length outgassing rate from the chamber wall at 10^{-9} torr. At this pressure, and pumping at a speed of 3 ℓ/sec per cm length, the ion current is only about 5 mA per ring[3]. The effect of the electric field on the particle beam due to the 5 kV anode voltage is negligible. This linear ion pump will be installed in all bending and quadrupole magnets.

In addition, at each 1.6 m straight section a conventional 100 ℓ/sec ion pump will be used because of the poor conductance of the chamber and to maintain a reasonable vacuum when the ring magnets are turned off.

Conventional titanium sublimation-getter pumps are used in the beam crossing insertions. These pumps work very well down to 10^{-12} torr and, at this pressure, should have essentially infinite life. It may be more efficient and economical to mount the titanium filaments of the getter pump directly inside the vacuum chamber and sublimate titanium onto the chamber wall for use as the getter surface. Development work is needed to study this possibility.

(C) Cryosorption Pump

For storage rings using either cryogenic aluminum coils at 16°K or superconducting Nb-Ti coils at 4.2°K, it is natural to use cryosorption pumping. With the vacuum chamber wall at a temperature of 16°K the vapor pressures of all materials are less than 10^{-11} torr, except H_2 and some inert gases. These gases can be pumped out by cryogenically cooled absorptive materials. These so-called cryosorption pumps have been developed and extensively studied recently[4,5,6]. The best absorbent developed so far is Molecular Sieve 5A - a class of synthetic zeolite. When bonded to a metal plate cryogenically cooled to 16°K this material gives an absorption pumping speed of about 2 ℓ/sec per cm^2 for H_2 and about 1 ℓ/sec per cm^2 for He. Thus such an absorbing strip 1 cm wide mounted on the side wall along the length of the vacuum chamber will provide more than

adequate pumping speed. The absorptive capacity of the strip is such that pumping at 10^{-9} torr pressure or lower, its useful lifetime is essentially infinite.

With this design it is natural and convenient to extend the cryosorption pumping to the beam crossing insertions. A pressure of 10^{-11} torr should be easily obtainable. The beam pipes are enclosed inside a jacket of cryogenic-coolant and vacuum-insulation. In an experimental insertion, the coolant jacket may have to be interrupted at the window where secondary particles emerge. The exact arrangement will depend on the requirement of specific experiments to be performed.

(D) Sector Valves

Sector valves will be installed at both ends of all beam crossing insertions to isolate the insertions from the regular lattice. The valves will be located at the ends of the central long drift spaces just inboard of the quadrupoles. Sector valves will also be installed in the injection transport lines to isolate them from the accelerator main ring and from the storage rings. These valves will be compressed air operated, non-magnetic, and all metal in construction.

In general the vacuum system in an experimental crossing will have to be constructed as an integral part of the experimental set-up. It is visualized that the complete experimental set-up, including a section of vacuum chamber and the associated pumping system, will be assembled and checked out in the assembly and test area. The entire unit will then be brought into the experimental hall to be mounted onto the storage ring replacing a

corresponding section of the storage ring vacuum chamber and the pumping system.

(E) Clearing Electrodes

Even at the average pressure of 10^{-9} torr a large number of electrons are produced from ionization of residual gas atoms by the beam. The negatively charged electrons are trapped in the positively charged proton beam and will totally neutralize the beam if allowed to remain. The effect of neutralization is to increase the betatron oscillation frequencies. Loss of beam will result when the betatron oscillation frequencies reach resonant values.

To clear the electrons out of the beam, a transverse electric field must be applied across the beam. This field will act on the electrons to overcome the attractive field of the beam. In the present design a modest voltage of ± 5 kV across the beam is adequate[7]. However, to apply this clearing field inside a magnet will take up valuable magnet gap space. Happily it can be shown[8] that inside a magnet the transverse magnetic field together with the electric field due to the beam causes the electrons to precess out of the magnet along the beam. The speed of motion compared to the production rate of the electrons is such that there will be no appreciable build up of electrons in the beam as long as they are cleared out of the beam immediately when they emerge from the ends of magnets. Therefore clearing electrodes are needed only immediately outside the ends of magnets.

A pair of electrodes will be mounted on stand-off insulators above and below the beam inside a widened section of the vacuum

chamber between magnet coil end cross-connections, as shown in Fig. V-2. The electrodes will be made of titanium and will have dimensions spanning the width of the vacuum chamber and extending 10 cm along the beam. For the design in which a linear ion pump is used, the + 5 kV voltage on one of the electrodes could be taken directly from the anode of the linear ion pump element. The polarities of these clearing electrodes will be alternated from pair to pair to reduce the effect of the electric field on the beam.

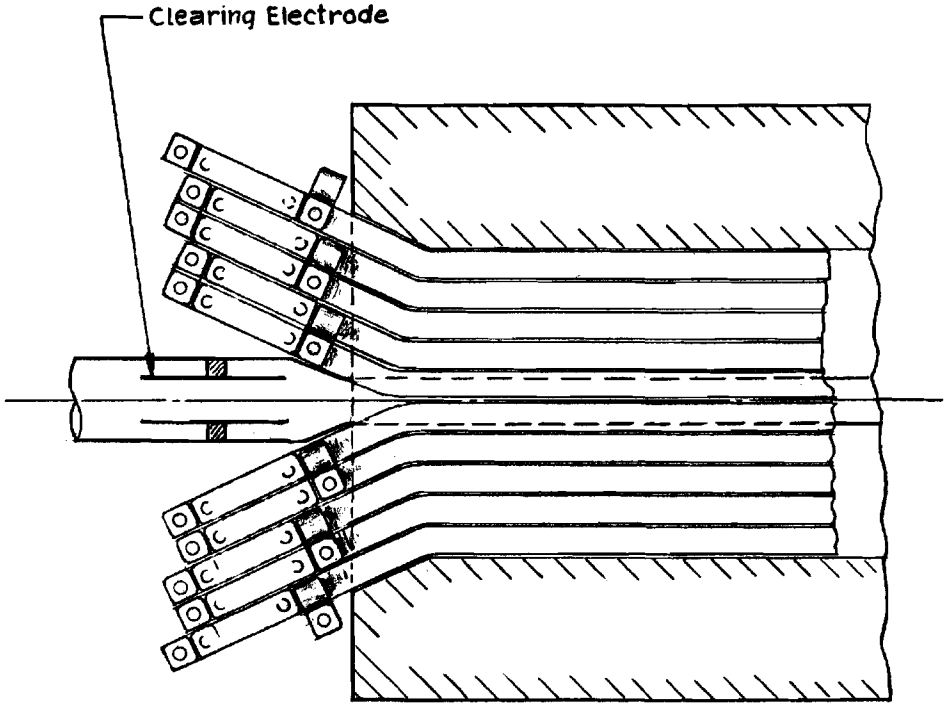

Figure V-2 Clearing Electrodes

References

1 Earl Hoyt, Effect of Surface Treatment and Baking on the Outgassing Characteristics of 304 Stainless Steel Pipe, SLAC-TN-64-5, January, 1964.

2 L. C. Teng, Empirical Formulas for Ion Pumping - Information Obtained from Nuclear Physics Institute, Novosibirsk, NAL Report TM-84, October 28, 1968.

3 S. L. Rutherford, Sputter-Ion Pumps for Low Pressure Operation, Varian Assoc. Report VR-27, January, 1964.

4 S. A. Stern, J. T. Mullhaupt, R. A. Hemstreet, and F. S. DiPaolo, Cryosorption Pumping of Hydrogen and Helium at 20^{o}K, J. of Vac. Sci. and Tech. 2, 165, 1965.

5 S. A. Stern, R. A. Hemstreet and D. M. Ruttenbur, Cryosorption Pumping of Hydrogen at 20^{o}K, J. of Vac. Sci. and Tech. 3, 99, 1966.

6 G. E. Grenier and S. A. Stern, Cryosorption Pumping of Helium at 4.2^{o}K, J. of Vac. Sci. and Tech. 3, 334, 1966.

7 E. Keil, B. W. Montague, Electric Field Required for De-Neutralizing the Stacked Beam in the NAL Storage Rings, NAL Report TM-25, September 3, 1968.

8 E. Fischer, Clearing Fields for the ISR, ISR-VAC/66-15, June 3, 1966.

VI. RADIOFREQUENCY SYSTEM

Beam stacking in the storage ring requires a maximum momentum reduction of about 1.2% for moving the injected beam from the outer radius of the vacuum chamber aperture into the beam stack at the inner radius. The rf system to provide this beam manipulation must meet the following requirements:

1) Beam-Cavity interaction must be controlled throughout the range of cavity voltage and in the presence of circulating beam current up to about 20 A.

2) Cavity voltage must be programmed during stacking to provide rf buckets which match bunch shape at capture and fit the bunches tightly at the moment of release in the stack.

3) The cavity voltage must be sufficient to decelerate the beam from the injection orbit to the stacking orbit in the time between main ring pulses. At peak voltage 10 kV and synchronous phase $\phi_s = 30^o$ it will take 1.7 sec to move the beam from the injection to the farthest stacking orbit.

Phase space matching of the accelerator main ring bunches to the shape of storage ring buckets will be carried out prior to beam transfer by adiabatic reduction of the rf voltage in the main ring. Since the transfer will be effected without debunching and rebunching, the rf frequency required in the storage ring is the same as that in the main ring. At 100 BeV the main ring rf is 53.10279 MHz (harmonic number $h_{MR} = 1113$). The orbit

frequency of the storage ring at 100 BeV and $\frac{1}{3}$ km radius is 143.1342 kHz, corresponding to harmonic number $h = \frac{1}{3} h_{MR} = 371$.

(A) RF Cavity

A single cavity should suffice to meet the requirements. The one shown in Figure VI-1 provides a low-impedance source of voltage to decelerate the injected beam into the beam stack. The perturbing effects on the cavity which must be considered in the design are the following:

(1) The injection transient - The bunched beam injected into the storage ring abruptly excites a component of rf cavity current not previously present. This current includes predominately a dc component, a component at the circulation frequency of 143 kHz, and a component at the fundamental rf frequency of 53.1 MHz. Each turn of beam from the 1 km radius main ring when injected (3 turns) into the 1/3 km radius storage ring produces a beam current envelope rising to 1.16 A in three successive steps of 386 mA each.

(2) Azimuthal charge density variations at the circulation frequency and harmonics - The 3-turn injected beam will in general have longer-period azimuthal charge density variations as well as missing bunches. These latter occur at predictable locations as a consequence of missing bunches in the main ring.

(3) Variations in real and reactive loading at the phase oscillation frequency ($\simeq$ 20 Hz).

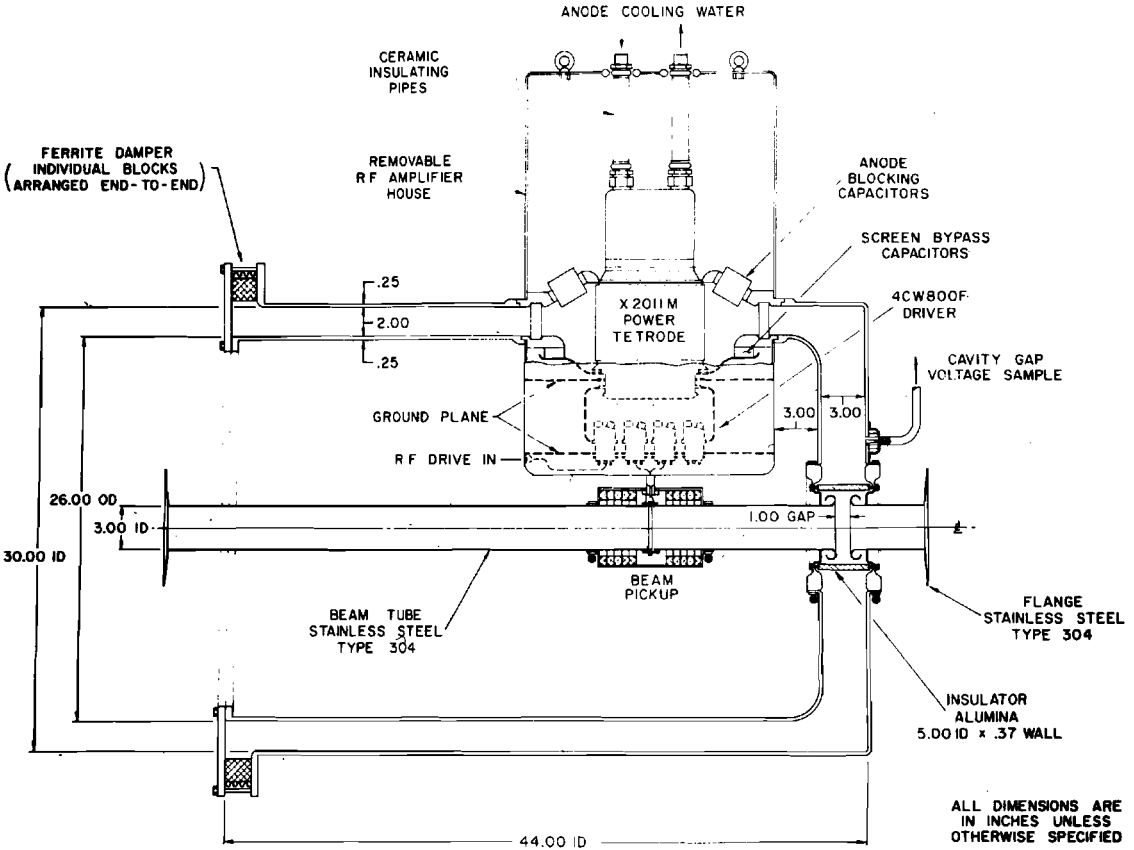

Figure VI-1 RF Cavity

The cavity is a coaxial line of 10 Ω characteristic impedance tuned to a quarter-wave resonance at 53.1 MHz. The design gap voltage is 10 kV peak. Ferrite damping blocks placed at the short-circuited end of the resonator provide strong absorption of rf energy and make the cavity gap appear to the beam as an ohmic resistance nearly equal to the characteristic impedance of the cavity at all harmonics of 53.1 MHz above the first. To achieve this frequency-selective coax termination it is necessary to choose a ferrite (such as Stackpole 12) having a steep falloff in Q with respect to frequency in the interval between 53.1 MHz and 106 MHz. Mechanically the cavity is designed to be constructed in two shells, removable without disturbing the vacuum.

(b) RF Supply and Control

The cascode rf power amplifier includes 6 parallel Eimac 4CW800F tetrodes dc coupled to a 100 kW tetrode X2011M. Transient beam loading is handled by a beam pickup signal which feeds a 50 W drive to three of the 4CW800F tetrodes. Electrically, the amplifier is connected to the point in the cavity line where the voltage is approximately 70% of the gap voltage. Mechanically, the amplifier is readily removable and replaceable as a unit.

Control of the cavity gap voltage is provided by a negative feedback loop, shown in Fig. VI-2. Long term differences between the cavity gap voltage and the reference voltage (standard rf signal) act to restore the cavity voltage to the programmed

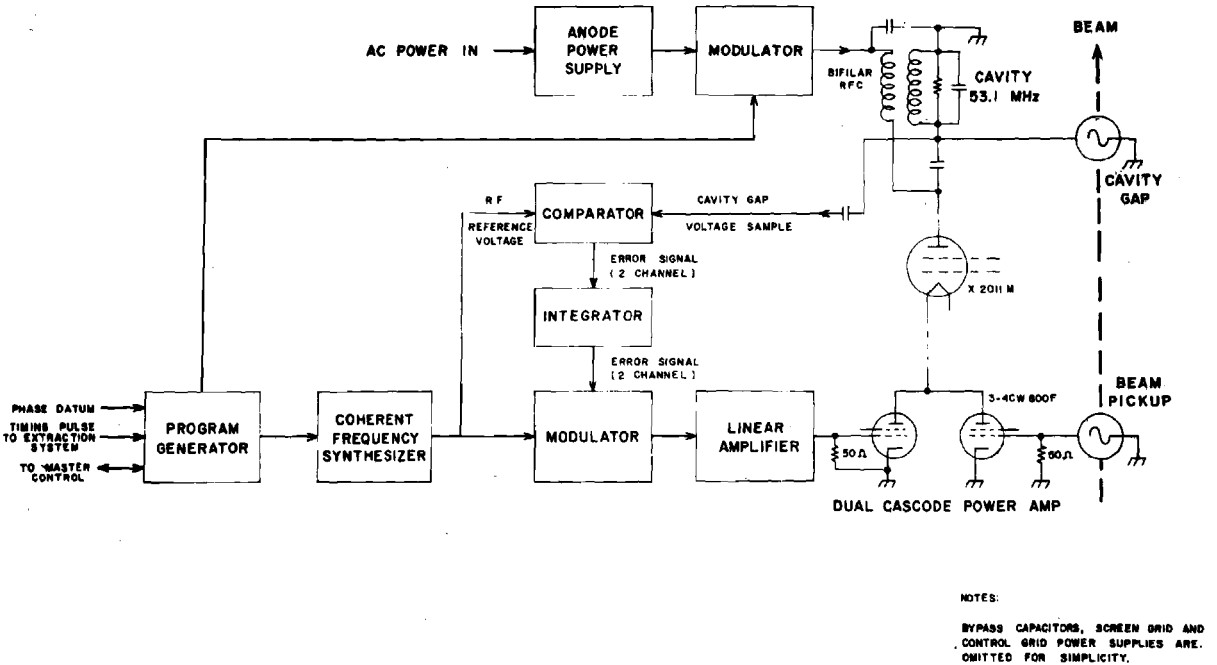

Figure VI-2 RF Power Supply and Controls

value. The integrators included in the feedback circuit increase the loop gain for decreasing disturbance frequency. The design value of stabilization factor, which is unity at 20 kHz, rises to 10^3 at 20 Hz, the synchrotron oscillation frequency.

Low-impedance design of the high-power portion of the rf system is not sufficient to guarantee the required rf voltage at the cavity gap. Accurate derivation of the low-level control signal is equally important. We plan to generate the control signal via a coherent frequency synthesizer. Prior to beam transfer, the synthesizer is phase-locked to the main ring rf. After injection into the storage ring, the synthesizer under stored program control increases the frequency to move the beam into the stack.

The maximum required $\frac{\Delta f}{f}$ for stacking is 7.5×10^{-5}, while the frequency spread in the beam stack due to momentum spread is about 4.4×10^{-5}. The precision of the final frequency at stacking should be a factor of 10 smaller, namely about 4×10^{-6}. The frequency synthesizer in connection with a program generator permits such a precise control of frequency and also of amplitude as required for maximum stacking efficiency. Furthermore, the choice of a software program control permits complete freedom in adjusting details of the stacking process such as time rate of momentum change and bucket area vs. frequency. A suitable integrated-circuit synthesizer will provide frequency increments of 0.01 Hz and frequency stability of 1 part in 10^9.

VII. INJECTION AND BEAM TRANSPORT

(A) Injection Beam Transport

The proton beam accelerated to 100 BeV in the main ring of the accelerator is extracted in one turn from the long straight section immediately downstream from the one for injection and external proton beam. The same fast horizontal extraction system as that described in Section 13 of the NAL Design Report will be used. Immediately following the last septum magnet of the extraction magnet chain a section of magnet elements is added which reduces the momentum dispersion of the beam to zero ($x_p = x'_p = 0$). This non-dispersive beam is then switched to either one of two branch lines which transports the beam to the injection point of either one of the two storage rings.

The transport lines have a simple and economical design. One of the branches is kept straight and the other bends about 60° away from the accelerator main ring. This geometry requires the minimum total amount of bending, leads to the shortest total transport length, and gives an adequate separation between the main ring and the storage ring. Only the separated function FODO lattices of the main ring and the storage ring are used in the design of the transport line lattice. This will simplify the design and will make it possible to use magnet elements identical to and interchangeable with those of the main ring and the storage ring.

For the straight branch, a short section of matching quadrupoles will match the optics of the non-dispersive beam to that of the regular lattice of the main ring. The beam is then transported by a succession of main ring normal cells with the bending magnets omitted. At a point near the injection crossing of the storage ring a section of optics matching quadrupoles and a section of dispersion matching magnets will prepare the beam with proper optical and dispersive properties for injection. The beam is then guided by a series of septum magnets to the injection point for horizontal injection into the storage ring from the outside.

The 60° bending branch of the transport lines uses a sextant of the storage ring lattice modified so that both ends are matched to zero dispersion as in the experimental insertion. The low-β_y matching quadrupoles at the front end are modified to match the optical properties of the beam from the main ring (after having been made non-dispersive) to those in the storage ring regular lattice; and the low-β_y quadrupoles at the tail end are modified to match the beam in the regular storage ring lattice to the regular main ring lattice. The, now, optically matched and again, non-dispersive beam will enter a straight lattice of main ring normal cells with bending magnets omitted. The remaining length of this branch is identical to that of the straight branch, and the beam is transported to the injection point for horizontal injection into the other storage ring. The layout of the beam transport lines as described above is shown in Fig. III-3. The total length of the transport lines

is about 5300 ft. Clearly, since the storage ring needs to be filled only once or twice a day and each filling takes only a few minutes, the injection transport line magnets only have to be energized during the few minutes of filling time per day.

(B) Injection Procedure

In the injection insertion of the storage ring, the beams travel outward. To avoid crossing of the injection line with the storage ring, it is necessary to bend the beam just before injection by an angle larger than the crossing angle of 50 mrad and to inject downstream of the crossing point. In the present design a total bending angle of 55 mrad is produced by a series of 8 dc septum magnets as shown in Fig. VII-1. Similar to the beam transport magnets these septum magnets need to be energized only during the few minutes a day when the storage rings are being filled. The injection point at the end of this chain of septum magnets is 21.2 m downstream of the crossing point. For the lattice design described in Section III, $\beta_x = 56$ m at the injection point. Assuming that the horizontal emittance of the injected beam is 0.916π mm-mrad, we get a beam half-width of $a = 7.16$ mm.

Conventional multi-turn injection scheme adapted to 3-turn injection is used[1]. In this scheme, the closed orbit is moved outward at the injection point to a position just inside the magnet septum by a pair of fast kicker magnets located approximately at 90° horizontal oscillation phase upstream and

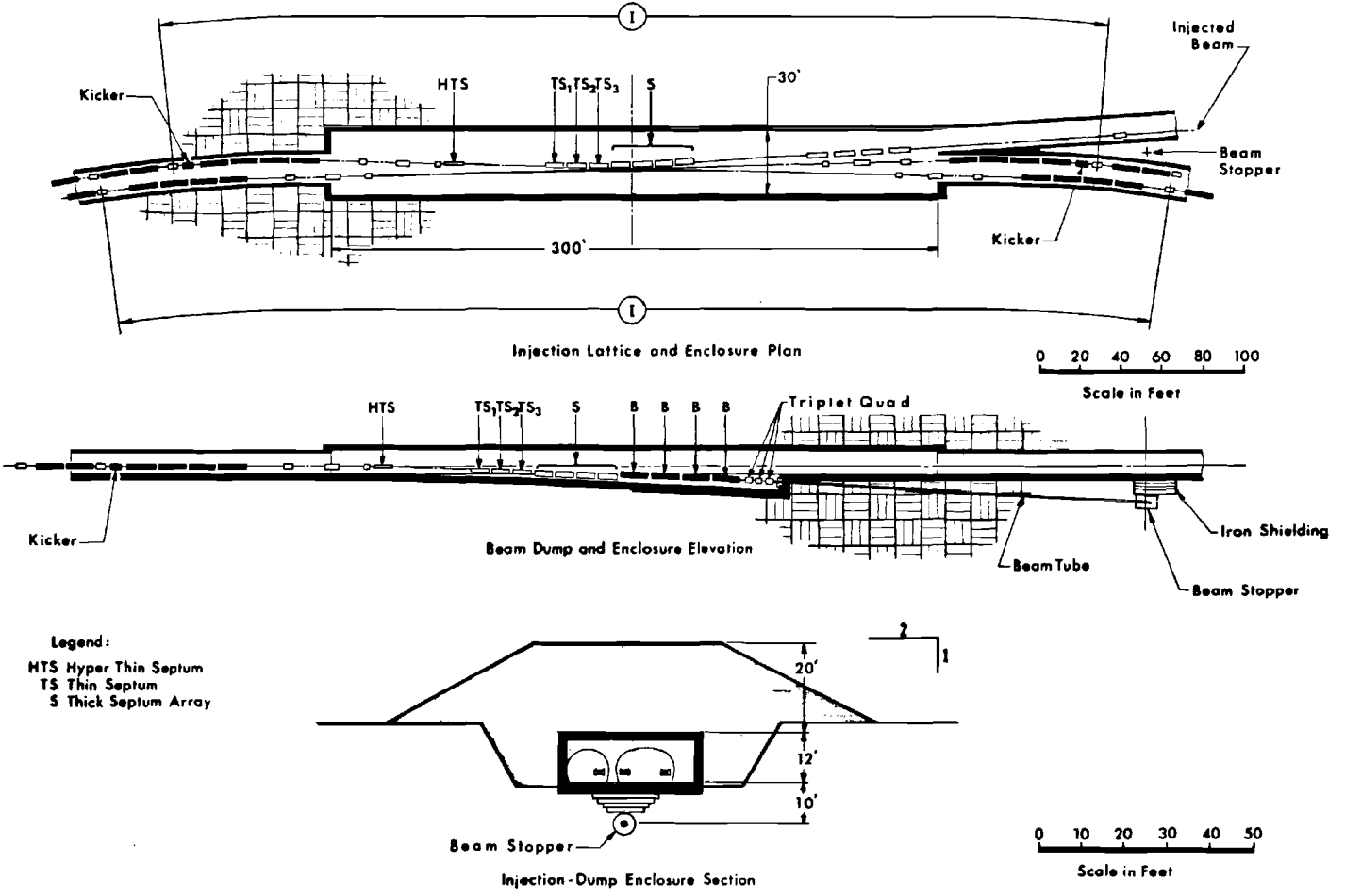

Figure VII-1 Top: Injection Septum Magnets and Beam layout.
Middle and Bottom: Side and End Views of Beam Dump System and Injection Crossing Enclosure

downstream from the injection point respectively. The horizontal oscillation wave number ν_x is tuned to approximately a 1/3 integral value. The beam entering the storage ring on the opposite side of the magnet septum from the closed orbit will oscillate about the closed orbit with a small amplitude. Because of the 1/3 integral value of ν_x the oscillating beam will miss the septum for two revolutions and will hit the septum on the third revolution. At that time, the injection kicker magnets are turned off suddenly, the closed orbit is moved inward back to its normal position far enough inside the septum for all 3 turns to miss it. This procedure is shown in the phase space diagram in Fig. VII-2 except that in our case, since β_x is not a maximum at the injection point the phase space of the beam is not a circle but an oblique ellipse and the tuning for maximum phase space density is not exactly ν_x= 1/3 (integer). Further modification of the lattice will give better optimized tuning conditions. For the present lattice with a septum thickness of 2 mm, exact calculation[2] gives A = 17.9 mm, and the necessary orbit displacement by kickers is d = 17.7 mm. The average phase space density in the large circle is reduced, compared to that of the injecting beam, by a factor $3a^2/A^2 = 0.48$.

(C) Kicker Magnet

To obtain the necessary orbit displacement, a pair of full-aperture fast kicker magnets have to be placed on either side of the injection point, spaced so that the horizontal oscillation

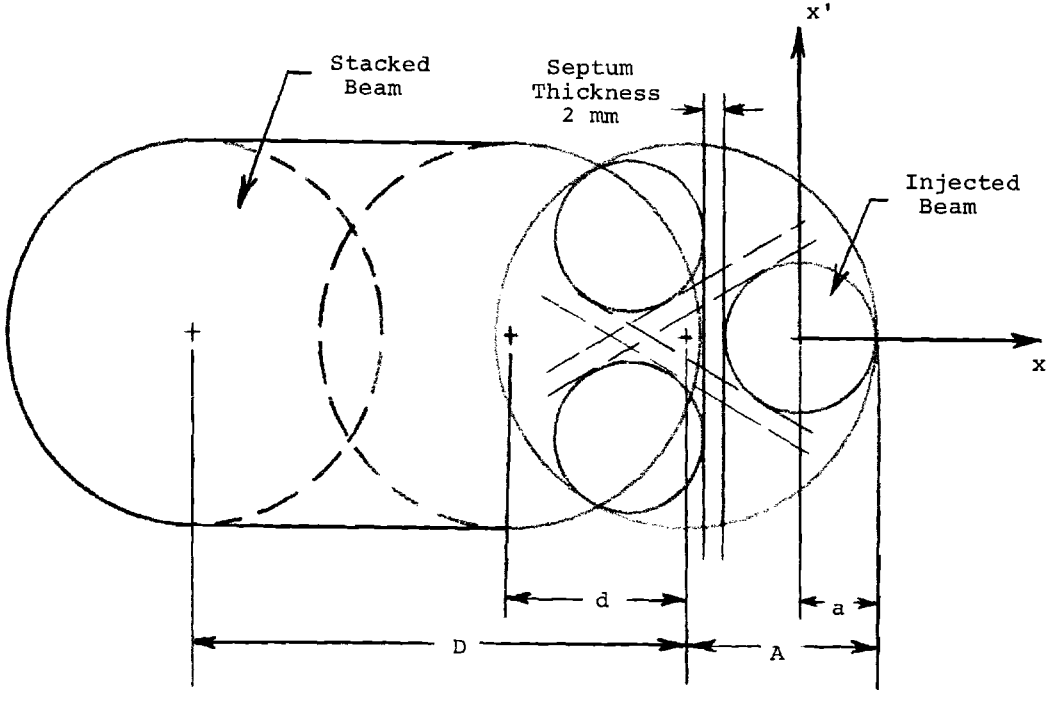

Figure VII-2. Phase Space Diagram Showing Injection and Stacking Procedures

phase difference between them is 180^{o}. In our lattice, this is accomplished by placing the kickers in the drift spaces at either end of the matching insertion. At these points, $\beta_x \approx 11$ m, and to obtain the orbit displacement of 17.7 mm, the kickers must deflect the orbit by an angle

$$\delta = \frac{d}{\sqrt{\beta_k \beta_s}} = \frac{17.7 \times 10^{-3}}{\sqrt{11 \times 56}} = 0.713 \text{ mrad}$$

where β_k and β_s are β_x at the kicker and the septum. This requires a kicker strength of 2.12 kGm. At the same time, the kicker must have a rise time, or rather a fall time, of 20 nsec in order to avoid scraping a part of the beam on the septum (20 nsec is approximately the interval between bunches).

Although possible, this is a severe requirement. The kicker strength requirement can be alleviated by modifying the matching insertion so that β_k and β_s are larger, thus reducing the necessary kick angle δ. As mentioned in Section III, the present design of the matching insertions is only an intermediate solution. Effort to improve the design is continuing. The fall time requirement would be relaxed if the radius of the storage ring were slightly more than 1/3 the radius of the main ring. For then there would be a longer gap between the end of injection and the time the first injected protons arrive at the septum after their third turn. However, this produces an undesirable 2/3 intensity gap in the beam.

We have chosen to use full aperture kickers[3]. This avoids

the need for the electromagnetic shields between the stacked beam and the partial aperture kicker magnets which enclose only the injected beam, and reduces the very costly vacuum chamber and magnet gap width. These electromagnetic shields would have to be movable screens which shield the kicker fields from affecting the stacked beam during injection and which are removed after injection to allow the injected beam to move out of the kicker magnets and into the stack. However, since the full aperture kickers affect also the stacked beam, any inequality in the fields of the two kickers during the fall time of 20 nsec will cause residual horizontal oscillation in the part of the stacked beam affected. Fortunately, 20 nsec is a very short time compared to the revolution period of about 7 μsec. Even though the stacked beam is kicked on the average 10 times by the kicker magnets for injection of 20 main ring pulses, the part of the stacked beam affected during the 10 x 20 = 200 nsec is still rather small. In any case, with improved technology, it should be possible to build kicker magnets which behave alike during the fall time to a high degree of precision.

The kicker magnet as presently visualized will have a design similar to that used for extraction from the 10 BeV booster of the NAL accelerator. The magnet shown in Fig. VII-3 will be made up of individually energized modules. Each module will be a ferrite loaded transmission line short-circuited at one end to form a one-turn current loop and will be driven from an impedance-matched pulse line with triggered switches at both ends.

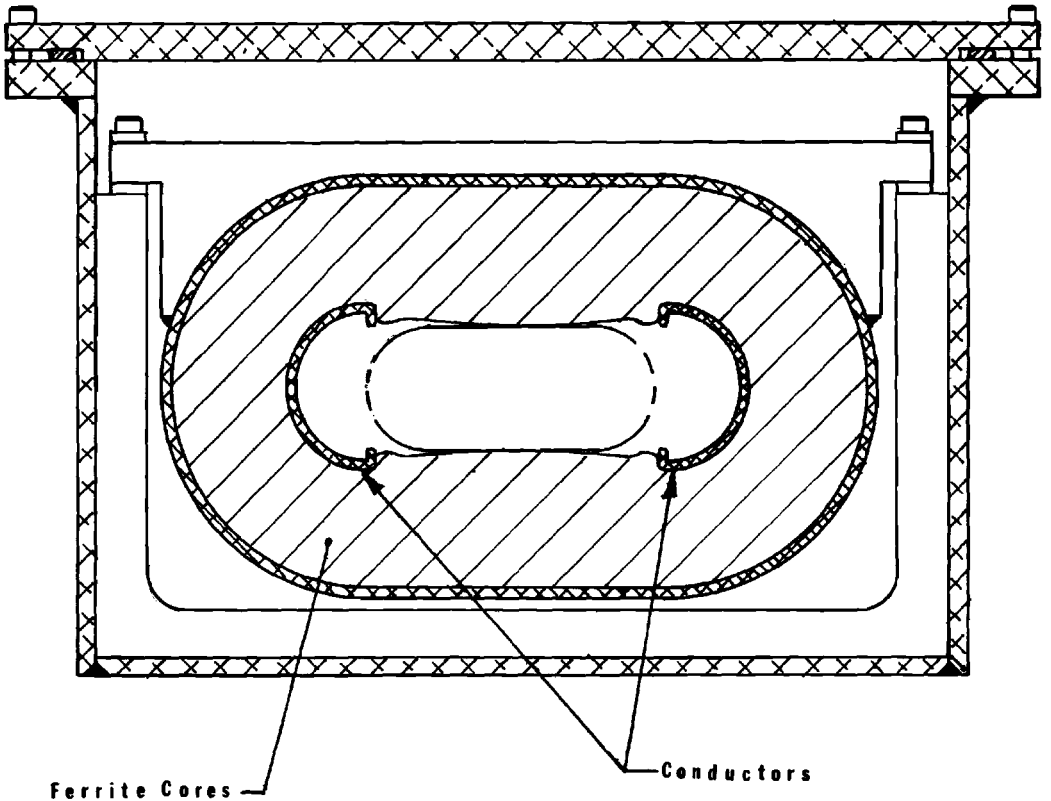

Figure VII-3. Cross Section of Kicker Magnet

The switch between the pulse line and the magnet will switch the magnet on and does not have to be fast. The switch at the far end of the line is switched on to terminate the pulse and hence must provide a fast, low-jitter pulse. This fast current switch may be either a spark gap or a deuterium thyratron. This type of pulsed magnet has been operated at a field of about 1 kG. At this field the injection kicker magnets for the storage ring will have to be more than 2 m long each. It may be possible by extending present technology to increase the field and shorten the magnet. However, a better and simpler solution is to modify the design of the injection insertion to reduce the requirement on the kick angle.

(D) Beam Stacking

The injected beam still retaining the bunch structure of the main ring rf is synchronously captured into the storage ring rf buckets. To reduce the storage ring rf voltage required for phase space matching the beam should be debunched in the main ring by reducing the main ring rf voltage adiabatically before extraction. Since the beam is injected from the outside of the storage ring, stacking is accomplished by decelerating the beam and moving the orbit inward. The procedure of beam stacking in the momentum phase space using rf had been studied extensively by MURA[4].

In our case, the good field aperture width of B1 is 2.5 in. or 63.5 mm and β_x at B1 is 37 m. This gives an aperture width at the injection point of $6.35\sqrt{56/37} = 78$ mm. Referring

to Fig. VII-2 we see that the maximum and minimum orbit displacements to be accomplished using rf are 42.2 mm and 17.7 mm respectively (assuming the closed orbit errors have been corrected). With x_p= 3.59 m at the injection point, these displacements correspond to $\left(\frac{\Delta p}{p}\right)_{max} = 11.8 \times 10^{-3}$ and $\left(\frac{\Delta p}{p}\right)_{min} = 4.9 \times 10^{-3}$. The deceleration could be supplied very slowly by the rf over the long time of 3 sec between main ring pulses.

The rf voltage at capture should be adjusted to give a bucket shape matching that of the beam bunch after appropriate debunching in the main ring. But as the beam is decelerated toward the stack, the rf voltage should be adiabatically reduced to shrink the bucket tightly around the beam bunch so as not to stir empty phase space into the stacked beam.

Properly, after the beam reaches the stacking momentum, it should debunched completely by turning the rf off adiabatically. This is a slow process. It has been shown[5], however, that even if the rf is turned off abruptly, when a large number of pulses have been stacked in this non-adiabatic manner, one gets a fairly good statistical filling of the available phase space with an efficiency as high as 90%. The stacking procedure is, therefore, to decelerate the beam by a random amount somewhere between $\left(\frac{\Delta p}{p}\right)_{min}$ and $\left(\frac{\Delta p}{p}\right)_{max}$ and deposit the beam abruptly simply by turning the rf off. Of course, the rf voltage still has to be adjusted to give a tight fitting bucket around the beam bunch.

References

1 E. Keil, Aperture Requirements at Injection into the NAL Storage Ring, NAL Report FN-169, August 27, 1968.

2 E. D. Courant, Phase Space Dilution in Three Turn Injection, NAL Report FN-174, November 1968.

3 A. van Steenbergen, Injection Criteria Storage Ring, NAL Report FN-171, August 28, 1968.

4 K. R. Symon and A. M. Sessler, Methods of Radiofrequency Acceleration in Fixed Field Accelerators with Application to High Current and Intersecting Beam Accelerators, CERN Symposium 1956, Vol. 1, p. 44, 1956.

5 Report on the Design Study of Intersecting Storage Rings (ISR) for the CERN Proton Synchrotron, p. 110, AR/Int. SG/64-9, May 12, 1964.

VIII. RADIATION, SHIELDING, AND BEAM DUMP SYSTEM

For the purposes of estimating radiation levels and shielding requirements for the storage ring, four mechanisms of particle loss must be considered. Nuclear interactions in the residual gas cause particle loss accompanied by the creation of secondaries, which are chiefly responsible for a general level of radiation around the ring. Multiple Coulomb scattering in the residual gas causes the beam to grow in size until it intercepts the vacuum chamber; however, it is planned to make routine use of beam scrapers as aperture stops, so that the resultant radiation will be localized to one or two places around each ring. Injection errors and finite rise and fall times of injection kicker magnets give rise to larger amplitude betatron oscillations which will be clipped by the scrapers. Finally, the beams must be dumped periodically in preparation for refilling the rings when the luminosity has decreased or beam size increased beyond tolerable limits. The dumping is accomplished by using a fast kicker magnet followed by a beam transport system to guide the beam onto a beam stopper capable of handling the thermal shock and sufficiently removed from the ring tunnel not to affect the radiation level in the tunnel. However, the finite rise time of the dumping kicker will lead to some beam loss on the septum of the first septum magnet. These situations will be examined in detail.

(A) General Shielding

The radiation level over the major portion of the ring is determined by the rate of nuclear interactions in the residual gas, which depends only on beam intensity and the density and composition of the residual gas. Assuming a time average intensity of 10^{15} protons per ring and nuclear cross-sections of 40 and 380 mb for H_2 and N_2 respectively, one arrives at the loss rates given in Table VIII-1.

Table VIII-1 Proton loss per second per ring

	Residual gas	
Pressure	H_2	N_2,CO
10^{-8} torr	0.9×10^{9}	0.8×10^{10}
10^{-9} torr	0.9×10^{8}	0.8×10^{9}

There is some doubt at this point as to what the composition of the gas would be; however, as will be seen below, 10^{-8} torr of N_2 would be intolerable on the basis of beam lifetime. Thus, for the purpose of estimating shielding, we assume a loss rate of 10^{9} protons per second per ring which, at 100 BeV, corresponds to a power of 32 W for the two rings. Since, in this energy range, the intensity of secondary radiation to be shielded against is approximately proportional to the power dissipated, the required shielding can be estimated by comparing this power figure with that used in Section 12 of the NAL Design Report as a basis for computing the accelerator main ring shielding in the so-called quiet areas. In that case, a loss of 480 W is predicted for a ring of three times the circumference of the storage

ring, so that the intensity in the storage ring will be $\frac{3x30}{480} = \frac{1}{5}$ of that in the main ring. The difference in shielding corresponding to this intensity factor amounts only to a few feet of earth and so it was decided to use the same minimum thickness of shield as for the main ring, namely, 17 ft of earth.

Although this calculation is crude, it is safe to say that the radiation level in the storage ring tunnel is far from negligible and is, in fact,comparable to that anticipated in the accelerator tunnel.

(B) Beam Scrapers

Aperture limiting beam scrapers will be used to define the available aperture at all times. For experiments requiring a precise definition of beam interaction volume the scraper jaws will be closed down to fit tightly around the stacked beam. The scrapers will localize beam loss due to excessive beam size caused by either injection errors or multiple Coulomb scattering.

The beam scrapers consist of four pairs of remotely adjustable jaws located just upstream of the injection beam crossing point in each ring: two pairs each for defining the horizontal and the vertical apertures. The two pairs of horizontal aperture defining jaws are placed at locations along the beam where the horizontal oscillation phases are 180° apart and where the horizontal beam widths are large; the vertical jaws are similarly located. The jaw blocks should be about 3 m thick in the beam direction and should be made of either carbon or

beryllium. The adjusting mechanism for the jaw opening should give a precision of the order of 0.01 in.

To estimate the radiation intensity we assume an extreme case in which all losses occur in one pair of vertical jaws, and the jaws are set at an aperture corresponding to the predicted vertical beam emittance of 0.36π mm-mrad. The loss rates[1] are listed in Table VIII-2 together with the periods of time in which luminosity decreases to 70% (at constant emittance) due to Coulomb plus nuclear interactions.

Table VIII-2 Proton Loss Per Second and 70% Luminosity Time

Pressure	Residual Gas	
	H_2	N_2,CO
10^{-8} torr	2×10^9 (15 hr)	10^{10} (3/4 hr)
10^{-9} torr	2×10^8 (150 hr)	10^9 (7 1/2 hr)

It is illuminating to compare these figures with septum losses in the accelerator main ring slow extraction system. In that case a 1% loss at 10^{13} p/sec represents a local source of 10^{11}p/sec at 200 BeV. If we exclude the case of 10^{-8} torr of N_2 because of the excessively short life-time, we see that the radiation problem is one or two orders of magnitude less severe for the scrapers than for the main ring extraction system. One should add to these figures beam loss on the scrapers during injection; however, even assuming 10% loss (10^{14} protons per fill) the loss figures in Table VIII-2 are at worst doubled if the 70% luminosity time is taken to be the refilling time.

Shielding for this localized higher radiation level will be provided for by increased thicknesses of the concrete tunnel and the earth backfill over the injection beam crossings.

It should be remarked that while the nuclear interaction cross-section is roughly independent of energy in this energy range, the Coulomb interaction cross-section varies as $(\text{momentum})^{-2}$. Since the emittance of the injected beams varies as $(\text{momentum})^{-1}$, the power loss at the scrapers is approximately independent of the beam momentum for a given number of stacked protons. Thus the shielding required at the scraper location is independent of beam momentum for the assumed case of tight collimation, although this mode of operation may be unattractive at energies much less than 100 BeV because of the reduced beam lifetime.

(C) Beam Dump System

After the rings are filled, a process which should take only a few minutes, there will be a steady degradation of luminosity and a steady increase in interaction volume with a time scale as indicated in Table VIII-2. Depending on the requirements of the particular experiment in progress, it will eventually be advantageous to dump the degraded beam and refill the rings. In addition, for protection of the facility, it is imperative that it may be possible to remove the protons from the rings as rapidly as possible in the event of a malfunction of a critical machine component. The 16 MJ of energy carried

by the 10^{15} protons at 100 BeV could do serious damage to the machine if the protons are lost in the machine.

The beam dump system is shown in Fig. VII-1. Fast kicker magnets similar to those used for injection but deflecting the beam in the vertical direction will be installed in the injection insertion at the upstream end of the beam not occupied for injection. The kicker magnet should be positioned approximately at 90^{o} horizontal oscillation phase upstream from the beginning of the 68 m long drift space where the beam will be kicked vertically downward across a thin magnet septum. The beam is then channeled by a series of dc septum and bending magnets downward onto the beam stopper some 100 m away. A defocusing quadrupole triplet is placed immediately after the bending magnet chain to spread the beam so that the cross-sectional area of the beam is $\gtrsim 10$ cm^2 at the beam stopper. The beam stopper may be a steel cyclinder of 4 ft radius and 10 ft long with a cylindrical core of beryllium of 10 in diameter and 5 ft long as shown in Fig. VIII-1. The actual shape and dimensions will be determined after soil radioactivation and radionuclide leachability studies are completed. The beam striking the Be core may cause a local temperature rise of about $200^{o}C$ which is quite acceptable. The stopper is buried about 10 ft below the floor level of the tunnel. To reduce the radiation from the beam stopper to a negligible level in the tunnel, $4\frac{1}{2}$ ft of steel plates will be buried in the earth above the stopper.

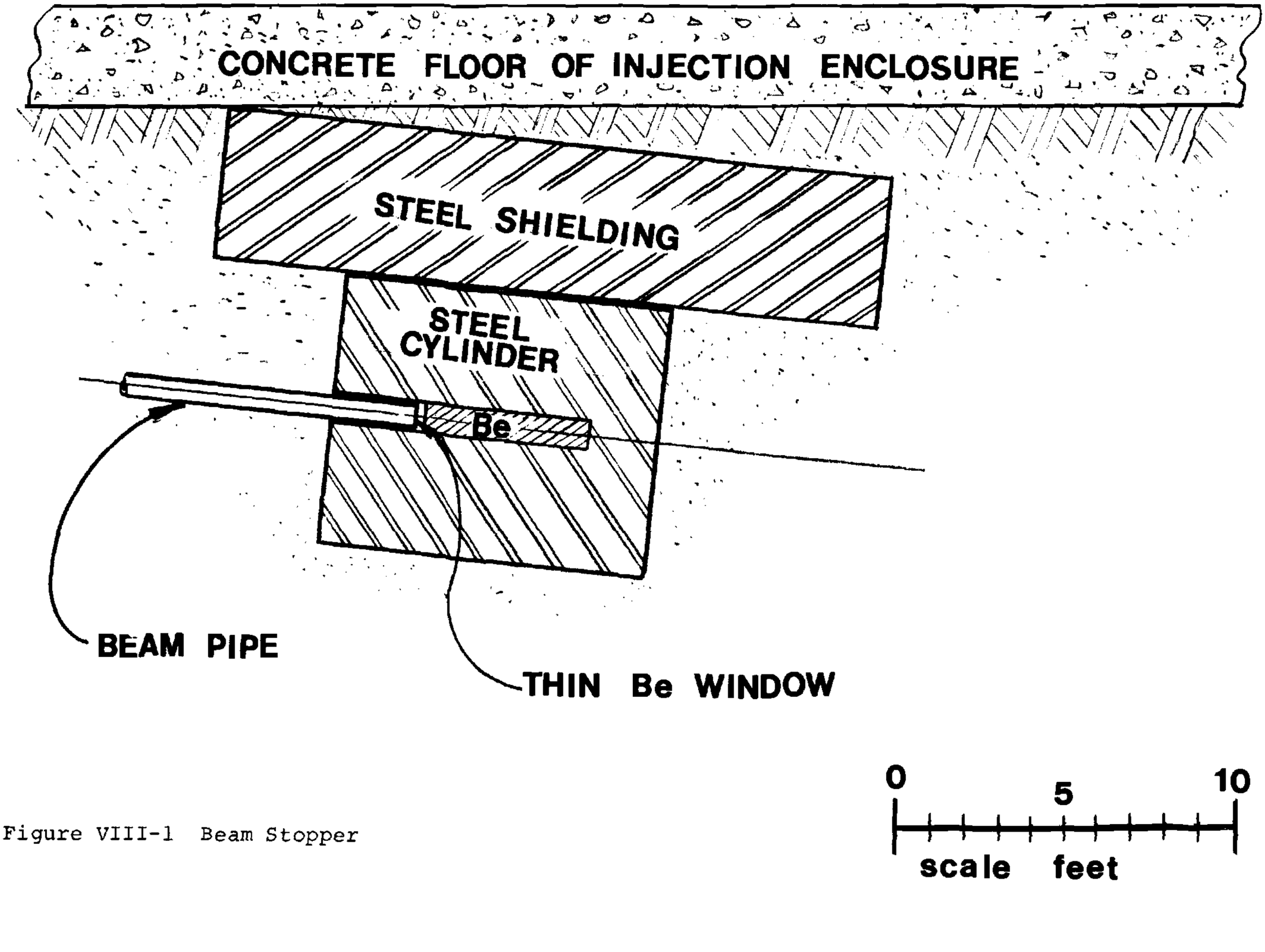

Figure VIII-1 Beam Stopper

The dumping kicker has a rise time of about 20 nsec which means that about 0.3% of the stacked beam will hit the first magnet septum. This is negligible compared to the beam loss on the scrapers. The kicker magnets are triggered either on command or by appropriate interlocks from various components of the storage ring. The interlocks should be sufficiently sensitive and fast that the kickers are triggered before the beams in the rings have strayed excessively from their normal orbits. Since the kicker magnets are the fastest components in the machine, these beam dumps should provide adequate protection for the entire storage ring system.

References

1 E. D. Courant, Nuclear and Coulomb Scattering in Storage Ring, NAL Report TM-69, October 7, 1968.

IX. MONITORING AND CONTROL SYSTEM

(A) Beam Monitoring

Beam monitors are required in the beam transport lines and the storage rings for observing beam intensity and position.

(1) Transport Line Beam Monitors

The beam in transit through the transport lines appears as a pulse train about 21 μsec long bunched at 53 MHz. Conventional ferrite window-frame monitors are used to feed sample-and-hold circuits in the control room. During adjustment of the beam the sample-and-hold circuits provide a continuous display of beam position in flight through the transport line.

A monitor designed for a mutual impedance of 2 Ω to the beam generates a 6 mV signal at 1% design beam current, namely about 3 mA. The energy signal-to-noise ratio $\frac{I^2Rt}{kT}$ corresponds to a voltage signal-to-noise ration of 10^5, permitting beam position measurement to an accuracy of ±1 mm at 1% design beam intensity and somewhat better at full intensity.

(2) Stacked Beam Position Monitors

The magnetic field of the stacked beam allows measurement of its radial and vertical positions. The lowest intensity to be handled is that due to a single pulse (5×10^{13} protons) from the main ring which produces a stacked current in the storage ring of I = 1.16A. The magnetic field intensity due to this current is given by $H \text{ (in G)} = \frac{2\ I \text{ (in A)}}{10r \text{ (in cm)}}$. If ΔH is the error

in measurement of H the corresponding error in measurement of r will be $\Delta r = \frac{-5r^2}{I} \Delta H$.

At 10 cm from a 1 A circulating beam, a detector with an uncertainty of 10^{-5}G gives a position uncertainty (considering differential errors of a pair of detectors) $\Delta r \approx 0.1$ mm.

The flux-gate magnetometer detectors are mounted on a ceramic bobbin outside the vacuum chamber as in Figure IX-1. A 1 m long magnetic shield is provided at each detector location to shield the assembly from stray fields. The shield is supported to prevent the Villari effect and is provided with a degaussing coil.

The position signal from a pair of detectors is formed by the difference signal divided by the sum signal. The detectors are placed 2 per cell in the 1.6 m straight sections of 48 normal cells, and 4 per insertion in 6 insertions, giving a total of 120 beam monitors in each ring. To minimize the total quantity of associated electronics and in particular to simplify the electronics required inside the tunnel, the individual magnetometer assemblies are time-division multiplexed on a coax system to a central amplifier and display console.

A carrier signal is normally required in the operation of the flux-gate magnetometer. The magnetometer output consists of the even harmonics of the carrier (commonly the 2nd harmonic is chosen). It appears probable that a trapezoidal carrier-current signal (rather than the commonly-used sine wave carrier)

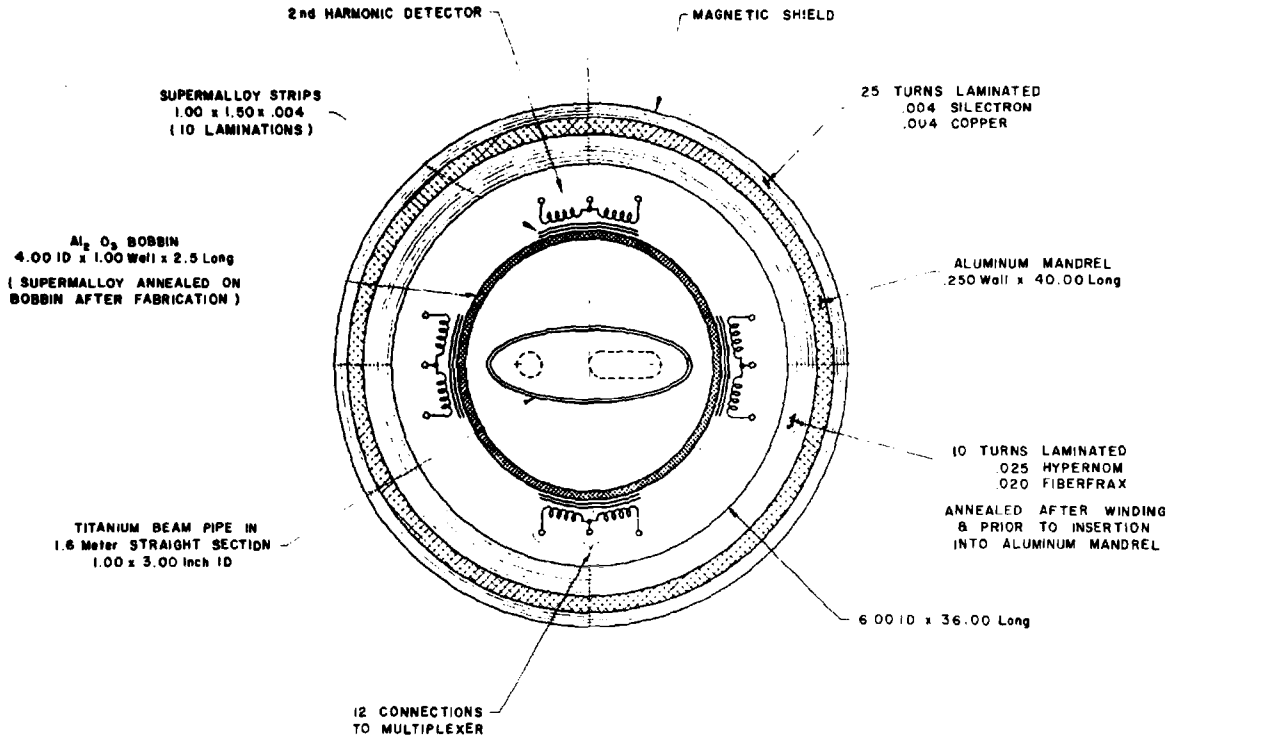

Figure IX-1 Beam Monitor

will produce sufficient output from the Supermalloy detectors so that no amplifiers will be needed in the machine tunnel.

(3) Beam Intensity Measurement

Beam current transformers are provided to measure the total dc beam currents and to monitor azimuthal charge density variations which may arise. These transformers will be of the 4-core type using MnZn ferrite toroids and Supermalloy cores and will be placed in each ring to provide current monitoring over the frequency range from dc to 50 MHz. The beam intensity signal is transmitted over a matched-impedance 50 Ω coax line to the control room.

(B) Control System

The control system required for the storage ring is similar to that for the main ring of the 200 BeV accelerator and will follow a similar pattern. The types and numbers of control functions for the storage ring system are estimated to be

Number of Status Points	2000
Number of Video Monitoring Points	500
Number of On-Off Controls	400
Number of Analog Monitoring Points	2200
Number of Analog Controls	400
Total Signals	5500

Most of the control functions will be carried out by a control computer located in the storage ring control center and interfaced to the central control computer of the accelerator. Similar to the accelerator, monitoring data of the storage ring will be

collected at a number of stations around the ring and transmitted to the control center by a time-shared multiplex system. It is assumed that the accelerator central control computer will have adequate capacity. For many operations such as filling of the storage ring, the operations of the storage ring must be in close conjunction with that of the accelerator. The interface between the accelerator and the storage ring multiplex systems will be located at the storage ring control room.

The multiplexing system is now conceived as a parallel transmission system with signals transmitted over twisted-pair wires at a relatively low rate. Further study may indicate that it is more economical to use serial transmission over better quality cables at a much higher rate.

In addition, for transmission of very fast signals and information that cannot be conveniently time coded, direct-wire systems with coaxial cables will be employed. The major systems for which direct-wire systems must be used are

(1) The rf system

(2) Beam injection, and beam dump control and interlock systems.

(3) Radiation-protection and personnel-access systems.

The storage ring control room will be located in the storage ring central laboratory building (see Fig. II-2). Although the storage ring is only $\frac{1}{3}$ the size of the accelerator main ring, the data transmission lines are still rather long. The average data transmission distance is approximately 1700 ft from the

storage ring control room with an additional 7000 ft when control is from the main accelerator control center.

X. RING ENCLOSURES AND EXPERIMENTAL HALLS

The storage ring system consists of three categories of components having different enclosure requirements. The basic function of the machine is served by the beam crossing areas where the colliding beams interact and where the experimental equipment is located. In these areas also are the special magnet elements inserted in the ring lattice to produce the desired beam characteristics at the intersection points. Between successive beam crossings are the bending and focusing magnets of the regular ring lattice, whose only function is to transport the beam between the crossings. Enclosures are also needed for the magnet elements forming the injection beam transport lines from the main ring of the accelerator. Of these enclosures, those housing the regular lattice and the injection transport lines constitute by far the major portion of the total length.

(A) Injection Transport Enclosure

The requirements for the enclosure of the injection beam transport lines are very similar to those of the 200 BeV accelerator main ring. The enclosure will be in the form of concrete tunnels with an omega-shaped cross-section of 10 ft maximum inside width and 8 ft center line ceiling height and is shown in View A of Fig. X-1. The tunnel will be either poured in place or formed of precast concrete sections. The two branches of the injection transport line will be enclosed in separate tunnels.

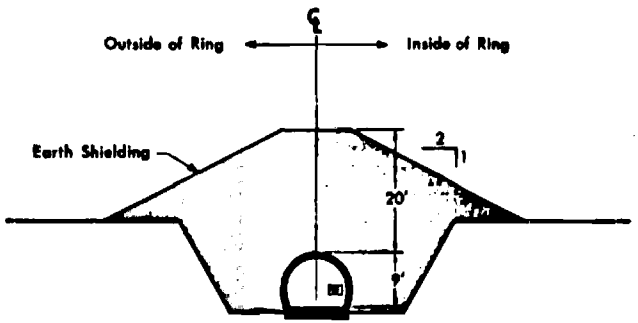

A. Standard Enclosure

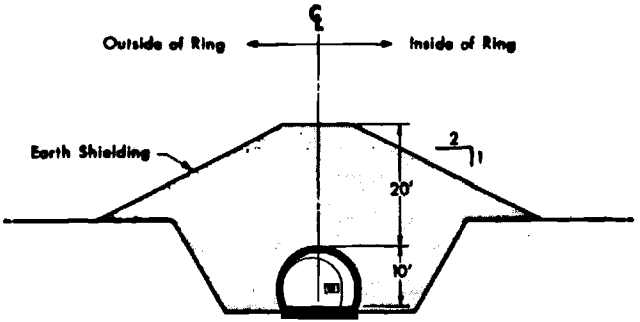

B. Standard Enclosure showing Enlarged Section

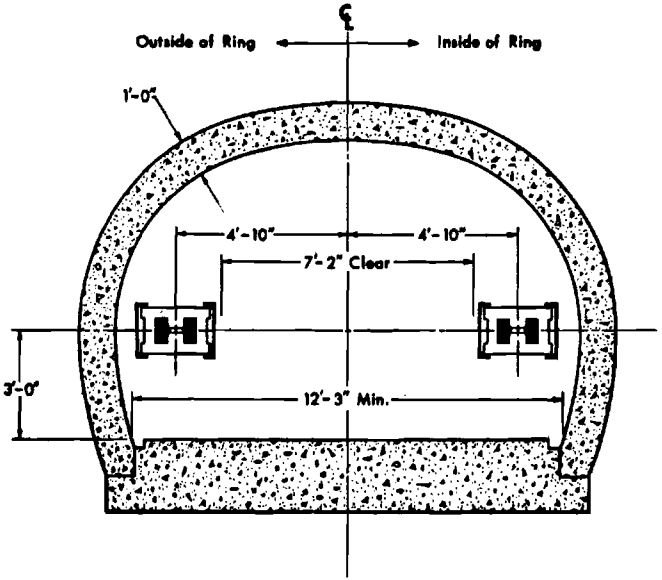

C. Enlarged View of Double Enclosure

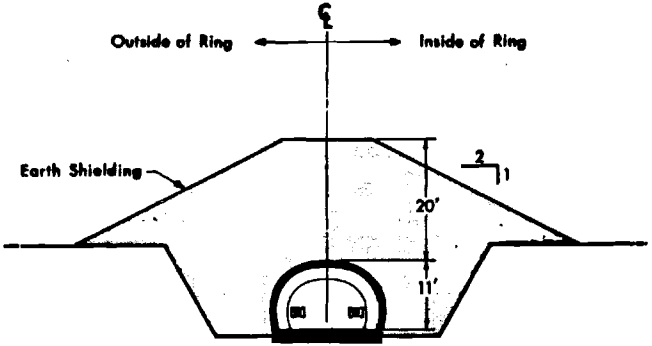

D. Double Enclosure showing Enlarged Section

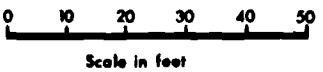

Figure X-1. Cross Sectional Views of Storage Ring and Injection Transport Enclosures.

At the points where magnet power and cooling leads from the service buildings are brought into the tunnel, the tunnel cross-section will be enlarged to 12 ft maximum inside width as is done in the main ring enclosure. This section is shown in View B of Fig. X-1. These tunnels will have the same patterns of utility penetrations and back-filled earth radiation shielding as the main ring tunnel.

(B) Enclosures of Regular Lattice and Injection Areas

The regular ring lattice enclosure differs from the injection transport enclosure principally in that the former has to house two beam lines and hence has to be wider. A modification of the injection transport tunnel is employed. The tunnel is simply split along the middle vertical plane and floor and roof sections of the appropriate width are inserted as shown in View C of Fig. X-1. The tunnel width is determined by the maximum spacing of the two beams and the center line ceiling height is about 8 ft. Of the several alternates considered, the one selected is considered a practical compromise for the following reasons: First, by adopting the same wall contour as for the injection transport tunnel, the designs for magnet stands, power and cooling leads, trays and other hardware can be used without modification. Second, the departure from the optimum circular cross-section for structural strength is offset by the reduction of back-fill earth shielding as compared to that required if the injection tunnel cross-section were merely photographically enlarged to provide the necessary width. At the center of each ring sextant, where power and cooling leads are brought in, the

tunnel cross-section is enlarged by 2 ft to provide space for utility cross-overs. View D of Fig. X-1 shows the enlarged section.

In each of two beam crossing areas 120° apart are located an injection system in one beam and a beam dump system in the other beam. These areas require special enclosures for a number of reasons. First, the injection transport tunnels and the storage ring tunnel merge at these points. Second, the beam stoppers of the beam dump systems lie below the level of the tunnel floor in the vicinity of these areas. Third, a large number of special magnets, both pulsed and dc, needed for injection and beam dumping are located in these areas. Fourth, beam losses at injection, scraping, and dumping produce higher radiation levels requiring extra shielding. In addition, the rf cavities and associated power supplies and modulators are located at the ends of these areas downstream of the injected beams. For these reasons, the enclosures for these two areas will take the form of concrete vaults with a rectangular cross-section. The necessary extra shielding will be provided by additional earth fill over the enclosures. Typical sections through these enclosures are shown in Fig. VII-1.

The three beam crossings where the beams are inwardly directed will be developed into experimental areas. The remaining beam crossing with magnet insertion similar to that of the crossing for injection and beam dump is reserved for future conversion into an experimental area. The enclosure for this

beam crossing will initially be identical to that of the regular lattice except that the utility penetrations are located such as to avoid the necessity of relocation during conversion.

(C) Experimental Halls

The experimental halls are designed to provide a minimum lateral clearance of about 17 ft all around the beams over a distance of 150 ft up and down-stream from the beam crossing point. The provision of space for shielding and access results in a building 100 ft wide and 300 ft long. The dimensions of the building are such that 10 ft of shielding may be placed on top and sides of the 17 ft clear space around the beams. Magnet elements in the lattice insertion are supported by narrow elevated platforms carried on a trestle structure at each end of the experimental hall. The floor of the experimental hall is at an elevation of about 712 ft or some 28 ft below nominal grade level. A 50 ton bridge crane spanning the building will be used to handle heavy experimental equipment and shielding blocks as well as to place servicing equipment at the entrances of the ring enclosure and to handle storage ring components. An outside ramp from the site level down to the floor level of the experimental hall will permit use of the building crane to unload equipment transported from the shops. The floor of the experimental hall will be designed to carry the loading of required shielding anywhere within the building. The structure of the experimental hall above ground will be steel framed with walls of insulated metal siding. Views A, B and C of Fig. X-2

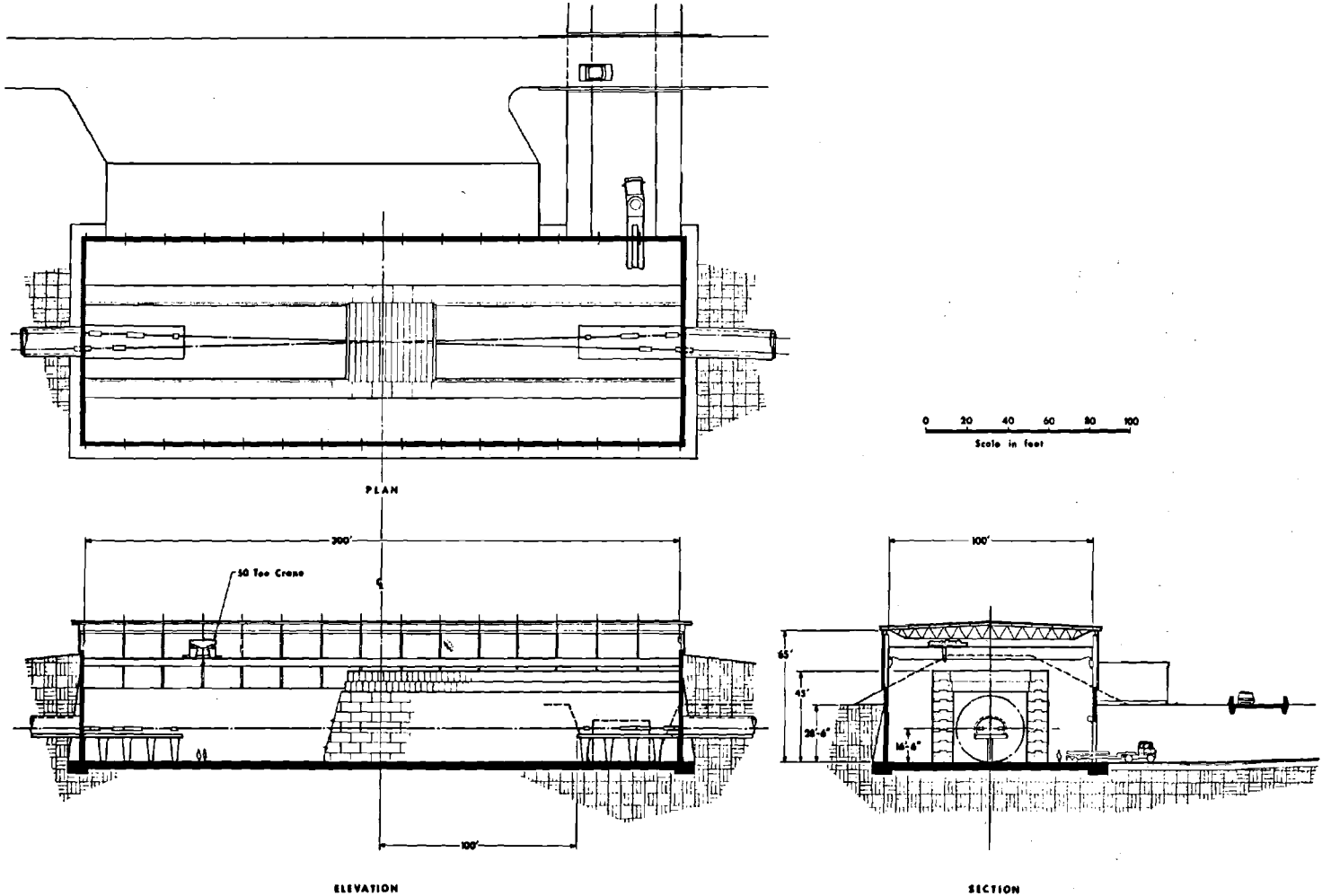

Figure X-2 Experimental Hall

illustrate the characteristic structure of the building as well as the important dimensions and shielding location.

Power for experimental equipment within the hall will be supplied at 4160 V and 480 V with terminal boxes distributed around the building perimeter to permit direct patching of magnet power supplies and other loads up to a maximum of 10 MW. Cooling water supply and return manifolds and water-to-air heat exchangers for dissipation of this maximum power will also be provided. Lighting, heating and ventilation standards for the accelerator experimental buildings are adopted for the storage ring experimental buildings.

XI. SUPPORT BUILDINGS AND UTILITIES

In addition to the ring enclosures and experiment halls, several other enclosures and buildings are required. Service buildings are required around the storage ring and along the injection transport lines to house magnet power supplies; control, monitoring, and communications equipment; cooling water pumps and heat exchangers; and ancillary equipment that must be distributed along with the storage ring lattice components. Central utilities which must be provided are electrical substations and vaults, sewage lift stations, and water reservoirs.

The storage ring system will have a central control room from which the system is operated. Provision will be made for housing the resident staff responsible for operation and maintenance of the storage ring system. Shops, offices, and light laboratory space must be provided for the scientific, professional, and technical staff, both permanent and temporary, engaged in the research programs.

(A) Service Buildings

At intervals around the storage ring enclosure and along the injection beam transport lines are located small service buildings. Their number and spacing is determined by the requirements of the equipment served. Twelve service buildings will be located on the inside of the ring at the beam crossings and the mid-points between crossings. The basic building module

has been set at about 35 ft by 70 ft. Each module houses a 1600 kW bending magnet power supply; cooling water pumps; water-to-air heat exchanger; and control, monitoring, and instrumentation stations. At the beam crossings the service buildings are lengthened to accommodate the power supplies for the other magnet elements of the lattice and for the injection and beam dump magnets at the injection beam crossings. Still further extension of the service buildings at the experimental halls provides space for experimenters' control and observation stations and for the additional electrical and cooling equipment required for the experiments. Tunnel purging fans will also be placed within the service buildings. The buildings will be lighted, heated and ventilated so that maintenance work can be performed and so that operating equipment may be maintained within reasonable temperature limits. The service buildings will have personnel access passages 3 ft by 9 ft cross-section leading into the ring and injection transport enclosures.

(B) Staff and Space Requirements

Inasmuch as the storage ring will be operated as an integral part of the Laboratory, the support facilities for operation of the storage ring will be derived from expansions of central laboratory facilities. However, for estimating space requirements and associated capital expenditures it has been assumed that size of staff and type of space will be typical for a high

energy physics laboratory of comparable investment.

Preliminary estimates give an initial annual operating budget of the order of $10 - $15 million and a staff of about 500. Assuming an average area of 250 ft^2 per person for all categories (excluding experimental area space requirements) and an average use factor of 0.70, we obtain a gross area of approximately 180,000 ft^2. This area is assumed to be distributed as in Table XI-1.

TABLE XI-1 SPACE DISTRIBUTION

Space Category	% of Gross Area	Area (ft^2)	Building
Office	20	36000	Storage Ring Central Laboratory (9 Story)
Light Lab*	40	72000	
Others +	5	9000	
Shops	20	36000	Storage Ring Shops (1-1/2 Story)
Stores	15	27000	

* Including control, counting, and computer areas.

\+ Library, lounge, and conference rooms.

The storage ring central laboratory will house about 400 people. Functions will include office and light laboratory facilities for resident and visiting physicists, engineering, storage ring operations and computer facilities. The storage ring central laboratory is designed to the standards of the

accelerator central laboratory.

The storage ring shops building has one-half of its width designated to be a long high-bay heavy shop and assembly area serviced by a 50 ton crane. The other half of the shop building comprises a two-story section with stores, electronic and mechanical fabrication areas, technician shops, smaller machine tool facilities, and shop offices. The building is designed to the standards of the central shops.

(C) Mechanical Utilities

In addition to the heating and ventilating requirements of the service buildings and the storage ring central laboratory and shops, other site requirements must be satisfied.

(1) LCW Systems - Low conductivity water (LCW) is required for filling, blow-down and make-up of the cooling systems of the magnets and other equipment. The central laboratory LCW supply is adequate to handle the additional needs of the storage ring system. Because of the very large make-up and blow-down water requirements of cooling towers for dissipating the design electrical load, an alternate LCW cooling system has been selected. This consists of forced-draft water-to-air heat exchangers designed to lower the water temperature from 51°C to 35°C for a hot-day design temperature of 89°F. For days when this temperature is exceeded, spray heads supplied from a water storage reservoir would wet the heat exchanging surfaces to lower the surface temperature and the resultant LCW outlet temperature. A 300,000 gallon elevated storage

tank will supply water for a 12 hour period. The storage tank will also pressurize the domestic water and fire protection systems.

(2) Utilities Layout - The layout of the mechanical utilities is shown in Fig. XI-1 with the essential components identified. All supply and waste connections are made at the ends of the utilities runs shown to be stubbed-out for service to the storage ring area on the NAL site drawings.

(3) Roadways - Paved aprons, parking lots and roadways are designed to the Laboratory standards. These are shown on both the site master plan, Fig. II-1 and the utilities layout, Fig. XI-1.

(D) Electric Power Distribution

Power for the storage ring will be transformed from 345 kV to 34.5 kV by a 90 MVA, 3 phase, 60 Hz transformer at the accelerator master substation. A 34.5 kV underground feeder will transmit all of this power to the main storage ring substation located near the central control. Fig. XI-1 shows the location of the storage ring substation and the buildings which house power supplies for the major loads. From the main storage ring substation power is distributed by loop type circuits to the major loads. The storage ring bending magnet loads are about 10 MVA each ring and are supplied by circuits separated from other loads and switched by the main circuit breakers. In a similar fashion the quadrupole magnet loads of the regular

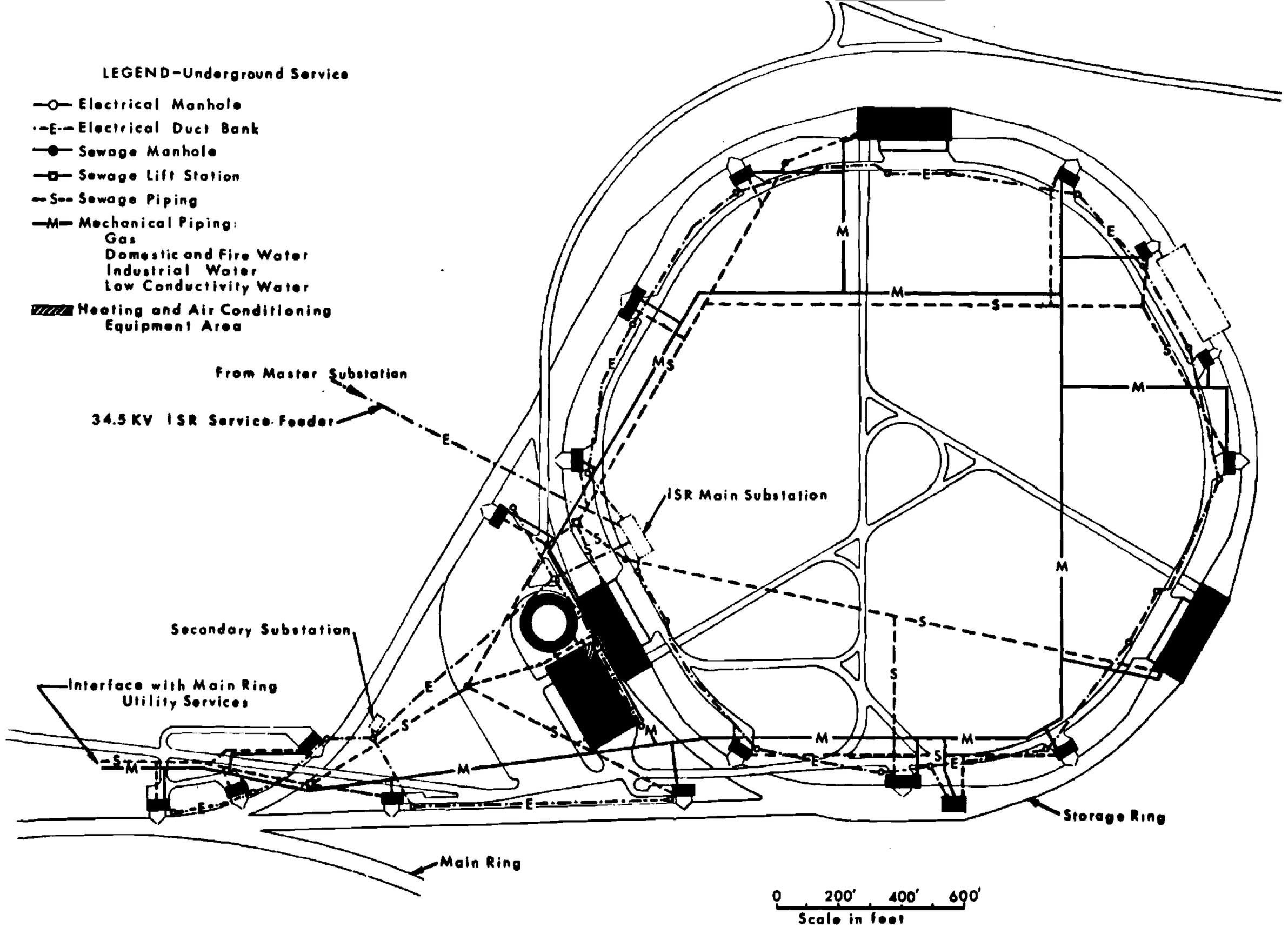

Figure XI-1 STORAGE RING BUILDINGS and UTILITIES LAYOUT

lattice will be supplied from 13.8 kV loops at a load capacity of about 1.2 MVA. The many individually controlled quadrupoles of the insertions in the storage ring will be supplied at 480 V. The 4.6 MVA power required by the injection transport magnets will be supplied from a secondary 13.8 kV substation located in the beam transport area. The experimental equipment in the experimental halls will be supplied at 4160 V and 480 V with a design connected load capacity of 11.5 MVA for each of the three experimental halls. The design loads of the storage ring central laboratory and work shops for lighting, air conditioning, etc. total 5.6 MVA. Power for fans of the forced-draft cooling systems, storage ring enclosures lighting, side services, and miscellaneous needs total some 12 MVA. The total design connected load is, therefore, some 78 MVA. The 90 MVA capacity of the substation transformer provides a reserve of 12 MVA for future additions. Fig. XI-2 shows the major components of the power distribution network.

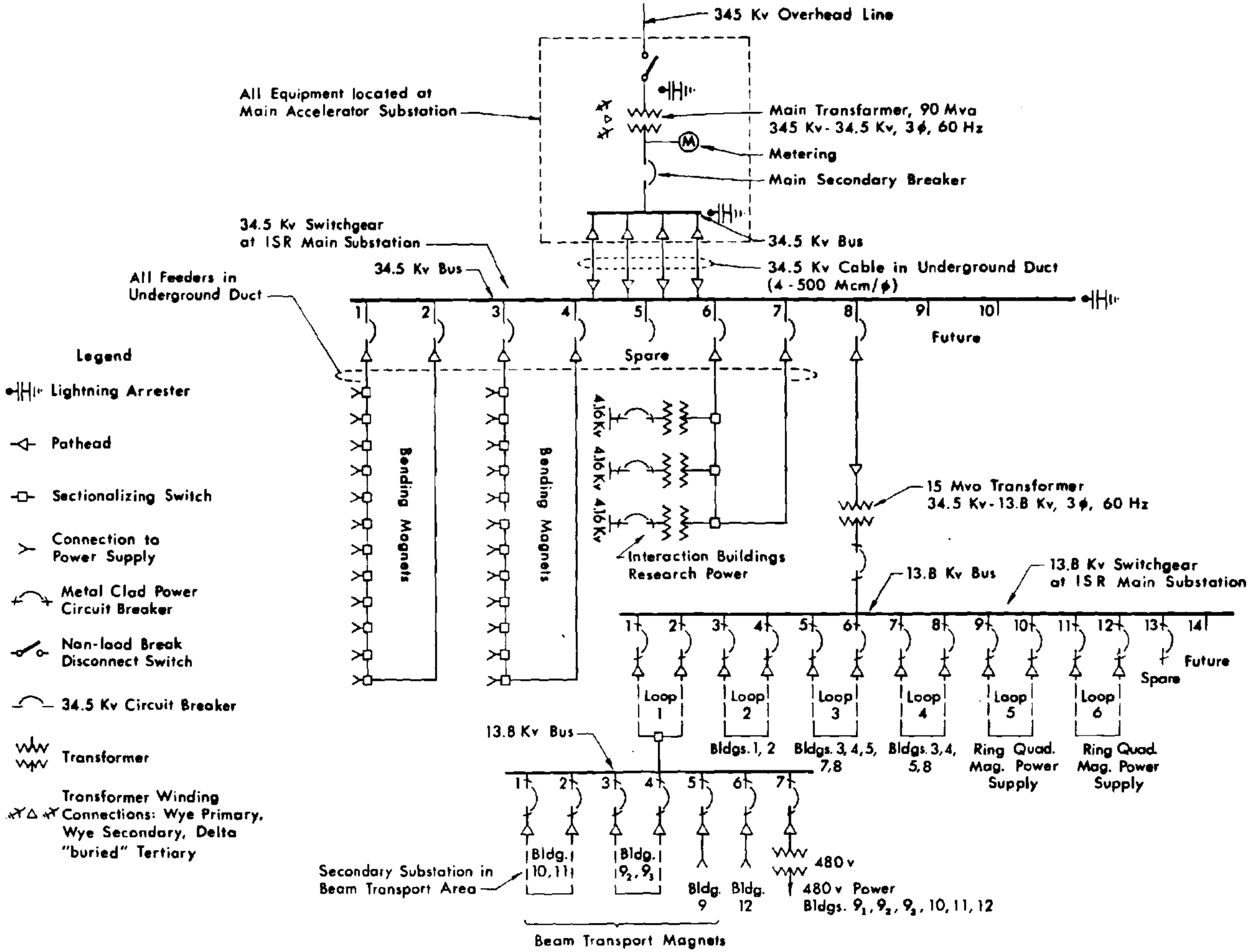

Figure XI-2 Power Distribution Network

XII. CONSTRUCTION COST ESTIMATE

The costs of the project were estimated by W. M. Brobeck and Associates. Installation costs of technical components were estimated separately and are shown explicitly as part of component costs. The costs of conventional facilities were estimated by commonly accepted methods based upon preliminary designs and layouts, and standards adopted for the National Accelerator Laboratory, insofar as available at this time, or otherwise upon standards of commercial practice.

EDIA costs on technical components are taken to be 25% of component costs. Contingencies on technical components are taken to be 25% of component and EDIA costs.

AEM costs on conventional facilities are taken to be 20% of facilities costs. Contingencies on conventional facilities are taken to be 15% of facilities and AEM costs.

This estimate does not include the cost of research equipment needed to carry out experiments but does include the costs of providing utilities in the experimental areas and of providing shielding for one of the three experimental halls.

All costs are given in 1968 dollars with no allowance for escalation.

CONSTRUCTION COST ESTIMATE
(ALL AMOUNTS IN THOUSANDS OF DOLLARS)

		CONVENTIONAL MAGNET SYSTEM	CRYOGENIC ALUMINUM COIL MAGNET SYSTEM	SUPERCONDUCTING COIL MAGNET SYSTEM
A. STORAGE RING TECHNICAL COMPONENTS				
1. RING MAIN MAGNETS		12,108	8,786	8,206
a. Bending magnets	7,738			
b. Normal quadrupoles	2,423			
c. Special quadrupoles	701			
d. Power and distribution system	480			
e. Assembly and installation	766			
2. RING MAIN MAGNET POWER SUPPLY		2,804	1,103	1,096
a. Bending magnet power supply	1,263			
b. Normal cell quadrupoles power supply	191			
c. Special quadrupole power supply	962			
d. Power supply installation	388			
3. HELIUM REFRIGERATION SYSTEM		-----	12,780	3,780
4. INJECTION TRANSPORT SYSTEM		1,521	1,521	1,521
5. TRANSPORT MAGNET POWER SUPPLY		818	818	818

A. STORAGE RING TECHNICAL COMPONENTS - Continued				
6. PULSED & AUXILIARY MAGNETS		2,284	2,444	2,444
7. PULSED & AUXILIARY MAGNET POWER SUPPLY		2,049	2,884	2,884
8. R. F. SYSTEM		203	203	203
9. VACUUM SYSTEM		3,711	1,767	1,767
a. Vacuum chamber and supports	694			
b. Linear ion pumps	491			
c. Sorbtion ion & sublimation pumps	1,430			
d. Sectionalizing system	194			
e. Gages, power supplies, cabling	835			
f. Cleaning and testing	67			
10. SUPPORT ALIGNMENT		852	852	852
11. SPECIAL HANDLING EQUIPMENT		192	192	192
12. BEAM DEVICES		548	548	548
a. Beam position detectors	281			
b. Beam dump system	267			
13. CONTROL AND INSTRUMENTS		1,375	1,375	1,375
a. Wiring and terminal	520			
b. Hard wire equipment	146			
c. Multiplex system	536			
d. Communications	22			

A. 13. Continued				
e. Beam monitoring	71			
f. Consoles, controls & displays	80			
SUBTOTAL		28,465	35,273	25,686
EDIA @ 25%		7,116	8,818	6,422
SUBTOTAL		35,581	44,091	32,108
CONTINGENCY		@ 25% 8,895	@ 30% 13,227	@ 30% 9,632
TOTAL-TECHNICAL COMPONENTS		44,476	57,318	41,740
B. STORAGE RING CONVENTIONAL FACILITIES				
1. ENCLOSURES		3,209	3,209	3,209
a. Ring	1,678			
b. Transport	1,088			
c. Injection-dump area	443			
2. EXPERIMENTAL HALLS		3,895	3,895	3,895
3. ENCLOSURES SERVICE BUILDING		850	850	670
4. CENTRAL LABORATORIES		3,415	3,415	3,415
5. WORKSHOPS		1,556	1,556	1,556
6. POWER DISTRIBUTION		4,109	3,814	2,806
7. MECHANICAL UTILITIES		1,848	1,813	1,519
8. EXCAVATION & EARTHWORK		1,116	1,116	1,116
9. SITE IMPROVEMENTS		908	908	908

B. STORAGE RING CONVENTIONAL FACILITIES - Continued			
10. MOVABLE SHIELDING	2,133	2,133	2,133
SUBTOTAL	23,039	22,709	21,227
AEM @ 20%	4,608	4,542	4,245
SUBTOTAL	27,647	27,251	25,472
CONTINGENCY @ 15%	4,147	4,088	3,821
TOTAL-CONVENTIONAL FACILITIES	31,794	31,339	29,293
PROJECT TOTAL	76,270	88,657	71,033

Appendix A HIGH FIELD SUPERCONDUCTING MAGNET STORAGE RINGS

The use of superconducting magnets at fields higher than the saturation field of iron in the storage ring will considerably reduce the overall length of magnetic field required, and thus the cost of the tunnel and utility runs. In this appendix 40 kG and 60 kG superconducting bending magnet designs for storage rings are briefly described and rough cost estimates are given for 100 BeV storage rings using these magnets.

For the same overall length of magnetic field the higher field strengths obtainable using superconducting magnets would give higher energies. As mentioned in Section II the storage ring geometry described in this report would give 200 BeV at 40 kG and 400 BeV at 80 kG. The costs with present technology for such storage rings could be obtained by scaling the figures for the 100 BeV designs. No detailed cost estimates for these options are given since they are so dependent on future developments in the superconducting field.

(A) Description of Bending Magnets

A 40 kG supercondcuting bending magnet is shown in cross section in Fig. A-1. The beam requires a uniform field region 2.5 in. in diameter. The required field uniformity is ± 0.5% per meter in the direction transverse to the beam, so that the maximum tolerable variation is .03% or 12 gauss over the useable aperture. In addition, the field intensities of all the bending magnets in the storage ring must be equal to one another to within ± 5×10^{-4}.

This implies that the reproducibility of the field in a given magnet must be good to this accuracy. While a transverse magnetic field of 40 kG is easily achieved using superconductors, this high degree of uniformity and reproducibility remains to be demonstrated. For transverse field superconducting magnets all effort so far has been concentrated on the attainment of a particular central magnetic field. The achievement of uniformity and reproducibility, while not neglected, has played a very minor role.

It is assumed in Fig. A-1 that with an inner diameter of the windings of 3.5 in. the required uniformity and reproducibility can be attained. The windings are shaped so as to give a high degree of field uniformity in the bore. The current density assumed is that of "stable" superconducting windings made with a composite conductor of copper and Nb-Ti. This type of conductor is the natural choice now and in the near future because of its low cost, reliability, and general ease of construction. The magnetic forces tending to push the two conductor bundles apart are taken up by a structure which surrounds the windings.

The complete superconducting winding and structure are placed inside a liquid helium container. Large voids in this space should be filled up with suitable filling material so as to reduce the amount of liquid helium required. The inner bore of the magnet is at $4.2^{\circ}K$, which automatically provides cryopumping for the required vacuum.

Figure A-1 40 kG Storage Ring Bending Magnet (Cold Bore)

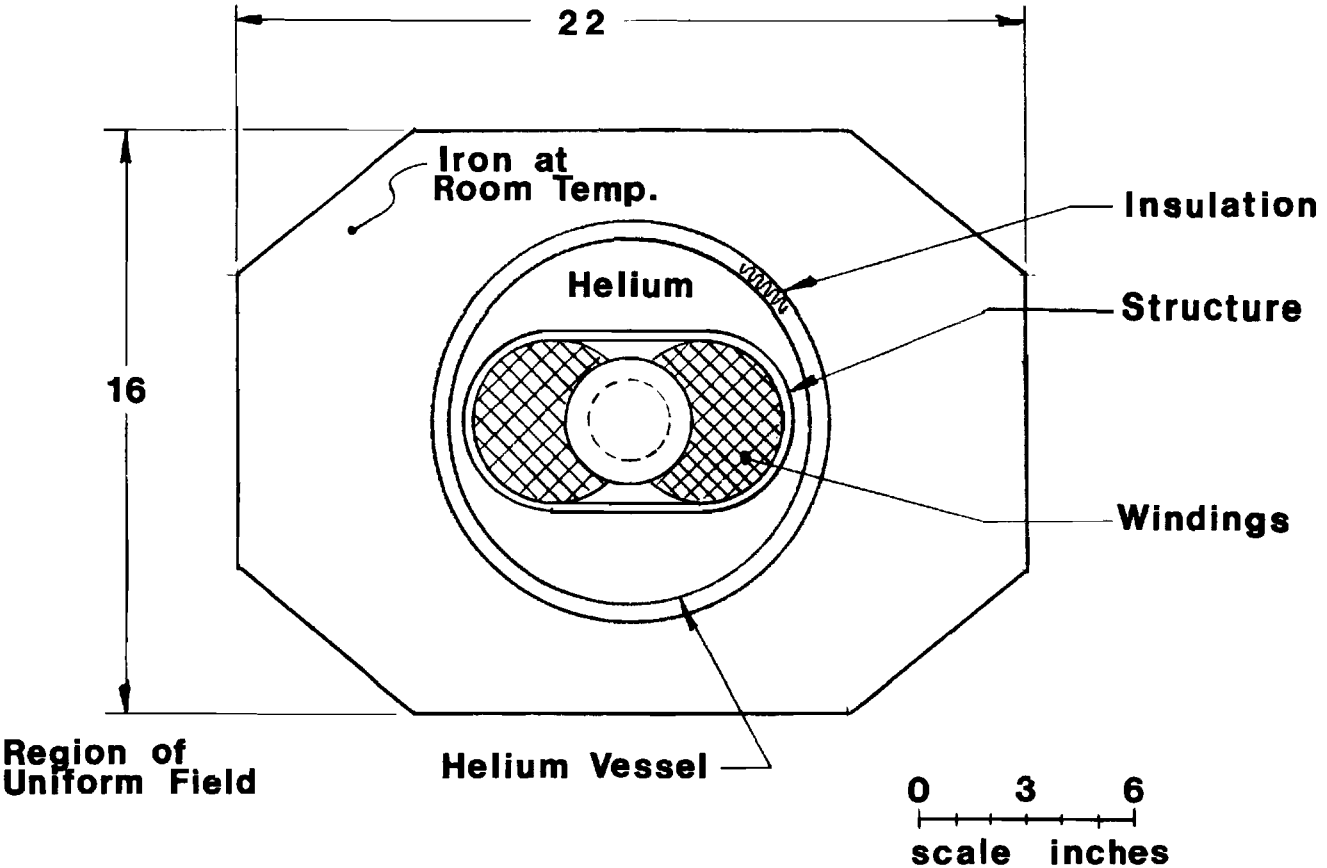

The helium container is thermally insulated with multiple reflecting insulation in vacuum, and a thick iron magnetic flux return shield serves as the outer room temperature wall. The insulation itself has very little mechanical load bearing capability if good insulation properties are to be maintained. Therefore a bicycle wheel type of tension structure at each end of the magnet must be used to position the inner helium vessel accurately with respect to the outer room temperature iron block. Additional supports may be required to prevent excessive sagging of the magnet under its own weight.

The thickness of the iron shield is such that at maximum operating magnetic field the iron can still carry all the flux so that flux leakage as well as magnet to magnet flux interaction is kept at a minimum. Under these conditions it contributes slightly less than 10 kG to the central magnetic field.

Figure A-2 presents an alternate 40 kG magnet design. The current density in the superconducting windings is twice that of the design shown in Fig. A-1. This current density is higher than that normally considered "stable"; i.e. at this high current density a normal region is self propagating once it nucleates. There is at the present insufficient experimental information as to how coils operate at current densities higher than that considered to be "stable". It would be imprudent to commit to this higher current density at this time.

Figure A-3 shows a 60 kG magnet design. The current density

Figure A-2 **40 kG High Current Density Superconducting Magnet for Storage Ring (Cold Bore)**

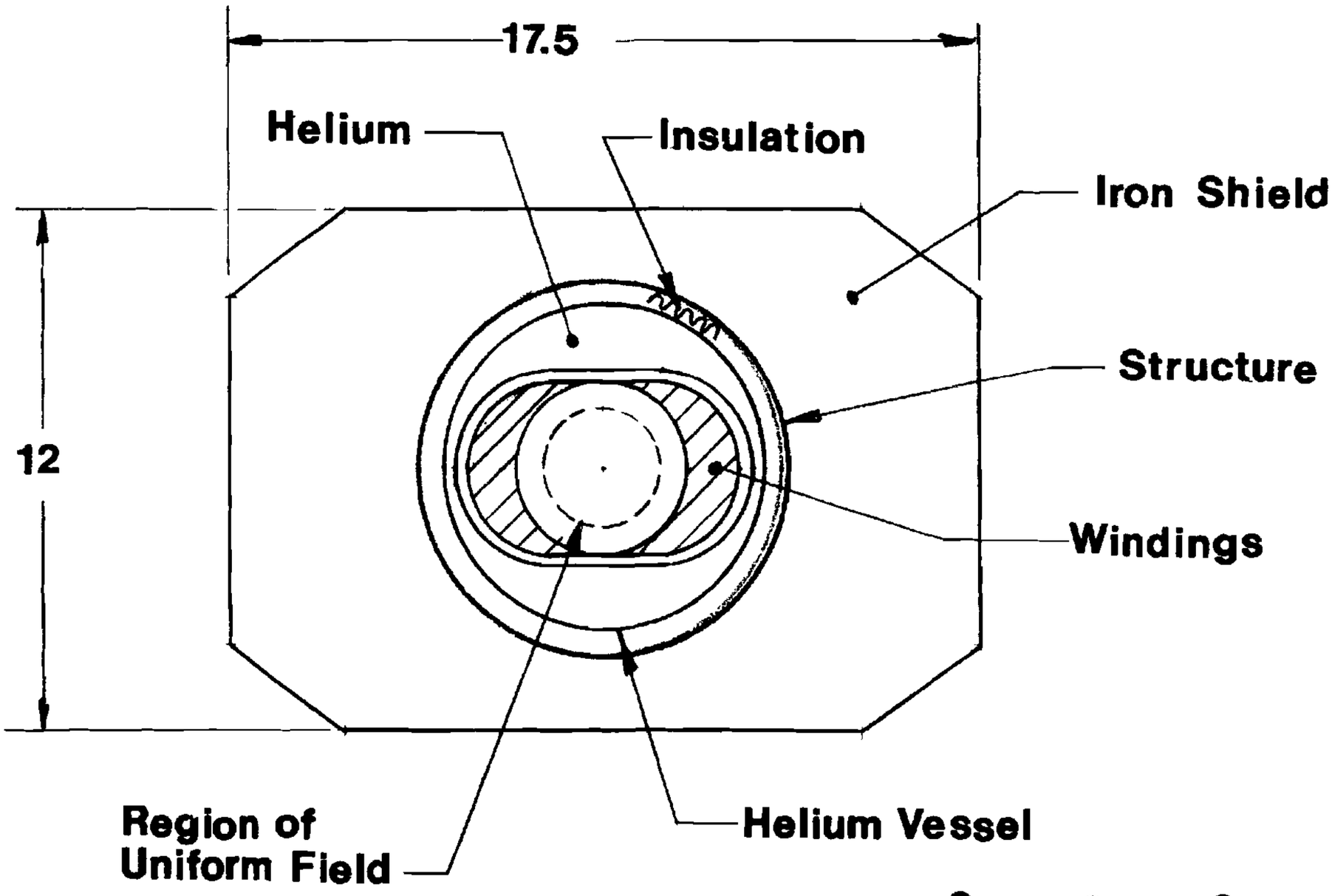

Figure A-3 60kG Storage Ring Bending Magnet

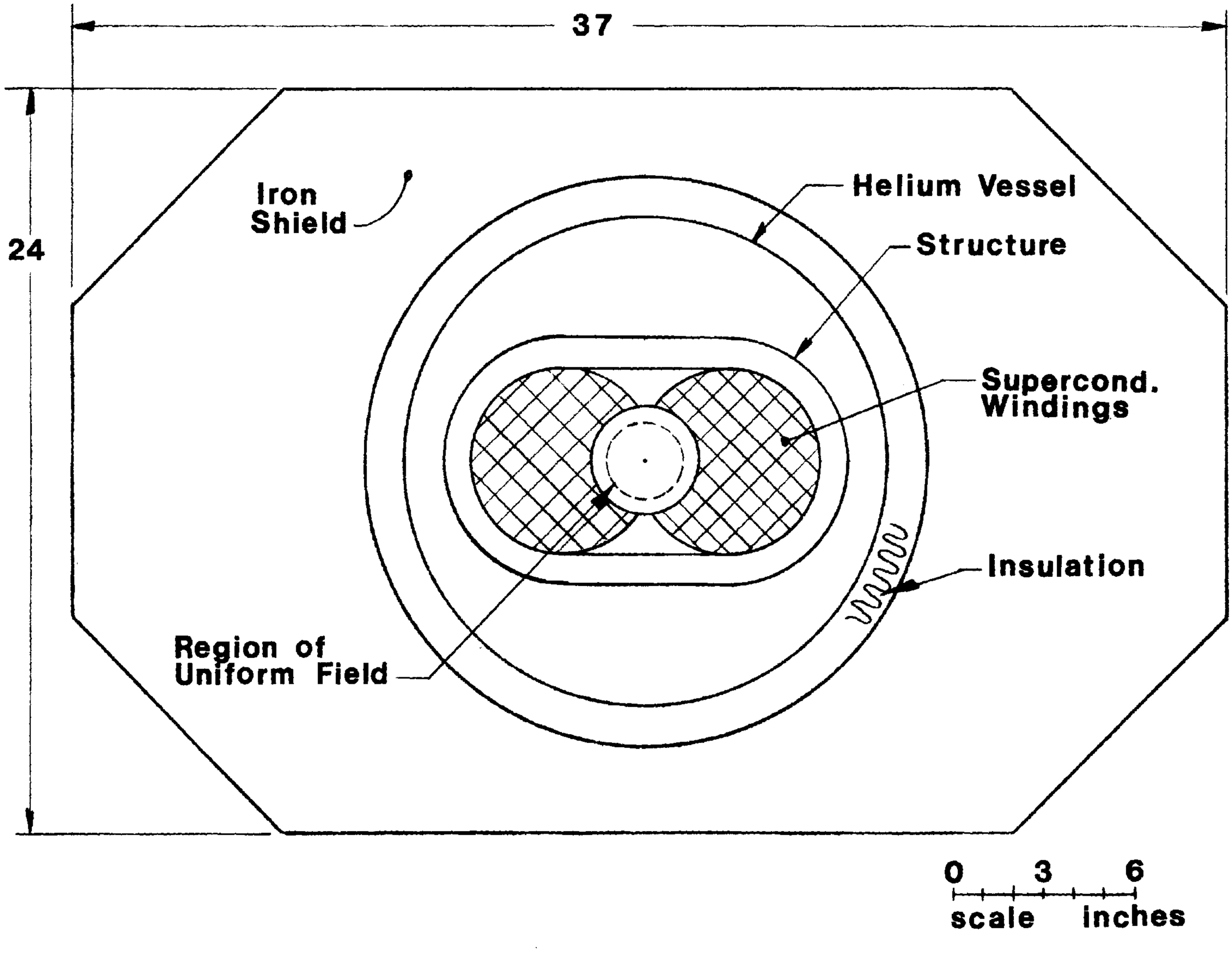

chosen is that typical of a Nb-Ti composite. For this design stability is no longer the limiting factor. Stability generally increases with increasing magnetic field because the lower current carrying capacity of a superconductor at higher field tends to make the conductor more "stable". Nb_3Sn conductors can generally operate at higher current densities, however compared to Nb-Ti its less desirable operating characteristics as well as reproducibility tend to balance out its obvious advantage of high field. The important parameters of the three designs for a 100 BeV storage ring are given in Table A-1.

Table A-1 Major Bending Magnet Parameters

	Design 1	Design 2	Design 3
Energy (BeV)	100	100	100
Magnetic field (kG)	40	40	60
Total length of bending field (each ring) (m)	529	529	352
Ring radius (m)	222	222	167
Length of bending magnet (m)	3.67	3.67	2.44
Number of bending magnet (each ring)	144	144	144
Diameter of uniform field region (in.)	2.5	2.5	2.5
Overall dimensions of magnet	22in.x16in.	17.5in.x12in.	37in.x24in.
Conductor type	Composite Cu and Nb-Ti	Composite Cu and Nb-Ti	Composite Cu and Nb-Ti
Refrigerator power (5 W/magnet) (kW)	1000	1000	1000

(B) Cost Estimates

The estimated costs for the magnet systems are summarized in Table A-2. As expected the costs are least for the smallest magnet. For the cryogenic system we assumed a heat load of 5 W per magnet and an installed refrigeration capacity of 10 W per magnet. It is expected that significant cost reduction will be possible for the 60 kG magnet when a reliable high current density low cost conductor becomes available.

Table A-2 Cost Estimates of Magnet Systems

(All numbers in million dollars)

(Not including EDIA and contingency)

	Design 1	Design 2	Design 3
Bending Magnets			
Magnets	19.40	8.15	29.30
Refrigeration (10 W/magnet) and containers	5.75	5.75	5.75
Power supplies	0.50	0.50	0.50
Subtotal	25.65	14.40	35.55
Misc. 15%	3.85	2.16	5.33
Subtotal	29.50	16.56	40.88
Quadrupoles (40% of Bending Magnet)	11.80	6.62	16.35
Total	41.30	23.18	57.23

A rough cost estimate of the entire 100 BeV storage ring project using these superconducting magnets are given in Table A-3. This Table is constructed as follows: Starting from the estimate

given in section XII for the design most closely related to the superconducting magnet application, namely that using iron-core magnets with superconducting coils, we first replace items A1, 2, and 3 by the totals in Table A-2. The remaining items fall, generally, into two categories: those which scale roughly as the ring radius and those which are essentially independent of the radius. There are items which do not belong to either category in a clear cut manner. However errors made this way are small and tend to average out in the project totals. Because of the lack of experience with the design and fabrication of these magnets on a mass production basis both the EDIA and the Contingency of the technical components are taken to be 30%.

Table A-3 Cost Estimates of 100 BeV Storage Rings

(All numbers in million dollars)

	Design 1	Design 2	Design 3
A. Technical Components			
1. Ring magnets, refrigeration, and power supply	41.30	23.18	57.23
2. Injection transport magnets and power supply	1.56	1.56	1.17
3. Pulsed and auxiliary magnets and power supply	5.33	5.33	5.33
4. RF system	0.20	0.20	0.20
5. Vacuum system	1.18	1.18	0.88
6. Support alignment	0.57	0.57	0.43
7. Special handling equipment	0.19	0.19	0.19
8. Beam devices	0.45	0.45	0.41
9. Control and instruments	1.20	1.20	1.12
Subtotal	51.98	33.86	66.96
EDIA @30%	15.59	10.16	20.09
Subtotal	67.57	44.02	87.05
Contingency @30%	20.27	13.20	26.11
Total Technical Components	87.85	57.22	113.16

	Design 1	Design 2	Design 3
B. Conventional Facilities			
1. Enclosures	2.14	2.14	1.60
2. Experimental halls	3.90	3.90	3.90
3. Enclosures service building	0.45	0.45	0.34
4. Central laboratories	3.42	3.42	3.42
5. Work shops	1.56	1.56	1.56
6. Mechanical utilities	1.01	1.01	0.76
7. Excavation and earthwork	0.74	0.74	0.56
8. Site improvements	0.61	0.61	0.45
9. Movable shielding	2.13	2.13	2.13
Subtotal	15.96	15.96	14.72
AEM @20%	3.19	3.19	2.94
Subtotal	19.15	19.15	17.66
Contingency @15%	2.87	2.87	2.65
Total Conventional Facilities	22.02	22.02	20.31
Project Total	109.87	79.24	133.47

We see from Table A-3 that the cost of the design using the high current density 40 kG magnet is already competitive with those of the 20 kG designs given in Section XII. It is entirely possible that designs using 60 kG or even 80 kG superconducting magnets will be technically and economically feasible at the time the project starts.

Appendix B LIST OF PARAMETERS

(100 BeV Storage Ring Using Conventional Magnets)

A. Principal Parameters

1.	Energy	100 BeV
2.	Ring radius	1/3 km
3.	Lattice type	Separated function FODO cells with 6 matched insertions
4.	Beam intersecting angle	49.87 mrad
5.	Number of experimental intersection	3
6.	Drift lengths next to experimental intersection	32.55 m(outside)+ 39.97 m(inside)
7.	Number of injection intersection	3
8.	Drift lengths next to injection intersection	29.49 m(outside)+ 39.28 m(inside)
9.	Number of accelerator pulses to fill each ring	20
10.	Number of protons stacked in each ring	10^{15}
11.	Stacked beam current	23 A
12.	Emittance of stacked beam	
	a. Horizontal	5.7π mm-mrad
	b. Vertical	0.36π mm-mrad
13.	Momentum spread of stacked beam $\frac{\Delta p}{p}$	$\pm 10^{-3}$
14.	Luminosity	$10^{32} cm^{-2} sec^{-1}$
15.	Refilling time	10 - 100 hr. (depending on experiment)

B. Lattice Structure and Orbit Parameters
(*Numbers in parentheses are bending magnet field and quadrupole field gradient)

B. Continued -

1. Normal cell (C)

a. Length of bending magnet (B1 and B2)	4.20 m	(19.99kG)*
b. Length of cell quadrupole magnet (QF and QD)	1.40 m	(248.5kG/m)
c. Length of minimum separation between magnets (0)	0.30 m	
d. Length of short straight section (00)	1.60 m	
e. Cell structure	(QF/2)00(B1)0(B2)0-(QD)00(B2)0(B1)0(QF/2)	
f. Total length of cell	24.00 m	
g. Number of cells in each ring	48	

2. Injection insertion (I)

a. Length of end quadrupole (QDI=QD/2)	0.70 m	(248.5kG/m)
b. Length of bending magnet (BI)	4.20 m	(19.99kG)
c. Lengths of quadrupoles in triplets		
QFI1	1.30 m	(237 kG/m)
QDI2	2.14 m	(-190 kG/m)
QFI3	0.85 m	(141 kG/m)
d. Drift lengths between		
QDI and B2 (LI1)	3.40 m	
BI and BI (0)	0.30 m	
BI and QFI1 (LI2)	6.14 m	
QFI1 and QDI2 (LI3)	4.70 m	
QDI2 and QFI3 (LI4)	3.86 m	
QFI3 and crossing point (inside) (LI5)	39.28 m	
Crossing point and QFI3 (outside) (LI6)	29.49 m	
e. Insertion point in normal cell	Midpoint of QD	
f. Structure of insertion I (in beam direction from inside to outside)	(QDI)LI1(B2)0(B1)0(BI)0(BI)LI2(QFI1)LI3(QDI2)LI4(QFI3)LI5-LI6(QFI3)LI4(QDI2)LI3(QFI1)LI2-(BI)0(BI)0(B1)0(B2)LI1(QDI)	
g. Total length of I insertion	149.35 m	
h. Number of I insertions	3	

3. Experimental insertion (E)

a. Length of end quadrupole (QFE)	0.94 m	(248.5 kG/m)
b. Length of bending magnet (BE)	4.20 m	(19.99kG)
c. Lengths of quadrupoles in outer triplet		
QFE1	1.80 m	(214kG/m)
QDE2	2.50 m	(-196kG/m)
QFE3	1.40 m	(165 kG/m)

B. 3 Continued -

	Lengths of quadrupoles in inner triplet		
	QDE4	1.80 m	(-179kG/m)
	QFE5	2.50 m	(183kG/m)
	QDE6	1.40 m	(-120kG/m)
d.	Drift lengths between		
	QFE and B1 (LE1)	0.78 m	
	BE and BE (0)	0.30 m	
	BE and QFE1 (LE2)	1.93 m	
	QFE1 and QDE2(LE3)	4.03 m	
	QDE2 and QFE3(LE4)	3.86 m	
	QFE3 and crossing point (LE5)	32.55 m	
	Crossing point and QDE4(LE6)	39.97 m	
	QDE4 and QFE5(LE7)	3.54 m	
	QFE5 and QDE6(LE8)	4.68 m	
	QDE6 and BE(LE9)	5.29 m	
e.	Insertion point in normal cell	Midpoint of QF	
f.	Structure of insertion E (in beam direction from outside to inside)	(QFE)LE1(B1)0(B2)0(BE)0-(BE)0(BE)0(BE)LE2(QFE1)-LE3(QDE2)LE4(QFE3)LE5-LE6(QDE4)LE7(QFE5)LE8-(QDE6)LE9(BE)0(BE)0(BE)-0(BE)0(B2)0(B1)LE1(QFE)	
g.	Total length of E insertion	164.78 m	
h.	Number of E insertions	3	

4. Superperiod

a.	Half cells	
	from mid-QF to mid-QD	$\frac{C}{2}$
	from mid-QD to mid-QF	$\frac{C}{2}$
b.	Structure of superperiod	$ECCCCCCC\frac{C}{2}I\frac{C}{2}CCCCCCC$
c.	Total length of superperiod	698.13 m
d.	Number of superperiods	3

5. Orbit properties

a.	Orbit length	2094.4 m(2π/3km)
b.	Radius in bending magnet	168.45 m
c.	Revolution frequency	143.134 kHz
d.	Betatron oscillation phase advances	
	Normal cell	
	μ_x	0.203(2π) rad
	μ_y	0.204(2π) rad

B. 5 Continued -

Injection insertion

μ_x	0.522(2π) rad
μ_y	0.951(2π) rad

Experimental insertion

μ_x	1.168(2π) rad
μ_y	0.733(2π) rad

Superperiod

μ_x	4.937(2π) rad
μ_y	4.948(2π) rad

Revolution

$\mu_x = \nu_x(2\pi)$	14.81(2π) rad
$\mu_y = \nu_y(2\pi)$	14.85(2π) rad

e. Betatron oscillation amplitude function

Normal cell

$\beta_{x\ max} = \beta_{y\ max}$	39.5 m
$\beta_{x\ min} = \beta_{y\ min}$	10.2 m

Injection insertion

$\beta_{x\ max}$	140 m
$\beta_{y\ max}$	102 m

Experimental insertion

$\beta_{x\ max}$	224 m
$\beta_{y\ max}$	618 m

Experimental crossing point

β_x	27 m
β_y	4 m

f. Momentum excursion function x_p

Normal cell (max)	2.18 m
Normal cell (min)	1.20 m
Injection insertion drift space	3.65 m
Experimental insertion drift space	0 m

C. Magnet System Parameters

1. Cell bending magnets B1 and B2

C. 1 Continued -

		B1	B2
a.	Number of units	216	216
b.	Length (2 sections each)	2x2.10 m	2x2.10 m
c.	Gap height	1.00 in	1.25 in
d.	Good field width	2.50 in	2.00 in
e.	Field strength	19.987kG	19.987kG
f.	Number of coil turns	40	50
g.	Current	1169A	1169A
h.	Power	32.2kW	41.6kW
i.	Inductance	0.042H	0.053H
j.	Cooling water pressure drop	100 psi	100 psi
k.	Number water paths/coil	4	5
l.	Water temperature rise	14°C	14°C

2. Cell quadrupoles QF and QD

a.	Number of units	180
b.	Length	1.40 m
c.	Pole contour	$xy=0.3125\ in^2$
d.	Field gradient	±248.5kG/m
e.	Number of coil turns	31 per pole
f.	Current	258A
g.	Power	6.04kW

3. Matching bending magnets BI and BE

		BI	BE
a.	Number of units	24	48
b.	Length (2 sections each)	2x2.10 m	2x2.10 m
c.	Gap height	0.85 in	2.75 in
d.	Good field width	4.00 in	3.00 in
e.	Field strength	19.987kG	19.987kG
f.	Number of coil turns	34	110
g.	Current	1169A	1169A

4. Matching quadrupoles

		Number of Units	Length (m)	Contour (xy) (in^2)	Field Gradient (kG/m)
a.	QDI+QD/2	12	1.40	0.3125	248.5
b.	QFI1	12	1.30	1.100	237
c.	QDI2	12	2.14	1.100	-190
d.	QFI3	12	0.85	1.100	141
e.	QFE+QF/2	12	1.64	0.3125	248.5
f.	QFE1	6	1.80	1.875	214
g.	QDE2	6	2.50	1.875	-196
h.	QFE3	6	1.40	1.875	165

C. 4 Continued -

i.	QDE4	6	1.80	3.150	-179
j.	QFE5	6	2.50	3.150	183
k.	QDE6	6	1.40	3.150	-120

5. Magnet weight

		Core steel	Coil copper
a.	Bending magnets B1+BI	1390 ton	255 ton
b.	Bending magnets B2+BE	2160 ton	430 ton
c.	Cell quadrupoles	390 ton	53 ton
d.	Matching quadrupoles	990 ton	136 ton
	Total	4930 ton	874 ton

6. Power consumption

a.	Bending magnets B1+BI	7.9 MW
b.	Bending magnets B2+BE	13.3 MW
c.	Cell quadrupoles	1.2 MW
d.	Matching quadrupoles	3.0 MW
	Total	25.4 MW

7. Power supply — Silicon controlled rectifier

8. Magnet foundation and support

a.	Foundation	Slab on ground. No piles
b.	Support	Two channel irons: one on each side of magnet

9. Trimming magnets

a.	Number	228
b.	Length	0.3 m
c.	Maximum multipole moments	
	Dipole (B)	±0.6kG
	Quadrupoles (B')	$\pm 2.5 kG/m_2$
	Sextupole (B")	$\pm 700 kG/m^2$

D. Vacuum System

1. Average pressure — 10^{-9} torr
2. Pressure in experimental insertion — 10^{-11} torr
3. Vacuum chamber

a.	Construction	All metal with welded joints
b.	Material	Stainless steel
c.	Thickness	0.05 in
d.	Treatment	Chemically etched and pre-baked for >48 hr at 400°C No bakeout after installatic

D. 3 Continued -

e. Cross-section in B1	Elliptical 1.00inx2.50in
f. Cross-section in B2	Elliptical 1.25inx2.00in

4. Pumps

a. Linear ion pump	Inside vacuum chamber along length of all magnets
b. Sputter-ion pump	100 ℓ/sec, one in each 1.6 m drift space
c. Sublimation-getter pump	In all insertions
d. Roughing pumps	Portable units

5. Isolation valves

a. Number	24 (one at each end of an insertion)
b. Type	All-metal and non-magnetic

6. Clearing electrodes

a. Location	Outside ends of all magnets and along drift spaces
b. Voltage	± 5kV

E. RF System

1. Frequency	53.1028 MHz
2. Harmonic number	371
3. Frequency modulation	0.0075%
4. Required precision of stacking frequency	$\frac{\Delta f}{f} = 4 \times 10^{-6}$
5. Peak cavity voltage	10kV
6. Cavity	Single ferrite tuned cavity
7. Debunching	Beam properly debunched in accelerator main ring before injection into storage ring

F. Injection System

1. Beam transport

a. Lattice	Combination of main ring and storage ring FODO cells
b. Geometry	One beam straight, one beam bent 60^{o}

F. 1 Continued -

c.	Magnet elements	
	Number x length of bending magnets	42x4.2 m
	Field of bending magnet	~ 20 kG
	Number of quadrupole	~ 60
	Field gradient of quadrupole	~ 250 kG/m
d.	Total length of both beams	5300 ft
2.	Extraction from accelerator	Fast one-turn extraction
3.	Injection	
a.	Mode	3-turn injection
b.	Septum magnets	Similar to main ring septum magnets
c.	Kicker magnets	
	Strength	2.12 kGm
	Number	4 (2 per ring)
	Rise time (fall time)	20 nsec
	Type	Ferrite loaded transmission line
	Switch	Spark gaps

G. Beam Scraper and Dump System

1.	Beam scrapers	
a.	Number	One horizontal and one vertical pairs of jaws per ring
b.	Location	Upstream of injection crossing point; jaws in each pair 180° betatron phase apart
c.	Jaw material	Beryllium
d.	Jaw thickness	~ 3 m
2.	Beam dump system	
a.	Number	One per ring
b.	Location	Injection insertion, on beam not used for injectior
c.	Direction of beam extraction	Vertical
d.	Kicker and septum magnets	Similar to those for injecf ion but vertical
e.	Beam stoppers	Steel cylinders with beryllium cores

Appendix C BIBLIOGRAPHY

M. S. Livingston, Study Paper on the NAL Storage Ring Design, FN-162, July 2, 1968.

P. J. Reardon, Cost Guestimate for Storage Rings, July 25, 1968.

M. S. Livingston, Storage Ring Study Paper #2, TM-3, August 14, 1968.

A. A. Garren, Storage Ring Study, TM-2, August 15, 1968.

E. Keil, B. Montague, W. Schnell and A. M. Sessler, An Estimate of Luminosity and ν Shifts, FN-168, August 27, 1968.

E. Keil, Aperture Requirements at Injection into the NAL Storage Ring, FN-169, August 27, 1968.

E. Keil and B. Montague, Kicker Requirements for Phase-Plane Interchange Injection into NAL Storage Ring, FN-170, August 28, 1968.

A. van Steenbergen, Injection Criteria Storage Ring, FN-171, August 28, 1968.

E. Keil, Space Charge Limit for a Neutralized Beam, TM-31, August 29, 1968.

W. Schnell, RF Considerations for 100 GeV Intersecting Storage Rings, TM-28, August 29, 1968.

W. Schnell, Bunching the Beam in the Storage Rings, TM-34, August 29, 1968.

M. S. Livingston, Dimensional Study of Intersecting Storage Rings, TM-24, August 30, 1968.

E. M. Rowe, Some Remarks Concerning the Achievement of Pressures in the Low 10^{-9} Torr Range, or Better, in the NAL Storage Ring, TM-89, September, 1968.

E. Keil and B. Montague, Electric Field Required for De-Neutralizing the Stacked Beam in the NAL Storage Rings, TM-25, September 3, 1968.

E. D. Courant, Nuclear and Coulomb Scattering in Storage Ring, TM-69, September 7, 1968.

R. B. Britton, Summary of Ideas for a Superconducting Storage Ring, TM-88, September 13, 1968.

M. Green, A Cost Estimate for the NAL 100 GeV Intersecting Storage Rings Using Superconducting Magnets - A Comparison Between 50 kG and 60 kG Machines, TM-99, September 15, 1968.

S. C. Snowdon, Conventional Bending Magnets for Storage Ring, TM-44, September 16, 1968.

J. M. Paterson, Vacuum and Shielding Requirements for 100 GeV Proton Storage Rings, TM-61, September 17, 1968.

L. C. Teng, FODO Lattice for Storage Rings, TM-55, September 20, 1968.

R. R. Wilson, A Superferric Storage Ring, FN-173, September 25, 1968.

E. D. Courant, Choice of Radius for NAL Storage Ring, TM-66, October 3, 1968.

C. A. Heusch, General Comments on the Use of Proton Storage Rings, FN-175, October 4, 1968.

S. C. Snowdon, Conventional Bending Magnets for Storage Ring (II), TM-75, October 8, 1968.

R. Little, NAL pp Storage Rings 100 GeV, Very High Energy Cosmic Ray Experiments, TM-73, October 11, 1968.

L. C. Teng, Empirical Formulas for Ion Pumping - Information Obtained from Nuclear Physics Institute, Novosibirsk, TM-84, October 28, 1968.

L. W. Jones, Proton-Proton Elastic Scattering with 2x100 GeV Colliding Beams, TM-85, October 29, 1968.

A. D. Krisch, A Storage Ring Interaction Station for Measuring Proton Proton Elastic Scattering in the Vertical Plane, TM-90, October 31, 1968.

L. W. Jones, Miscellaneous Comments and Observations on NAL 100 x 100 GeV Colliding Beam Storage Ring, TM-91, October 31, 1968.

E. D. Courant, Phase Space Dilution in Three Turn Injection, FN-174, November, 1968.

L. C. Teng, 200 BeV Storage Ring Parameters, TM-100, December 5, 1968.

Richard Wilson, Measurement of Luminosity, FN-176, December, 1968.

C. Heusch and L. Stevenson, Search for the W Boson at the NAL ISR, FN-177, December, 1968.

C. Heusch, Non-pp Experimentation at the NAL ISR, FN-178, December, 1968.

A. A. Garren and J. A. MacLachlan, Modification of the Lattice of the Colliding Beam Storage Ring for the National Accelerator Laboratory, TM-103, December, 1968.